SPECTRUM SHARING IN

NEXT GENERATION WIRELESS COMMUNICATION NETWORKS

by
Ying He

Dissertation submitted in fulfilment of the requirements
for the degree of

DOCTOR OF PHILOSOPHY

under the supervision of

Prof. Eryk Dutkiewicz

School of Computing and Communications
University of Technology Sydney
Sydney, Australia

February 2017

ABSTRACT

In recent years, the wireless communication systems have dramatically changed the world by connecting people and devices. We are currently standing at the 4th generation (4G) in the evolution and drawing the picture for the next generation (5G) wireless communication systems. For which, we are aiming at 1000x increase in capacity. Despite all efforts on the coding and modulation techniques, the growth of capacity is physically restricted by the limited spectrum resource. Therefore, spectrum sharing has been proposed to break this constraint. This thesis studied the emerging spectrum sharing frameworks and enabling spectrum sharing in cellular networks.

Our work focuses on two main spectrum sharing frameworks: Spectrum Access System (SAS) in the U.S. and Licensed Shared Access (LSA) in Europe. We address the common and differing factors, then propose access and interference mitigation methods for SAS and LSA. SAS is a hierarchical access model with three tiers of users: incumbents, Priority Access Licensees (PAL) and General Authorised Access (GAA) users. We propose a PAL-GAA co-channel interference mitigation technique that does not expose base station locations. The distribution of the aggregate interference is derived using Probability Density Function and Characteristic Function. The optimal exclusion zone size is found through an approximation of a convex problem and our approach reduces the exclusion zone size substantially. We also propose the access methods between different tiers in LSA and SAS, regarding the interference measurement and user selection of secondary users, efficient PAL detection with sub-sampling and LTE/WiFi

coexistence in the unlicensed band. These access and coexistence methods guarantee that the interference requirements are met.

Furthermore, we studied one of the key enabling technologies in the future cellular networks - Cloud Radio Access Network (C-RAN). By modelling C-RAN with the Distributed Antenna System (DAS), we analyse the capacity of C-RAN in multiple aspects. We derive closed-form upper and lower bounds in efficiently computable expressions for differential capacity (DCAP) using the Moment Generating Function (MGF) of the Signal-to-Noise-Ratio (SNR). We then propose to leverage Coordinated Multi-Point (CoMP), Fractional Frequency Reuse (FFR) and Multi-User Multiple-Input-Multiple-Output (MU-MIMO) in the C-RAN system to boost the capacity through coordination. Moreover, the emerging LSA framework is applied on the C-RAN to further increase the capacity. Additionally, we use Multiset to model the Inter-Cell Interference (ICI) of C-RAN and optimise the FFR resource allocation. We investigate the dynamic decision making and derive the transmitting SNR threshold for C-RAN.

In summary, spectrum sharing on the next generation wireless communication has not yet been fully studied. This thesis proposes spectrum sharing methods that contribute to the interference mitigation and capacity growth for spectrum sharing frameworks and C-RAN in the future 5G networks.

CERTIFICATE OF ORIGINAL AUTHORSHIP

I certify that the work in this thesis has not previously been submitted for a degree nor has it been submitted as part of requirements for a degree.

I also certify that the thesis has been written by me. Any help that I have received in my research work and the preparation of the thesis itself has been acknowledged. In addition, I certify that all information sources and literature used are indicated in the thesis.

Name of Student: Ying He

Signature of Student:

Date: 20/02/2017

ACKNOWLEDGMENTS

First and foremost, I would like to acknowledge that this work has been supported by University of Technology Sydney, Macquarie University, Intel Corporation - University Research Office and Chinese Academy of Sciences.

I would like to express my sincerest gratitude to my supervisor Prof. Eryk Dutkiewicz (University of Technology Sydney) who has been supporting me with the precious opportunities to learn, explore and improve.

I would like to thank Prof. Jinglin Shi (Institute of Computing Technology, Chinese Academy of Sciences) who led me to the road of research.

I am grateful to Dr. Markus Mueck and Dr. Srikathyayani Srikanteswara (Intel Corporation) who have broaden my perspective with the latest technologies in industry.

I would like to thank my co-supervisor Dr. Beeshanga Abewardana Jayawickrama (University of Technology Sydney) who has been my mentor and best friend.

I would like to thank Dr. Gengfa Fang (University of Technology Sydney) who has influenced me with his energetic spirit.

I would like to especially thank my colleagues and friends in Australia and China.

Finally, I wish to thank my sister, nephew and brother in law for their unconditional support and to my parents for their love.

Contents

List of Figures

List of Tables

List of Publications

Journal publications

The IEEE journal publications including submitted papers of the author are as follows:

- **Ying He**, Beeshanga Abewardana Jayawickrama, Eryk Dutkiewicz, Srikanteswara Srikathyayani and Markus Mueck, "Priority Access and General Authorised Access Interference Mitigation in Spectrum Access System", in *IEEE Transactions on Vehicular Technology*, 2016, under review.

- Beeshanga Abewardana Jayawickrama, Eryk Dutkiewicz, Markus Mueck and **Ying He**, "On the Usage of Geolocation Aware Spectrum Measurements for Incumbent Location and Transmit Power Detection", *IEEE Transactions on Vehicular Technology*, vol. 65, no. 10, pp. 8177 - 8189, Oct. 2016.

Intellectual property

Patent filings and intellectual property disclosures of the author during her PhD studies are as follows.

The following patents have been filed or accepted for filing through Intel Corporation:

- Srikanteswara Srikathyayani, Markus Mueck, **Ying He**, Beeshanga Abewardana Jayawickrama, Eryk Dutkiewicz, Zhibin Yu, Christian Drewes, Biljana Badic, "SAS PAL GAA co-channel interference mitigation", Application No. P98713Z.

- Markus Mueck, **Ying He**, Beeshanga Abewardana Jayawickrama and Srikanteswara Srikathyayani, "Uplink Interference Management in Shared Spectrum Networks", Application No. P86405.

- Markus Mueck, **Ying He**, Beeshanga Abewardana Jayawickrama and Eryk Dutkiewicz, "Methods and Devices for User Detection in Spectrum Sharing", Application No. P97272.

- **Ying He**, Beeshanga Abewardana Jayawickrama, Eryk Dutkiewicz, Markus Mueck and Christian Drewes, "Communication Device and Method for Communicating using a Frequency Range", Application No. P83877.

- Beeshanga Abewardana Jayawickrama, **Ying He**, Eryk Dutkiewicz, Markus Mueck and Srikanteswara Srikathyayani, "3.5 GHz Spectrum Sharing - Measurement reliability management for a SAS Non-dedicated ESC network", reference No. 138757, accepted for filing.

- Beeshanga Abewardana Jayawickrama, **Ying He**, Eryk Dutkiewicz, Markus Mueck, Srikanteswara Srikathyayani and Drewes Christian,"Distributed PAL protection area interference mitigation with GAA power allocation and beamforming", accepted for filing.

The following patents have been submitted to Intel Corporation patent committee and are under review:

- **Ying He**, Beeshanga Abewardana Jayawickrama, Eryk Dutkiewicz, Markus Mueck and Srikanteswara Srikathyayani, " SAS PAL Protection Area Interference Mitigation", reference No. 137524, under review.

- **Ying He**, Beeshanga Abewardana Jayawickrama, Eryk Dutkiewicz, Markus Mueck and Srikanteswara Srikathyayani, " Network Virtualization enhanced SAS", under review.

- **Ying He**, Beeshanga Abewardana Jayawickrama, Eryk Dutkiewicz, Markus Mueck and Srikanteswara Srikathyayani,"Spectrum Access System (SAS) Spectrum Sharing with fine-grained protection/exclusion zone differentiation", under review.

The following patents have been filed through Institute of Computing Technology, Chinese Academy of Sciences:

- Jian Wang, **Ying He**, Zhentao Kou, Jisheng Peng and Jinglin Shi, "LTE PRACH baseband signal generating methodology and system", Application No. CN101938329A.

- Yongtao Su, Shoujun Huang, **Ying He**, Yanbin Yao and Jinglin Shi, "Method and device for detecting number of transmitting antennae of base station of long term evolution (LTE) system", Application No. CN102594424A.

- Jian Wang, Shoujun Huang, Yongtao Su, Juan Zheng, **Ying He**, Jisheng Peng and Jinglin Shi, "Implementation and Methodology of LTE cell searching", Application No. CN102045815A.

- Shoujun Huang, Jian Wang, Shan Tang, Jisheng Peng, **Ying He**, Baideng Tian and Jinglin Shi, "LTE Timing and Frequency Synchronization", Application No. CN101827052A.

Conference publications

The conference publications of the author are as follows.

- **Ying He**, Eryk Dutkiewicz, Gengfa Fang and Markus Mueck, "SNR Threshold for Distributed Antenna Systems in Cloud Radio Access Networks", in *Proc. IEEE Vehicular Technology Conference (VTC)*, pp. 1-5, 2015.

- **Ying He**, Eryk Dutkiewicz, Gengfa Fang and Markus Mueck, "Fractional Frequency Reuse in Distributed Antenna Systems in Cloud Radio Access Networks", in *Proc. IEEE International Conference on Communications (ICC) Workshop*, pp. 907-912, 2015.

- **Ying He**, Eryk Dutkiewicz, Gengfa Fang and Markus Mueck, "Licensed Shared Access in distributed antenna systems enabling network virtualization", in *Proc. International Conference on 5G for Ubiquitous Connectivity (5GU)*, pp. 76-80, 2014.

- **Ying He**, Eryk Dutkiewicz, Gengfa Fang and Jinglin Shi, "Downlink capacity in cloud radio access networks with fractional frequency reuse", in *Proc. International Symposium on Wireless Personal Multimedia Communications (WPMC)*, pp. 424-428, 2014.

- **Ying He**, Eryk Dutkiewicz, Gengfa Fang and Jinglin Shi, "Differential capacity bounds for distributed antenna systems under low SNR conditions", in *Proc. IEEE International Conference on Communications (ICC)*, pp. 5550-5554, 2014.

- **Ying He**, Yongtao Su, Eryk Dutkiewicz, Xiaojing Huang and Jinglin Shi, "An Efficient Implementation of Uplink Baseband Signal Generator in LTE UE Transmitters", in *Proc. International Symposium on Communications and Information Technologies (ISCIT)*, pp. 444-448, 2012.

- **Ying He**, Jian Wang, Yongtao Su, Eryk Dutkiewicz, Xiaojing Huang and Jinglin Shi, "An Efficient Implementation of PRACH Generator in LTE UE

Transmitters", in *Proc. International Wireless Communications and Mobile Computing Conference (IWCMC)*, pp. 2226-2230, 2011.

- Shoujun Huang, Yongtao Su, **Ying He** and Shan Tang, "Joint Time and Frequency Offset Estimation in LTE Downlink", in *Proc. International ICST Conference on Communications and Networking in China*, pp. 394-398, 2012.

- Jisheng Peng, Na Guan, Gang Sun, **Ying He** and Jinglin Shi, "Analysis of diversity order and performance for phase hop diversity in Rayleigh fading channel", in *Proc. IEEE International Conference on Communication Technology and Application*, pp. 621-625, 2009.

Other Publications

- Pierce Rixon, Gengfa Fang, **Ying He**, Huiyang Wang, Markus Mueck, Eryk Dutkiewicz, Michael Heimlich, Beeshanga Abewardana Jayawickrama, Panagiotis Demestichas, Andreas Georgakopoulos, Chapter 6: Licensed Shared Access, in Novel Spectrum Usage Paradigms for 5G, IEEE Technical Committee on Cognitive Networks Special Interest Group Cognitive Radio in 5G, 2014.

Chapter 1

Introduction

To achieve the high capacity requirements of the next generation wireless communications systems, regulatory bodies and operators have been promoting spectrum sharing frameworks. Interference mitigation and resource allocation technologies are the main focus in spectrum sharing research.

This Chapter introduces and provides the background to spectrum sharing from three aspects: 1. The necessity of using and studying spectrum sharing, 2. Limits on other existing technologies and 3. Challenges on solving spectrum sharing problems.

1.1 Background

According to Ericsson's forecast, there will be a massive growth of mobile data traffic for the next five years (2016-2020) [1]. As shown in Figure 1.1, by 2021, there will be 9 billion mobile subscriptions, 7.7 billion mobile broadband subscriptions and 6.3 billion smartphone subscriptions. A similar prediction was drawn in [2]

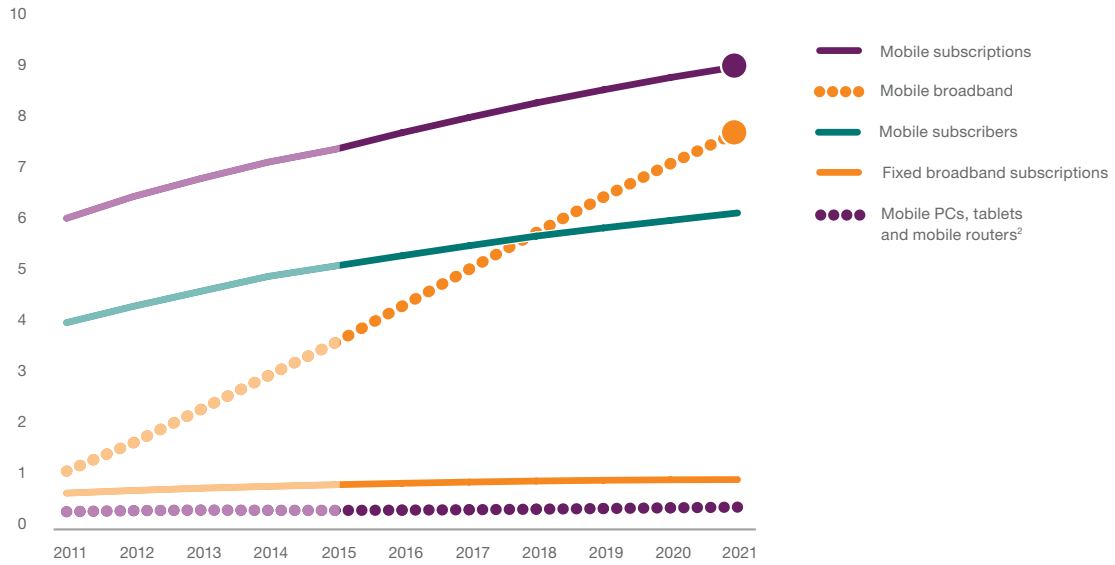

Figure 1.1: Ericsson mobile subscription outlook [1].

In the past few decades, many technologies have been developed and contributed with achieving high capacity in wireless networks. While we are seeking higher diversity in time, frequency, space and code domains, limited spectrum resources have remained a constraint. On our way to the next generation wireless communication [3], i.e. 5G, new approaches for effective utilisation of limited spectrum are needed to break the physical constraint and to help to reach the goal of 5G: 1000 times higher capacity [4] [5]. Shannon has proposed a theoretical capacity bound given as:

$$C = BW \times \log_2\left(1 + \frac{P_t}{I + N}\right) \tag{1.1}$$

where C is the capacity, BW is the bandwidth, P_t is the transmit power, I is the interference power and N is the noise power. Existing technologies without the use of spectrum sharing are targeting at obtaining higher Signal-to-Interference-and-Noise-Ratio (SINR). Four main domains have been explored: time, frequency, space

and code. Media Access Control (MAC) layer methods contribute more in time domain technology by increasing the efficiency and decrease the delay. Physical layer signal processing is more focused on finding diversity and multiplicity in frequency, space and code domains. Orthogonal Frequency-division multiplexing (OFDM) is the current widely used method in 4G Long-Term Evolution (LTE) network and is believed to be able to achieve promising frequency domain gain. Quadrature amplitude modulation (QAM) is able to carry more bits per symbol as it moves towards higher orders i.e 64QAM. However, with the same total transmit power, if the order of QAM increases, the distance between neighbour QAM constellation complex points decreases that will cause worse demodulation performance. Like OFDM, the multiple-input and multiple-output (MIMO) technology has been standardised and applied in 4G LTE and WiFi networks. One of the main features is using orthogonal spatial multipath to transmit and receive signals. Furthermore, beamforming and diversity methods are used to enhance the performance. Recently, massive MIMO, also known as Large-Scale Antenna Systems, has been proposed and has shown potential as being a candidate technology for 5G. However, it is constrained with regards to the applicable scenarios and size of the devices.

Another very timely topic in both research and industry is millimetre wave transmission. By using the higher frequency, the antenna size can be reduced due to that the antenna size is proportional to wavelength. As a result, more antennas can fit in one mobile device which further enables MIMO. All these features propelled millimetre wave transmission to become another candidate for 5G networks. From the spectrum resource perspective, millimetre wave also has the advantage that there are not so many occupants in the millimetre wave frequency bands, also known as the Extremely High Frequency (EHF) range. However, millimetre wave transmission is facing a main problem that due to the short wavelength, wireless signal experiences large fading during transmission. Thus the feasible transmission distance is not long enough for large macro cellular networks. Many efforts have been put on the research to increase the transmission distance using millimetre wave. So far more promising applications are more targeting at short-distance transmission, for example Device-to-Device (D2D) transmission instead of traditional cellular network transmission.

All the above technologies have been effective in increasing SINR. Nevertheless, they cannot compensate for the shortage of spectrum, which corresponds to the BW factor in (1.1).

Recently, regulatory bodies have been promoting spectrum sharing to facilitate this capacity growth. Two prominent spectrum sharing frameworks are 1) Licensed Shared Access (LSA) and 2) Spectrum Access System (SAS). LSA is being developed by European Telecommunications Standards Institute (ETSI) in Europe for the 2.3-3.4 GHz band [6]. SAS focuses on the 3.55-3.7 GHz band in the US, and it is being developed by the FCC [7]. Both schemes open up the access previously restricted to mobile communications bands below 6 GHz. [8] gives a comprehensive and comparative overview of LSA and SAS. [9] provides a review on different interest groups' viewpoint on the SAS architecture.

LSA proposes a two-tier sharing architecture between incumbents and licensees. Mobile Network Operators (MNO) get access to the licensed spectrum when incumbents are absent or not in the same geo-location area. There will be no co-channel interference between incumbents and licensees. In contrast, SAS proposed a three-tier sharing model. Incumbent users represent the highest tier in the framework and receive interference protection from Citizens Broadband Radio Service users. The Citizens Broadband Radio Service itself consists of two tiers - Priority Access and General Authorised Access (GAA) both authorised in any given location and frequency by an SAS. Priority Access Licensees (PALs), defined as an authorisation to use a 10 MHz channel in a single census tract for three years, will be assigned up to 70 MHz of the 3.55 - 3.7 GHz portion of the band. GAA is allowed to use 150 MHz throughout. Priority Access operations receive protection from GAA operations but GAA users will receive no interference protection.

In the cellular networks, there has been growing interest in the area of Cloud Radio Access Network (C-RAN), that has been proposed in [10] and [11], as an efficient and flexible architecture for 5G networks. All signal processing and computing are performed in a central unit, such as a super base station. Previous existing base stations become Remote Antenna Units connected to the central unit through fiber with an RF switch. Since they are geographically separated they can be deployed

as antennas in a Distributed Antenna Systems (DAS) in the cellular network.

By using the C-RAN, power consumption can be decreased and performance can be increased. According to [11], more than 46% of the power consumption is due to air conditioning systems in base stations. Reducing the number of base stations will reduce the number of air conditioning systems making the cellular network more power efficient. Cloud computing and centralised processing solve the cooperation difficulties caused by the large amount of information that needs to be otherwise exchanged between base stations on the backhaul. These features make efficient cooperation and spectrum sharing between cells possible and show potential in improving cell edge user performance.

1.2 Challenge and motivation

ETSI has proposed the LSA framework [6]. In Europe the 2.4 GHz band has been used for digital cameras by journalists and multimedia companies [12]. Digital camera usage is random and unpredictable. The transmission duration of these devices is considered short, as it is limited by the battery life of the camera. However, the propagation characteristics of 2.4 GHz channel is well suited for wireless communications. For example, 2.49 GHz band is defined as Time Division LTE (TD-LTE) band 40 in 3GPP specifications [13] and 2.4 GHz band is defined as one of the two most popular WiFi bands (the other WiFi band is 5 GHz). Thus for more spectrum and better compatibility, LSA framework is proposed to share the 2.4 GHz spectrum. Incumbents (digital cameras), make random use of the frequency band, in terms of location and duration of use. It is difficult for the LSA licensees to keep a high Quality-of-Service (QoS) in the licensed band without a sharing agreement, as they have to quit the spectrum and offload the users every time incumbents come back into the spectrum. VTT in Finland has demonstrated the first LSA trial in 2.3-2.4 GHz [14]. Key features are dynamic detection of incumbents and the shut down of a femto cell base stations or a relative sector of a macro cell base station. LSA has shown the capability of increasing the network capacity. However, controlling the interference from secondary users to incumbents and offloading a large

number of cellular users from the LSA bands are new challenges introduced by the LSA technology.

FCC has proposed the SAS framework [7]. In SAS, incumbents are non-commercial systems, such as the naval shipborne and airborne radars. Unlike the digital cameras (incumbents in LSA), naval radar systems are far away from the MNO base stations on the ground. However the transmit power of SAS incumbents is substantially higher [15]. Similar to many other countries in the world, in the U.S. the population density is higher in the coastal cities, such as San Francisco, New York and Boston, than other area. Therefore, implementing spectrum sharing techniques, such as SAS, is much focused on adding as much capacity as possible in the coastal cities that are closest to the radars. Further in contrast to LSA, SAS divides the secondary users into two tiers: Priority Access Licensees (PAL) and General Authorised Access (GAA). Therefore the interference mitigation in SAS is more challenging.

Other countries around the world will face similar spectrum shortages in the near future. In Australia, the situation is that the non-commercial networks receive interference from the cellular network. For example, it has been found that the LTE signal will cause significant degradation of probability of detection in radars [16]. Thus, spectrum sharing with other feasible bands is a key technology to enable next generation communication systems. This is the motivation of studying the spectrum sharing frameworks in this thesis.

As mentioned in the previous section, C-RAN is a novel centralised cellular network architecture. It is proposed to increase the spectrum efficiency and save the cost. Technologies that have been used in conventional network architectures where base stations are separately located cannot be directly applied to C-RAN. The central unit is connected to multiple remote radio units. The number of remote radio units can be significantly large due to the coverage and density of the next generation wireless communication networks. With the enhancement of MIMO techniques, there are various methods to jointly transmit through multiple antennas. Thus the capacity of multiple connected antennas is a key problem in C-RAN. Moreover, the centralised architecture enables the implementation of efficient spectrum sharing and

coordination algorithms across multiple cells. The coordination between cells can reduce the inter-cell interference (ICI). Therefore, the resource allocation algorithm of spectrum sharing between cells is also an important factor in C-RAN.

In summary, the two aspects in spectrum sharing for the next generation wireless communication that are considered in this thesis are: 1. New problems introduced by using the emerging frameworks LSA and SAS and 2. Enabling spectrum sharing in cellular networks.

1.3 Contributions

The main contribution of this thesis is given as follows:

Chapter 3:

- *Proposed a PAL-GAA co-channel interference mitigation technique that does not expose base station locations.*

  We solve the problem of PAL-GAA co-channel interference which is a mandatory requirement in SAS. We model the census tract with a closed polygon shape. Multiple PALs and GAAs are considered. We propose to use exclusion zones to protect the PALs. The distribution and number of transmitters of GAAs are shared with the PAL network and the exclusion zone size of PALs is shared with the GAA network. Despite the sharing of this information, neither network can locate the base stations of the other network.

- *Analytically deriving the distribution of the distance from a GAA transmitter to a PAL receiver.*

  The distribution of the distance from a uniformly distributed GAA transmitter to a PAL receiver is derived. The analysis considers multiple PALs and the overlapping of the PAL exclusion zone. The distribution is based on the exact shape and locations of the census tract and the PAL exclusion zones.

- *Analytically deriving the aggregate interference from multiple GAA transmitters to a PAL receiver using the Characteristic Function.*

The distribution of the aggregate interference using the Probability Density Function and the Characteristic Function is derived. Instead of using the Moment Generating Function, we propose the use of the Characteristic Function as a new method which is simpler to implement.

- *Proposed a numerical approximation using Inverse Fast Fourier and Discrete Fourier Transforms*

  Inverse Discrete Fourier Transform (IDFT) and Discrete Fourier Transform (DFT) are used to implement the calculation of the distribution of the aggregate interference. The IDFT is further simplified into groups of smaller size Inverse Fast Fourier Transform (IFFT) to further decrease the computational complexity.

- *Found a lower bound for the optimisation problem for the exclusion zone size and analytically proved the convexity of the problem.*

  We formulate the exclusion zone size design as an optimisation problem. We derive a lower bound for the problem by tightening the constraints. The convexity of the lower bound is analytically proved so that optimisation tools can be used to obtain the solution. Our approach reduces the exclusion zone size by over 40%, which gives significantly more spectral opportunities to GAA in the spatial domain.

The work in Chapter 3 has been submitted as a journal paper "Priority Access and General Authorised Access Interference Mitigation in Spectrum Access System" and provisionally filed as a patent "SAS PAL GAA co-channel interference mitigation".

Chapter 4:

- *Proposed an interference measurement and user selection method for secondary users' access to the incumbent bands.*

  We propose to use the secondary users close to the incumbent area to measure the interference from the secondary network. We also propose a method to select users for uplink transmission. Compared to the random uplink user

selection method, our approach can achieve higher capacity and lower interference. When the incumbent is not sharing any information, our method effectively manages the interference within the secondary network which is a mandatory requirement in LSA and SAS. This work has been filed as a patent "Uplink Interference Management in Shared Spectrum Networks".

- *Proposed an efficient PAL detection method using sub-sampling.*

  We propose a novel detection method for GAA users to sense the PAL activities, which is a mandatory requirement in SAS, before GAA users access the PAL bands. Using our approach, the GAA users can detect multiple PALs and identify their Primary Synchronisation Sequence indices simultaneously. This work has been filed as a patent "Methods and Devices for User Detection in Spectrum Sharing".

- *Proposed a coexistence method for WiFi and LTE in the unlicensed band.*

  We propose to use unlicensed bands to offload the secondary users that have to quit the licensed band due to incumbents reclaiming of the spectrum. Our approach guarantees the fairness and avoids collisions between WiFi and LTE. The offloading solution prevents capacity drops when secondary users lose access to the licensed band. This work has been filed as a patent "Communication Device and Method for Communicating using a Frequency Range".

Chapter 5:

- *Analytically deriving closed-form upper and lower bounds in efficiently computable expressions for differential capacity of the Cloud Radio Access Networks.*

  The moment generating function (MGF) of SNR is used in the analysis. Bounds accuracy is evaluated and compared to results in the current literature. Numerical results corroborate our analysis and the analytic bounds on DCAP are tight in the low SNR regime. This work has been published as a conference paper "Differential capacity bounds for distributed antenna systems under low SNR conditions".

- *Analysed the capacity between MU-MIMO and SU-MISO in the Cloud Radio Access Networks.*

  Thorough comparisons on the performance are given between MU-MIMO and SU-MISO in terms of capacity CDF, costs and constraints. This work has been published as a conference paper "Downlink capacity in cloud radio access networks with fractional frequency reuse".

- *Analysed the capacity of the Cloud Radio Access Networks using Licensed Shared Access.*

  The LSA concept is leveraged in the Cloud Radio Access Networks. To the best of our knowledge, our analysis is the first considering C-RAN capacity in the context of LSA. This work has been published as a conference paper "Licensed Shared Access in distributed antenna systems enabling network virtualization".

Chapter 6:

- *Analytically found the optimum frequency division number for the resource allocation in the Cloud Radio Access Networks.*

  We model the optimisation problem using Multiset and obtain the optimum frequency division number for the resource allocation. This work has been published as a conference paper "Fractional Frequency Reuse in Distributed Antenna Systems in Cloud Radio Access Networks"

- *Analytically derived a novel threshold for the transmitting SNR to decide whether or not to use Coordinated Joint Transmission in FFR aided C-RAN.*

  We found that the SNR condition has an important impact on the Cloud Radio Access Networks, that the performance of coordination is not always better than non-coordination. We derive a new threshold for the transmitting SNR to decide whether to use coordination. This work has been published as a conference paper "SNR Threshold for Distributed Antenna Systems in Cloud Radio Access Networks"

1.4 Organisation of the thesis

This chapter introduces the background of the thesis. The rest of the thesis is organised as follows:

In Chapter 2, we summarise the key concepts, frameworks and methods in aspects of importance, relevance and quality. Section 2.1 gives an overview of Cognitive Radio. Section 2.2 includes spectrum sharing in the context of Cognitive Radio: LSA and SAS. The importance of spectrum sharing in next generation wireless communication is highlighted. Section 2.3 includes spectrum sharing in the domain of operators' network: C-RAN, DAS, FFR and CoMP. The principle of selection is established in this section. The limitations are addressed that lead to the motivation of the work in next chapters.

In Chapter 3, we propose a PAL-GAA co-channel interference mitigation technique that does not expose base station locations. We show how PAL can derive the distribution of the distance from a GAA transmitter to a PAL receiver in Section 3.2. The distribution of the aggregate interference using Probability Density Function and Characteristic Function is derived in Section 3.3. We also propose a numerical approximation using Inverse Fast Fourier and Discrete Fourier Transforms in Section 3.4. Additionally we formulate an optimisation problem for the optimal exclusion zone size in Section 3.5 . We analytically prove convexity of the problem.

In Chapter 4, we propose the spectrum access and coexistence methods for different tier users in LSA and SAS. The access of all the secondary users, such as LSA licensees, PAL and GAA in SAS, to the incumbents' bands is discussed in Section 4.1. GAA users sensing the PAL bands in SAS is discussed in Section 4.2. When the higher tier users, such as incumbents or PAL users reclaim their bands back, the lower tier users, such as secondary users or GAA users have to quit the bands and offload their users to other bands. We propose WiFi and LTE coexistence for the offloading in Section 4.3.

In Chapter 5, we study the capacity performance of Cloud Radio Access Networks (C-RAN) and introduce Coordinated Multi-Point (CoMP) and Fractional Frequency Reuse (FFR) to further enhance the coordination and mitigate the in-

terference. The system model is given in Section 5.1. The differential capacity of C-RAN with multiple coordinated antennas is analysed in Section 5.2. Multiple-Input-Multiple-Output (MIMO) techniques are introduced to the system and the performance is analysed in Section 5.3. The capacity of C-RAN with LSA is discussed in Section 5.4.

In Chapter 6, we investigate the resource allocation optimisation and SNR threshold in C-RAN. An optimum way to allocate resources in C-RAN with Fractional Frequency Reuse in order to maximise the capacity is proposed in Section 6.1. We modelled the optimisation problem using Multiset and found the optimum frequency division number for the resource allocation. We also found that the SNR condition has an important impact on the coordination performance. A new threshold for the transmitting SNR, to decide whether or not, to use Coordinated Joint Transmission in FFR aided C-RAN is derived in Section 6.2.

In Chapter 7, this thesis is concluded and future work is foreseen.

1.5 Summary

In this chapter, we introduced the background of spectrum sharing, the challenges and motivation of this thesis. Moreover, we summarised the contributions and organisation of this thesis. In the next chapter, we will present the literature review of the related work of spectrum sharing based on the background.

Chapter 2

Literature Review

Based on the background of spectrum sharing, this chapter summarises the key concepts, frameworks and methods in aspects of importance, relevance and quality. Section 2.1 gives an overview of Cognitive Radio. Section 2.2 includes spectrum sharing in the context of Cognitive Radio: LSA and SAS. The importance of spectrum sharing in the next generation wireless communications is highlighted. Section 2.3 includes spectrum sharing in the domain of the operators' network: C-RAN, DAS, FFR and CoMP. The principle of selection is established in this section. The limitations and improvements are addressed, which lead to the motivation of the work in the next chapters.

2.1 Cognitive Radio

Early stages of Cognitive Radio

The concept of Cognitive Radio was first introduced by Prof. Joseph Mitola III in [17] in 1999. Personalised devices will learn and understand the network's radio environment, user requirements and applications etc. Then they will make decisions about access and communication. The cognition cycle is supported by software defined radio to achieve the flexibility in the domain of time, space and frequency. FCC has defined Cognitive Radio as [18]:

"*Cognitive radio: A radio or system that senses its operational electromagnetic environment and can dynamically and autonomously adjust its radio operating parameters to modify system operation, such as maximise throughput, mitigate interference, facilitate interoperability, access secondary markets.*"

Cognitive radio enables dynamic spectrum access. Cognitive radio users can sense and capture a window to access a temporary vacant spectrum and control the interference to the other users in the band. Normally, the spectrum is allocated to incumbents, also called primary users who have a higher priority on using the band. Cognitive radio users are also called secondary users.

Standardisation of Cognitive Radio

The first Cognitive Radio network standard is IEEE 802.22 [19] which operates the Orthogonal Frequency Division Multiple Access (OFDMA) in the TV White space. Dynamic spectrum access is used in the coexistence of secondary users. Spectrum sensing management, geo-location management, incumbent database query and channel management are used in coexistence between primary and secondary users [20]. 802.11 af enabled WiFi to run in the TV White space [21]. Similar to 802.11 af, ECMA 392 defined a high speed video streaming and an internet access to TV white space [22]. To solve the coexistence problem between different networks, IEEE released the IEEE 802.19.1 standard in 2014 [23], [24]. However, the TV white space uses opportunistic access that cannot guarantee Quality-of-Service (QoS) for cellular network communication. Moreover, before the commercialisation of 4G,

the spectrum allocated to operators can fulfil the requirement of cellular network bandwidth. Thus in the past decade, operators have not been fully convinced by Cognitive Radio. However, with the boost of capacity requirements in 4G and the foreseen capacity requirements for 5G, operators have to seek additional spectrum. Cognitive Radio and spectrum sharing are believed to be an important research area in order to develop 5G [25], [9].

Research interests in Cognitive Radio

Research interests in Cognitive Radio are divided into three aspects: radio knowledge analysis, channel estimation and prediction as well as power and resource allocation [26]. Radio knowledge analysis includes radio knowledge collecting and processing. Spectrum sensing is a key component in the radio knowledge analysis field [27]. Typical spectrum sensing techniques are: energy detection, waveform-based sensing, cyclostationarity-based sensing, radio identification based sensing and matched-filtering. Through spectrum sensing, users can identify opportunities in different dimensions and develop algorithms based on the historical information. Main merits on the performance of spectrum sensing are the probability of detection and the probability of false alarm. Main constraints on the methods of spectrum sensing are sensing scheduling [28] [29], complexity [30] and adaptivity [31]. Spectrum sharing involves physical layer signal processing algorithms [32] and also MAC layer protocol designs [33].

Most previous Cognitive Radio studies are more focused on spectrum sensing. However, in the next generation wireless communication networks, interference between different tiers of users using cognitive radio and resource allocation are major issues. With privacy considerations, users in different tiers or different operators' networks do not want to share their location information. Therefore the interference and resource allocation issues in the new spectrum sharing frameworks cannot be solved by conventional interference mitigation methods.

2.2 Spectrum sharing frameworks

2.2.1 Licensed Shared Access

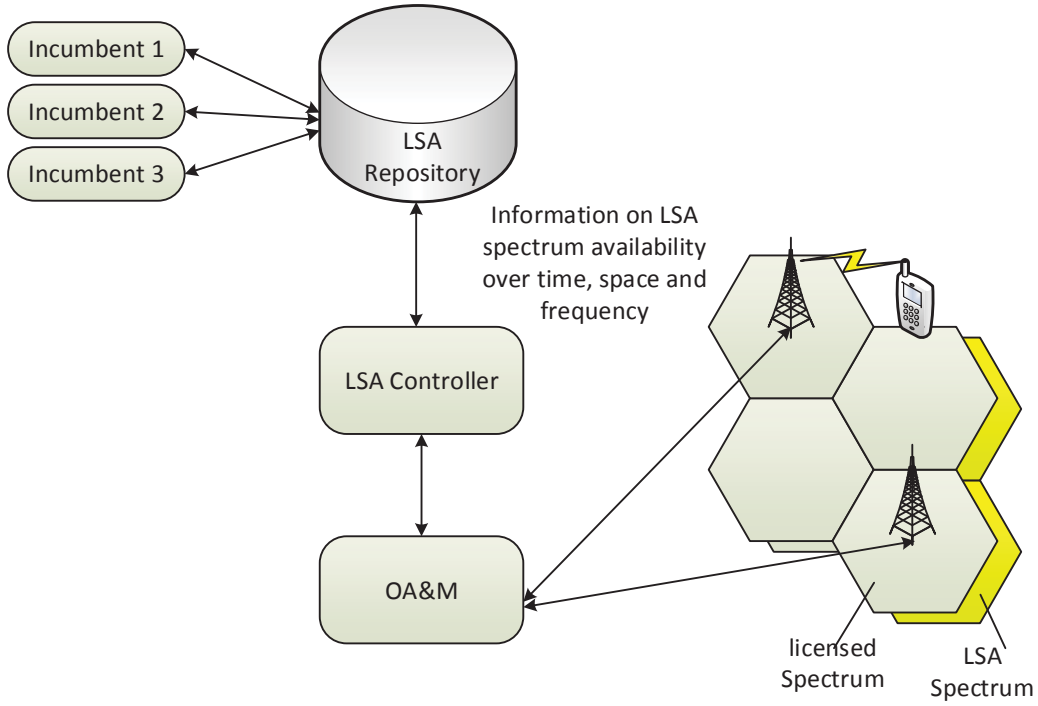

Figure 2.1: Licensed Shared Access architecture.

In order to enable spectrum sharing technologies in the next generation wireless communication systems, the European Telecommunications Standards Institute (ETSI) Reconfigurable Radio Systems Technical Standardisation Committee has proposed a new framework - Licensed Shared Access (LSA) [6]. LSA is a spectrum sharing framework to meet short-term to mid-term industry needs with a quasi-static allocation of shared spectrum to cellular operators. It allows a LSA licensee (i.e. a mobile network operator (MNO)) to access the spectrum that has already been allocated to an incumbent. During the sharing time, location or frequency that incumbents are absent, LSA licensees have full access to the LSA band under certain power and interference requirements [6]. Unlicensed users cannot access LSA bands. Therefore the quasi-static licensing agreement guarantees the QoS in a LSA licensee network. This is a major difference in comparison to the traditional cognitive radio

approaches such as IEEE 802.22, IEEE 802.11 af, IEEE 802.19.1 and ECMA 392. Those networks that allow access to TV white space on an unlicensed basis cannot guarantee the QoS.

The LSA architecture is shown in Figure. 2.1. The LSA system consists of a repository (LSA Repository) and a controller (LSA Controller). The repository has direct connections with the controller and incumbents. One typical implementation of a LSA repository is a database. The LSA repository stores information including the incumbents' spectral usage from a geographical, temporal and frequency point of view. The LSA controller reads information from LSA repository for calculation and decision making. It is also assumed, that the LSA system, in particular the controller and repository will be owned and maintained by a third party to ensure compliance of agreements between both the MNOs and incumbents within the framework.

The LSA repository will notify the LSA controller of any changes to the sharing agreements. This information is defined as LSA Spectrum Resource Availability Information [34]. The LSA controller will use the information from the repository and communicate with the respective MNO to ensure proper transmission and compliance of the agreement. The MNO can only access the secondary spectrum after it is granted by the controller, this is to make sure that the MNO does not interfere with incumbents. Therefore, the MNO is granted access to additional spectrum which increases its network capacity. This is further analysed in Section 5.4.

The current licensing agreement is suggested to cover the period in the order of years. This gives MNOs enough confidence on a relatively stable QoS level. However, a long-term agreement is not flexible enough for dynamic usage or more MNOs' requirements. It is expected in future releases of LSA design, that the agreement period will be reduced. Eventually, the LSA framework should be able to provide dynamic, short-term agreement as well as QoS guaranteed licensed shared access. To achieve the QoS target under a short-term agreement, the LSA system needs to adapt to the changes of availability of spectrum. When incumbents reclaim the LSA bands back, the LSA system needs to have a solution to offload the mobile network users to other bands in order to keep their connections. This is another major difference with conventional cognitive radio networks where secondary users

have to completely drop their connections when incumbents return. We propose to offload LSA users with LTE and WiFi coexistence. This is further discussed in Section 4.3.

Spectrum sharing in the LSA framework is binary. Either incumbents or LSA licensees can access one band at one location at one time. Therefore, spectrum is shared in two dimensions [6]:

- incumbents and LSA licensees use the same spectrum at the same time but at different locations. For example, if incumbents are digital cameras, they will be active in certain areas. LSA licensees can use the same spectrum in other areas, where there are no incumbents or from where they cause no interference to incumbents.

- incumbents and LSA licensees use the same spectrum at the same locations in time division. For example, the LSA agreement signed between incumbents and LSA licensees will indicate the period when incumbents are absent, so LSA licensees can use the spectrum. However, when incumbents come back, LSA licensees have to leave the spectrum.

In the first scenario, incumbents and LSA licensees can share the same spectrum at different locations. Thus LSA licensees may cause interference to incumbents not at the same location, but possibly nearby. Thus [35] has defined a geo-location area limitation for LSA licensees as follows:

- exclusion zone: area where LSA licensees are not allowed to transmit.

- restriction zone: geographical area within which LSA Licensees are allowed to operate radio transmitters, under certain restrictive conditions. For example, transmit power per antenna has to be below a certain threshold.

- protection zone: geographical area within which incumbent receivers will not be subject to harmful interference caused by LSA licensees' transmissions. For example, aggregate interference from LSA licensees to the incumbent receivers has to be below a certain threshold. The aggregate interference can be measured by sensing nodes. For the secondary users' downlink transmission, it

is easy to control the aggregate interference. Because transmitters are base stations, they can calculate the aggregate interference to incumbents. For the uplink transmission, transmitters are user equipments (UEs), and there will be random access transmission. Thus measurement from sensor nodes is necessary. This will be further discussed in Section 4.1.

In the second scenario, secondary users share the same spectrum at the same location but at different times. Therefore, when incumbents reclaim the spectrum, secondary users have to quit the bands. To keep the connections for secondary users, alternative bands have to be available for traffic offloading. Unlicensed bands are one of the potential candidates for offloading.

LTE and WiFi are the main transmission schemes used in the 4G and 5G cellular networks. LTE has some features that can integrate the LSA implementation. The LTE resource allocation unit is a resource block which contains 12 subcarriers and each subcarrier's bandwidth is 15 kHz. If the available spectrum is not a continuous band and the number of users increases but the bandwidth requirement from the users is not high, e.g. voice service or machine type communication, current LTE resource allocation can directly use the spectrum. If the users' bandwidth requirements also increase, e.g. many users are requesting services such as video downloading that consume large bandwidth, LTE-Advanced provides the carrier aggregation function which can assemble separate frequency resources together for single stream transmission. A constraint for using carrier aggregation, is that the aggregated frequency range has to satisfy the existing RF capability. LSA can leverage this carrier aggregation functionality that is already built in to the LTE standard to provide additional LSA spectrum to the MNO without significant modification to existing base station deployments. WiFi provides cellular network users with a complementary service to the MNOs existing infrastructure, enabling more coverage and higher density. The users access the WiFi networks provided by MNOs using their cellular network identifiers and the MNO can appropriately deliver the service that the users' rate plan entitles them. Both LTE and WiFi are possible transmission schemes for LSA networks and they are going to be active at the same time in the same network due to various device types. Therefore, the study on coexistence

of LTE and WiFi is necessary.

Current User Equipment (UEs), are built with both LTE and WiFi components. As UE manufacturers are different, and the components are highly integrated, e.g. baseband chips and RF front ends, it will be difficult to implement the coexistance between LTE and WiFi in the lower layers. In contrast, the coexistence can be implemented in the higher layers. For example, for the downlink transmission, one possible scheme is to change the software in the application layer, to schedule and decompose packets in the application layer of the base station then recover and combine the packets in the application layer of the UE. This requires a constraint that the base station transmits LTE and WiFi at the same time. However, this scenario only applies in cases where the LTE and WiFi networks are owned by the same MNO.

For LSA, the spectrum from the incumbent may become available by chance. The current potential frequency band, which can be used for LTE and WiFi transmission is 2.3-2.4 GHz. Coexistence of LTE and WiFi gives the MNO more choices in LSA. MNOs will, however, incur an extra cost in the computation for scheduling, resource allocation, optimisation and decision making for LTE and WiFi data streams. Also, a coexistence scheme needs to be designed to meet backward compatibility. The scheme should be able to switch to single transmission, LTE or WiFi, according to the user's application version, QoS requirement or channel quality.

Current mainstream technologies related to the coexistence of LTE and WiFi in the unlicensed band are LTE-U and LTE-LAA. LTE-U, is proposed by a group of industrial companies in the LTE-U Forum [36]. LTE-U uses Supplementary Downlink (SDL) and Carrier Aggregation (CA) techniques in LTE to combine the transmission of the cellular network band and the unlicensed band. LTE-LAA is standardised by 3GPP in [37]. LTE-LAA is a global framework solution for LTE operation in the unlicensed band. LTE-LAA includes both uplink and downlink. Most of the related work uses Listen-Before-Talk (LBT) techniques to avoid collisions. [38] studied the performance of LTE and WiFi coexistence in the unlicensed band with different MAC protocols.

In summary, LTE and WiFi coexistence is important in the licensed and unli-

censed bands. This is further discussed in Section 4.3.

2.2.2 Spectrum Access System

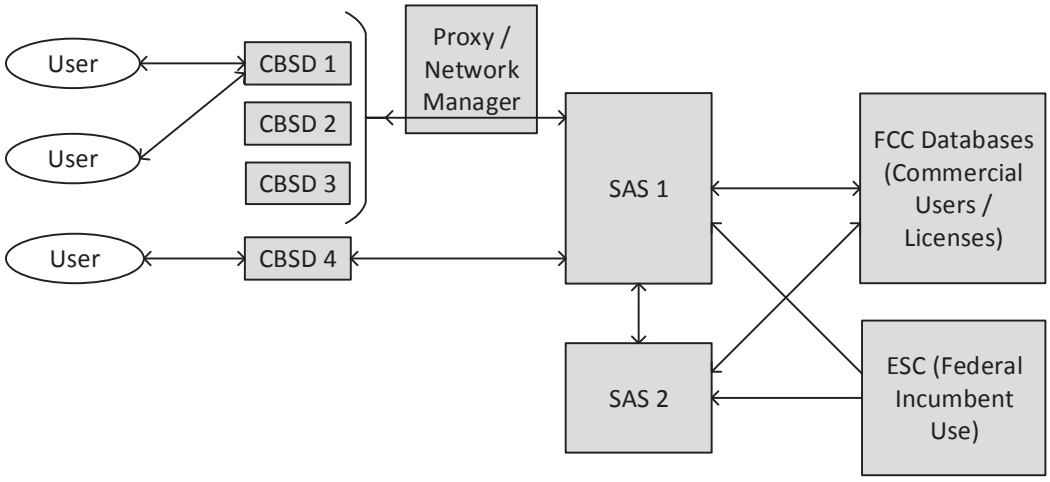

Figure 2.2: Spectrum Access System architecture.

Based on a Notice of Inquiry (NOI) and a Notice of Proposed Rulemaking (NPRM), the FCC released the Report and Order to the Citizen's Broadband Radio Service (CBRS) 3.55 - 3.7 GHz band in April 2015 [7], in which, FCC defines a spectrum access system and its architecture, function and regulations. In a released follow up document [39], the FCC adjusted some regulation items for secondary users, the interference protection area and Fixed Satellite Systems (FSS) incumbents protection.

FCC defines a three-tier model. This is different from the two-tier model in LSA. In SAS, the incumbent users represent the highest tier in the framework and receive interference protection from the CBRS users. The CBRS consists of two tiers - Priority Access and General Authorised Access (GAA), both authorised in any given location and frequency by a SAS. Priority Access Licensees (PALs), defined as an authorisation to use a 10 MHz channel in a single census tract for three years, will be assigned in up to 70 MHz of the 3.55 - 3.7 GHz portion of the band. A census tract is defined as a statistical subdivision of a county or equivalent entity. GAA is

allowed to use 150 MHz throughout. Priority Access operations receive protection from GAA operations, but GAA users will receive no interference protection.

The architecture of SAS is shown in Figure 2.2. It differs from LSA in that only the geo-location area limitation is defined. SAS is implemented in such a way that it protects incumbents by geo-location area limitation and interference measurements, and is divided into two phases:

- In phase one, SAS can access the spectrum outside of exclusion zones. The CBRS licensees will be permitted to deploy and utilise Category A Citizens Broadband Radio Service Device (CBSD)s in the 3550-3650 MHz band [7]. The exclusion zone is measured and defined by National Telecommunications and Information Administration (NTIA) in [40]. The exclusion zone will ensure that the aggregate interference from SAS outside is below a certain threshold. The threshold is defined in [40] as 6 dB below the noise floor. One illustration of the exclusion zone is shown in Figure 2.3. One typical average exclusion zone distance is 135 km in the east coast of U.S to protect the shipborne radars. In phase one, SAS gets access to a large area inland, yet some big cities along the coast such as New York and Boston are excluded from transmission. Thus the FCC defined phase two to further increase the coverage in the coast area.

- In phase two, exclusion zones will be turned into protection zones. Environmental Sensing Capability (ESC) is used to sense the spectrum availability in the protection zones and inform SAS when the band is vacant. ESC can be a network of sensors and it is a third party stand between SAS and incumbents. CBRS operations in the 3550-3650 MHz band will be permitted within protection zones, including major coastal cities, except when the ESC reports that incumbents are active in the area. Availability of an ESC will also allow use of Category B CBSDs in the 3550-3650 MHz band portion, provided that the relevant system parameters required to protect federal incumbent user operations at these higher levels are determined and implemented through the ESC approval process [7].

In contrast to LSA, the FCC divides secondary users in SAS into two tiers:

Figure 2.3: Shipborne radar exclusion zone for the lower 48 states (yellow line represents the fast track exclusion zone and blue line represents the revised exclusion zone).

PAL and GAA. GAA users can only access the spectrum when there are no PAL activities. Before transmitting, GAA users have to make sure the band is clear to transmit. The incumbent usage will be informed. However, the usage of PAL users are not directly informed and the transmit power may not be high enough to be detected by a simple method, e.g. energy detection. There are 7 channels, each with a 10 MHz bandwidth. If neither incumbent users nor PAL users are using the channel, GAA users can use the channel for general access purposes. GAA users will know if any channel is assigned to PAL users, but they need to determine whether the PAL users are currently using the channel, given that incumbents are not using the channel at the same time. To achieve more accurate detection results, we proposed to use certain features in the PAL signals for the detection instead of energy detection. We assume the PAL users are LTE base stations. One typical feature of LTE downlink signals is the Primary Synchronisation Sequence (PSS). It

is allocated in the third OFDM symbol of subframe 1 and subframe 6. The PSS is generated from a Zadoff-Chu (ZC) sequence with index 25, 29 and 34 for the base 63. Zadoff-Chu sequence is widely used in LTE specifications for reference and pilot signals. It satisfies a Constant Amplitude Zero Autocorrelation (CAZAC) property. ZC sequences of any length have an "ideal" cyclic autocorrelation (i.e. the correlation with its circularly shifted version is a delta function). Moreover, the absolute value of the cyclic cross-correlation function between any two ZC sequences is constant [41]. We propose to use PSS in LTE as the characterisation sequence for the detection. This is further discussed in Section 4.2.

PAL and GAA can be connected to the same or different SAS. Therefore, there are intra-SAS and inter-SAS interference between secondary users. The intra-SAS interference can be managed by resource allocation optimisation. SAS knows the locations and transmit power of all base stations connected to it. The inter-SAS interference needs advanced mitigation techniques, so it is the main focus in this thesis. One of the main interference requirements is from other secondary users to PAL users, since GAA users receive no interference protection. The constraint on the interference from other secondary users to a PAL is defined as:

- aggregate interference from co-channel and adjacent channel to a PAL user has to be below -40dBm. The detail of this requirement is as follows [7]:

  "*Priority Access Licensees must accept adjacent channel and in-band blocking interference (emissions from other authorised Priority Access or GAA CBSDs transmitting between 3550 and 3700 MHz) up to a power spectral density level not to exceed -40 dBm in any direction with greater than 99% probability when integrated over a 10 megahertz reference bandwidth, with the measurement antenna placed at a height of 1.5 meters above ground level, unless the affected Priority Access Licensees agree to an alternative limit and communicates that to the SAS.*"

We consider co-channel interference as the main contributor to the aggregate interference, and assume the adjacent channel interference can be neglected. There can be multiple GAA transmitters and multiple PAL receivers in the same census

tract. One possible way to control the interference is that the PAL network estimates the aggregate interference using the location information of the GAA transmitters. The interference can be controlled below a certain threshold by adjusting the transmit power of each GAA with either a binary decision or an optimised power level. The Radio Environment Maps [42] method can be used in such a scenario. However, this method is only applicable when the PAL/GAA network has precise information about the locations of the other network's base stations.

In a practical scenario, if the GAA transmitters and the PAL receivers belong to the same operator, the location information is known to all, since each PAL/GAA is obliged to regularly report about its location to the corresponding SAS [7]. However, if the GAA transmitters and the PAL receivers belong to different operators, the location information is not necessarily known. The locations of the base stations are regarded as private information by operators. The operators in the U.S. have taken a strong stance against sharing the site locations with all SAS users (including competitors) to a degree that they would opt out from using SAS if that was an obligation. One option would be for PAL to conservatively assign a large exclusion zone outside which GAA can be located anywhere, such that the interference constraints are met. However, such a conservative approach will result in a large decrease in the spectral opportunities of the GAA network in the spatial domain.

Previous studies on cognitive radio networks regarding aggregate interference are related to this topic. Some studies assumed Poisson Point Process (PPP) as the distribution of the users. [43] studied the aggregate interference from secondary users to a primary user by deriving the Moment Generating Function (MGF) and cumulants in a finite disk area. [44] studied the aggregate interference from secondary users to primary users in cognitive radio networks with exclusion zones around primary users and proposed approximations based on the Poisson cluster process. [45] analysed the aggregate interference in an underlay network of cognitive radio with Rayleigh fading and exponential path loss. [46] derived the results of the higher order moments of the Signal-to-Interference-plus-Noise Ratio (SINR) using the MGF and showed the existence of a tradeoff between the average SINR and rate performance in cellular networks. Some other studies assumed a uniform distribution for the

users. [47] considered that an independent and uniform distribution is more suitable for the cognitive radio network scenario and proposed to use a finite arbitrarily-shaped model for the network. [47] also introduced a numerical approximation of the Laplace transformation to perform the MGF. [48] studied secondary user activity protocols' effects on the performance of underlay cognitive radio networks. Both [47] and [48] are based on the distance distribution calculation in a finite area proposed in [49].

In the SAS scenario, a census tract is a closed area with possibly an irregular shape. The performance, such as network capacity, should depend on the physical boundary of the census tract. Thus we believe a finite arbitrarily-shaped model is more suitable for a census tract than a disk. Moreover, we adopt the assumption in [47] that the location of users follow an independent and uniform distribution. All the above papers used the MGF to derive the distribution of aggregate interference from the distribution of the interference from a single user. The Laplace transform used to perform the MGF has high computational complexity and it is difficult to implement. Furthermore, the previous related studies focused on one receiver scenario. However, in the SAS framework, there will be multiple PAL base stations in a census tract and we need to keep interference to all of them below the threshold.

A few recent studies are also based on using exclusion zones to protect primary users (i.e. incumbents) from secondary users (i.e. LSA/SAS licensees). Several methods are based on measurement and monitoring of interference. [40] provides the assumptions, methods and analyses of how to design exclusion zones in the 3.5 GHz band. [50] mentioned dynamically monitoring the activity of incumbents and informing secondary users. Other methods are based on distribution features of interference. [51] studied the optimal deployment of secondary users. [52] proposed and compared three exclusion zone designs and Media Access Control (MAC) protocols accordingly. [53] studied interference from secondary users to incumbents in SAS. [53] proposed a multi-tier exclusion zone design to improve the spectrum efficiency. [54] proposed a dynamic exclusion zone design in SAS to protect incumbents from secondary users by dividing a disk area into several annular sectors and provided aggregate interference distribution with an approximation. Both [53] and [54]

used annular sectors with the incumbent at the centre. The practical network deployment area is difficult to model with annular sectors, since it can be a finite area of any shape. Moreover, we can directly calculate the Probability Density Function (PDF) of the aggregate interference instead of using an approximation in Section 3.3.

There is so far no suitable solution for the aggregate interference mitigation between PAL (i.e. second-tier) and GAA (i.e. third-tier) in SAS. Therefore, it is important to develop a generic framework to find the smallest possible exclusion zones that guarantee interference protection to PAL, without exchanging the location information. This is the motivation of the work in Chapter 3.

2.3 Enabling spectrum sharing in cellular networks

2.3.1 Cloud Radio Access Network

The Cloud Radio Access Network (C-RAN), proposed in [10] and [11], has become a technology of great interest due to its efficiency and flexibility for future cellular networks. In C-RAN architecture, all signal processing and computing is performed in a central unit, such as a super base station. Conventionally deployed base stations become remote antenna units connected to the central unit through fiber with an RF switch. Since they are geographically separated they can be employed as antennas in the cellular network. C-RAN is supported by operators as it removes the distributed processing units which consume high amounts of electricity by powering the air-conditioning. According to [11], more than 46% of the power is used by the air-conditioners. The decreased number of base stations would reduce the number of air-conditioning units, making cellular networks more environmentally friendly. C-RAN also enables better cooperation between cells than conventional separately deployed base stations since all processing happens physically in one central unit.

C-RAN is regarded as one of the key enabling technologies for 5G. [55] proposed a user-centric architecture for 5G communication by repartitioning and redefining the function of the base stations in C-RAN. C-RAN is further enhanced by software-

defined air interface to achieve flexibility in frame structure, waveform, duplex mode, access mode and MIMO transmission. [56] also proposed that in 5G the conventional cell-centric architecture should evolve into a device-centric one. The C-RAN and CoMP technologies are an important trend and support for this evolution. [57] discussed the requirements and demands in 5G and how ultra-dense deployment and C-RAN are the two key enablers. By adding software functionality to C-RAN, the network will be turned into a service provider. Simulation results showed that a centralised architecture has higher average throughput. [58] summarised state of the art studies about C-RAN, including the advantages, key technologies and challenges. CoMP Joint transmission and Coordinated Beamforming are mentioned to be the technologies that can solve inter-cell interference and increase capacity. [59] proposed the heterogeneous cloud radio access networks (H-CRANs). Multiple base stations coordination results were given. The conclusion is that the increment in capacity, decreases with the number of cooperating base stations. [59] also summarised the potential of using the cloud-computing-based CoMP and resource management in C-RAN. However, no analytical work was given.

To analyse the capacity of C-RAN, we propose to use the Distributed Antenna System (DAS) to model the physical layer of C-RAN. The system model is presented in Section 5.1. A DAS is considered to be one of the mainstream technologies for the next generation wireless communication, especially for the cell edge users in cellular networks. The seminal work on DAS was presented in [60] and applications were used to improve the coverage of the indoor cellular networks and to reduce the outage without building extra base stations. Subsequently the concept was introduced into the cellular network by deploying multiple antennas in different sectors to improve performance within one cell [61].

By enabling C-RAN, the power consumption decreases while the performance increases. As proposed in [62], [63] and [64], most of the previous publications have explored the DAS Ergodic Capacity within only one cell with one central unit in the cell centre and symmetric distributed antennas in every sector of the cell. In [62], the number of antennas is up to 7, with one in the centre of the cell and 6 in each centre of a sector. However, for the C-RAN scenario, the number of

antennas could be far more than that and the distance between antennas would also be larger. [65], [66] and [67] discussed the antenna numbers, deployment and selection. Moreover, DAS shows potential in improving cell edge users' performance. [68] compared the performance between traditional microcellular system and DAS with frequency reuse. The capacity measurement and scaling have been obtained in [69]. [70] studied virtual MIMO performance in DAS with large-scale channel state information given and proposed an iterative algorithm to achieve the capacity and coverage. The DAS scenario used in [70] covers multiple cells in which each cell has a central processing unit with several remote radio heads separately distributed inside the cell. However, in the C-RAN, each cell has one remote radio head and multiple cells connect to one central processing unit. Other related works considered a large-scale DAS with a very large number of distributed antennas, possibly up to a few hundred antennas. [71] proposed a channel-gain-based antenna selection (AS) method and an interference-based user clustering (UC) method. MU-MIMO precoding and power control were used in [71] to achieve better energy efficiency. [72] used a similar large-scale DAS model as [71] by grouping the antennas into clusters to serve a group of users in cooperation. [72] optimised the cluster size to obtain the maximum capacity with imperfect channel information and inter-cluster interference. Yet, these papers consider system performance including cell boundaries' capacity under high SNR (17 to 20 dB), which may not be the most suitable case, because boundaries normally have low SNR values. For example, the Long-Term Evolution (LTE) standard specified by the Third Generation Partnership Project (3GPP), in which, the system SNR for cell edge users is much lower (-30 to 0 dB) [73] [74].

Therefore, how cooperative communication can increase the capacity of C-RAN for the cell edge users under low SNR values has not been fully investigated. C-RAN provides the platform for multiple cell cooperation. To what extent should the cooperation be is the problem we need to consider. We study the capacity of C-RAN cell edge users in Section 5.2. Different from the above mentioned papers that consider the downlink capacity, we analyse the Differential Capacity (DCAP) which represents the benefit on the capacity from increasing the number of cooperative

cells. With the increase of the number of cooperative cells, the overall capacity will increase, however the differential capacity will decrease. In comparison with the work in [69], we derived a pair of closed-form upper bound and lower bound of DCAP using the MGF under low SNR which is more suitable for cell boundaries. Whereas the upper bound in [69] is designed for high SNR values only. In addition, our upper bound performs tighter than the upper bound in [69] and better under the 3GPP specified LTE channel model.

2.3.2 Fractional Frequency Reuse and Coordinated Multi-Point

To further boost the capacity of C-RAN, we study the enhancement of C-RAN by using spectrum sharing techniques: Coordinated Multi-point (CoMP) and Fractional Frequency Reuse (FFR). These two technologies were proposed before the proposal of C-RAN. Compared to conventional cellular networks, C-RAN provides a better architecture for the application and implementation of CoMP and FFR.

Coordinated Multi-point was first standardised in [75] to improve the coverage and cell-edge users' downlink capacity. Two transmission schemes were given: Coordinated scheduling and/or beamforming (CB) and Joint processing/transmission (JT). The downlink signal transmitted to one UE is from one or multiple coordinated base stations. The field trial of CoMP was presented in [76] and their results showed that CoMP can significantly increase the capacity. CoMP is also believed to be one of the key technologies that can improve the performance of the next generation wireless communication [77]. The requirements to apply CoMP are: tight synchronisation between coordinated base stations, strong backhaul between base stations or from base stations to a central processing unit and good channel information feedback. All these needs are difficult to be fulfilled in the conventional network where cooperation between base stations is limited. However, the C-RAN architecture provides all these supports easily due to the centralised processing and fiber connection backhaul.

CoMP breaks the conventional cell boundary resource allocation with the co-

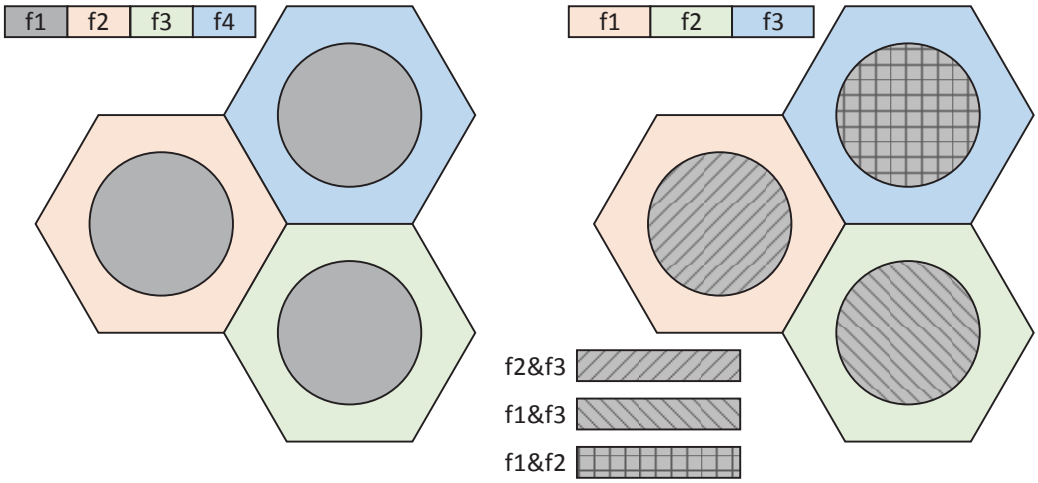

Figure 2.4: Illustration of strict FFR and soft FFR.

ordination of two neighbouring base stations. The coordinated base stations share the same frequency resource to transmit to the UE. Thus a new method to allocate the resource for the cell boundary users is required for using CoMP in C-RAN. We propose to use Fractional Frequency Reuse (FFR).

Fractional Frequency Reuse (FFR) was first proposed in [78] to decrease inter-cell interference in 4G networks by assigning neighbouring cells with different frequency resources. FFR is widely used in OFDM system. [79] proposed a Multi-sector Gradient (MGR) algorithm by dividing a cell into different sectors and applied FFR to improve the capacity of OFDM systems. FFR is futher developed to dynamic methods. [80] proposed a two-step method: first allocating the same frequency resource to all cells, and then allocating a frequency to each sector opportunistically. [81] compared two modes: Strict FFR and Soft Frequency Reuse (SFR) as shown in Figure 2.4. Strict FFR has no inter-cell interference and lower spectrum efficiency, while SFR has inter-cell interference and higher spectrum efficiency. The capacity of all users in average and cell edge users are simulated in [81]. SFR achieves higher overall capacity, while strict FFR obtains better performance on capacity for cell edge users. Therefore, from the aspect of cell edge users' capacity, we build our model based on the strict FFR and focus on cell edge users' capacity.

The spectrum efficiency of CoMP was also further improved with the MU-

MIMO technology [82] [83]. Multiple users on neighbouring sectors can be supported by multiple base stations in the same frequency band. MU-MIMO transmission scheme is applied to achieve spatial domain separation of the signal streams to different users.

The capacity of DAS using FFR and CoMP is analysed in Section 5.3. We use FFR to enhance the spectrum efficiency and use CoMP Coordinated Beamforming (CB) to obtain MIMO gain. Then we compare the capacity between SU-MISO with CoMP-JT and MU-MIMO with CoMP-CB.

As mentioned in Section 2.2, LSA shows potential for increasing the capacity of MNO users by obtaining more frequency resources. However, LSA is a novel approach and to the best of our knowledge the problem of FFR resource allocation in LSA DAS for cell edge users has not been fully investigated yet. Although the LSA concept was presented in [84] [85], no directly comparable work was found in literature. Thus we extend the results in 5.3 by adding usage of LSA in one cell and investigate how LSA will perform in DAS and C-RAN systems for 5G networks, the related work is presented in Section 5.4.

Beside overall capacity analysis, several related studies have explored the resource allocation and transmission schemes for DAS with FFR and CoMP. [86] proposed a Cooperative Frequency Reuse (CFR) to support CoMP joint transmission. CFR can further improve cell edge performance compared with universal frequency reuse (UFR) that means no frequency division within one cell. The frequency band in [86] has been divided into three parts for resource allocation. [87] proposed a frequency allocation scheme for joint transmission with omni-directional and 6-sector directional antennas which can improve spectral efficiency for cell boundary users. In [87] the frequency band has been divided into six parts for resource allocation. [67] studied the power allocation of CoMP in DAS.

Yet, none of these papers have compared the effect of different FFR resource allocation approaches on network performance. The FFR resource allocation in [86] could achieve a full frequency reuse but it will cause inter-cell interference (ICI). [87] considered a three antenna CoMP but the interfering cell set was not specified. [67] proposed several different arrangements, but under the assumption that the number

of users is equal to or less than the number of base stations. Thus the problem of optimal FFR resource allocation in DAS for cell edge users has not been fully investigated.

In section 6.1, we propose a Multiset based algorithm for calculating optimum FFR resource allocation in DAS. The results are compared with the resource allocation schemes proposed in [86] and [87].

In our work of C-RAN performance analysis, we noticed that the SNR of the network affects the performance of cooperation transmission. Indeed, C-RAN is suitable for coordinated transmission. However, we found that, under certain SNR conditions, it is not necessary to use coordinated transmission. This is an angle that has been missed in most of the related work, in which coordinated transmission is always assumed to perform better than non-coordinated transmission. In section 6.2, we derive an SNR threshold for coordinated and non-coordinated joint transmission. To the best of our knowledge, this is the first work that derives transmitting SNR threshold for FFR aided coordinated and non-coordinated joint transmission in C-RAN. The SNR threshold can provide a design guide for base station coordinated transmission schemes in network planning without the need of simulations.

2.4 Summary

In this chapter, we presented a literature review of the related work in spectrum sharing. We gave an overview of Cognitive Radio. Two main spectrum sharing frameworks: LSA and SAS, were introduced and compared. We also summarised the key concept and technologies in the C-RAN, such as DAS, CoMP and FFR. The limitations and improvements of the related work were addressed in this chapter. In the following chapters, research work of this thesis will be presented in detail.

Chapter 3

Priority Access and General Authorised Access Interference Mitigation in Spectrum Access System

To meet the capacity needs of next generation wireless communications, U.S. Federal Communications Commission has recently introduced Spectrum Access System (SAS). Spectrum is shared between three tiers - Incumbents, Priority Access Licensees (PAL) and General Authorised Access (GAA) Licensees. When incumbents are absent, PAL and GAA share the spectrum under the constraint that GAA ensures the interference to PAL is no more than -40 dBm with at least 99% confidence.

We propose a PAL-GAA co-channel interference mitigation technique that does not expose base station locations. We show how PAL can derive the distribution of the distance from a GAA transmitter to a PAL receiver in Section 3.2. The distribution of the aggregate interference using Probability Density Function and Characteristic Function is derived in Section 3.3. We also propose a numerical approximation using Inverse Fast Fourier and Discrete Fourier Transforms in Section 3.4. Additionally we formulate an optimisation problem for the optimal exclusion zone size in Section 3.5. We analytically prove the convexity of the problem.

3.1 System model

We consider the scenario, illustrated in Figure 3.1: one operator owns the census tract and it is running PAL. The other operator runs GAA in the same census tract using the same spectrum. We model the census tract as a closed polygon shaped area. We assume that the PAL and GAA are all the base stations with fixed locations and the GAA base stations are transmitting with a known power. We define PAL base stations as interference receivers and GAA base stations as interference transmitters. As interference receivers, the PAL network has full knowledge of all base stations in its own network. We assume that the small scale fading can be averaged out across time. Shadow fading or height differences of antennas are not considered in this chapter.

We use the exclusion zone concept to control the interference to the PAL base stations and mask their locations. Any GAA transmission inside of the exclusion zone is not allowed. We use each PAL base station j as the centre and draw a circle with a certain radius around it to form the exclusion zone. If two exclusion zones overlap, we group them into one combined exclusion zone with their non-overlapping boundary, and each PAL base station is still at the centre of its previous exclusion zone circle, as shown in Figure 3.3 and Figure 3.4. If more than two exclusion zones overlap, we use one circle to replace their exclusion zones with the minimum area that covers all the overlapping exclusion zones, while the PAL base stations may no longer be at the centre of the new circle, as shown in Figure 3.5.

For each PAL interference receiver j, the constraint on aggregate interference I_j is formulated as:

$$P(I_j \leq I_0) > P_0 \tag{3.1}$$

By default, $I_0 = -40$ dBm, $P_0 = 0.99$. Agreement between two SASs may change these parameters and they are constant during one round of interference mitigation operation. The aggregate interference at PAL receiver j from N_{TX} number of GAA transmitters is given as:

$$I_j = \sum_{i=1}^{N_{TX}} I_{ij} \tag{3.2}$$

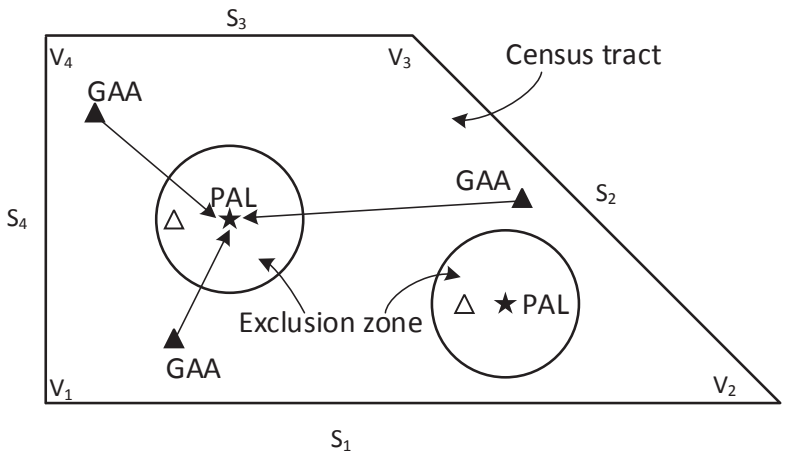

Figure 3.1: SAS PAL GAA co-channel interference illustration:★ are the PAL base stations, ▲ are the GAA base stations outside of exclusion zones that can transmit, △ are the GAA base stations inside of exclusion zones that have to remain silent. $V_i, i = 1, ..., 4$ are the vertices, $S_i, i = 1, ..., 4$ are the sides.

i is the index of the interference transmitters, i.e. GAA, $i \in \{1, ..., N_{TX}\}$. The interference from each transmitter i is given as:

$$I_{ij} = P_t L_{ij} \tag{3.3}$$

where P_t is transmit power and L_{ij} is the path loss between transmitter i and receiver j. We use the path loss model in [88],

$$L_{ij} = K \left(\frac{d_0}{d_{ij}} \right)^{\beta} \tag{3.4}$$

where d_{ij} is the distance from interference transmitter i to receiver j. K, β and d_0 are parameters related to the wireless environment [88].

We propose the process of the PAL-GAA co-channel interference mitigation as follows: The GAA network will initiate a request to the PAL network with the information of the distribution and the number of GAA transmitters. The PAL network will use the GAA information to obtain the PDF of the distance of one GAA transmitter to a PAL receiver, then use the transformation function to get the PDF of the interference from one GAA transmitter to a PAL receiver. The

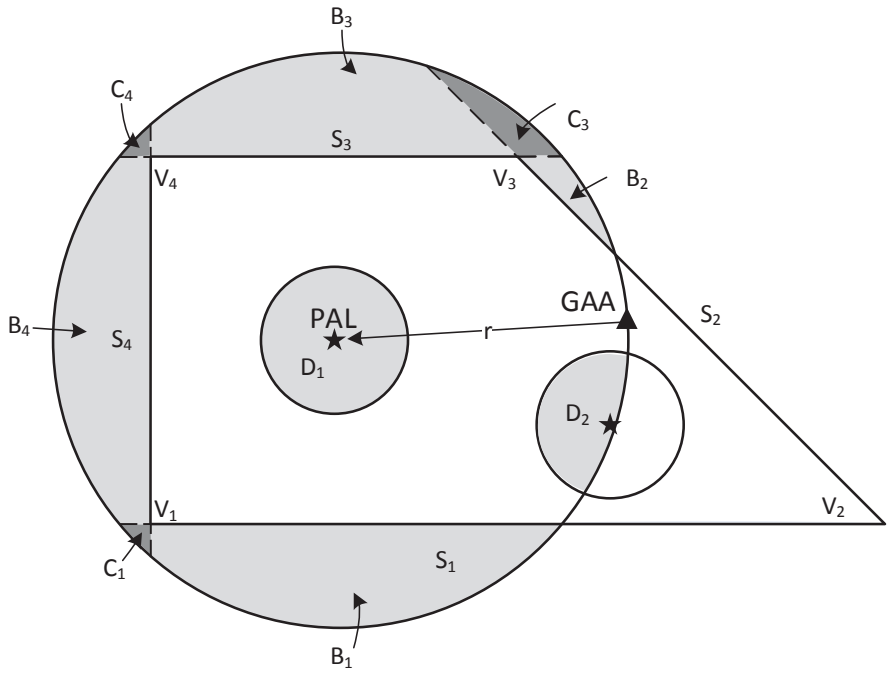

Figure 3.2: Illustration of CDF of the distance of GAA interference transmitters to a PAL interference receiver, B_l is the area outside of the side S_l of the census tract, C_j is the overlapping area of B_l and B_j and D_k is the overlapping area of the exclusion zone k and the circle of which the centre is the PAL interference receiver's location and radius is r.

Characteristic Function is leveraged to calculate the PDF of the aggregate interference from multiple GAA transmitters to a PAL receiver. The CDF of the aggregate interference from multiple GAA transmitters to a PAL receiver is the integral of the PDF. A numerical approximation of the CDF is implemented by IDFT, multiplication and DFT. From the CDF, the probability of the aggregate interference below a certain threshold is obtained. The PAL network then can optimise the exclusion zones around all PAL receivers and send the exclusion zone information back to the GAA network. After the GAA network receives feedback from the PAL network on the exclusion zones, it will launch the GAA transmission accordingly. This is a single round of the PAL-GAA interference mitigation. If any parameter in the GAA transmission changes, the GAA network will send a new request to the PAL network and that will trigger a new round of interference mitigation. The key components in the process are presented in detail in the following sections.

3.2 Distribution of distance of a GAA transmitter to a PAL receiver

Since we assume the interference transmitters' locations follow a uniform distribution inside of the finite census tract excluding the exclusion zone of each receiver, the distribution of the distance from the transmitter to a particular receiver can be derived [47]. In [47], the Cumulative Density Function (CDF) of the distance r from a transmitter to a certain receiver is defined as:

$$F_R(r) = \frac{1}{|A|}\left(\pi r^2 - \sum_l B_l + \sum_l C_l\right) \tag{3.5}$$

The difference is that we consider that GAA interference transmitters have to remain silent in other exclusion zones. Thus in this chapter, the CDF of the distance r from a transmitter to a certain receiver is given as:

$$F_R(r) = \frac{1}{|A^c| - \sum_{k=1}^{N_E} |A_k^e|}\left(\pi r^2 - \sum_l B_l + \sum_l C_l - \sum_{k=1}^{N_E} D_k(r)\right) \tag{3.6}$$

where $|A^c|$ is the area of the census tract, $|A_k^e|$ is the area of the k th exclusion zone and N_E is the total number of exclusion zones. One exclusion zone may contain more than one PAL base station, thus $N_E \leq N_{RX}$, N_{RX} is the number of PAL base stations. $B_l(r)$ and $C_l(r)$ depend on the location of PAL j and the shape of the census tract, shown in Figure 3.2 and given as follows:

$$B_l(r) = 2\int_{d_l}^{r} \tau \arccos\left(\frac{d_l}{\tau}\right) d\tau \tag{3.7}$$

$$C_l(r) = \int_{d_l}^{r} \left(\tau\left(-\pi + \delta_l + \arccos\left(\frac{d_l}{\tau}\right) + \arccos\left(\frac{d_{l-1}}{\tau}\right)\right)\right) d\tau \tag{3.8}$$

where δ_l is the inner angle of vertex l and other notations follow the definitions in [47].

$D_k(r)$ shown in Figure 3.2, varies with the exclusion zone and the number of PAL base stations inside of exclusion zone k. We divide this into two cases: calculate $D_k(r)$ with regard to its own exclusion zone with the PAL base station j inside and with regard to other exclusion zones.

3.2.1 Calculation of $D_k(r)$ for the exclusion zone k that covers the PAL receiver j

If only one PAL base station j is inside of its own exclusion zone, the PAL base station j is at the centre of the exclusion zone circle, $D_k(r) = 0$ when $r \leq R_k$ and $D_k(r) = |A_k^e|$ when $r > R_k$.

If two PAL base stations are inside of their own exclusion zone of two combined circles with radius R_{k_1} and R_{k_2}, we assume R_{k_1} is the radius of the circle with PAL base station j as the centre.

$$D_k(r) = 2\int_{r_{min}}^{r} \tau\xi_{jk_2}(\tau)d\tau \tag{3.9}$$

where

$$\xi_{jk_i}(r) = \arccos\left(\frac{r^2 + d_{jk_i}^2 - R_{k_i}^2}{2d_{jk_i}r}\right) \tag{3.10}$$

and $r_{min} = R_{k_1}$. d_{jk_2} is the distance between PAL base station j to the other PAL base station k_2 in the same exclusion zone. $\tau = r'$.

If more than two PAL base stations are inside of their own exclusion zone k,

$$D_k(r) = 2\int_{r_{min}}^{r} \tau\xi_{jk}(\tau)d\tau \tag{3.11}$$

where $\xi_{jk}(r)$ follows (3.10), r_{min} is the minimum distance from PAL base station j to the boundary of exclusion zone k, d_{jk} is the distance between PAL base station j to the geometric centre of exclusion zone k.

3.2.2 Calculation of $D_k(r)$ for the exclusion zone k that does not cover the PAL receiver j

If there is only one PAL base station in another exclusion zone k that does not cover PAL base station j,

$$D_k(r) = 2\int_{r_{min}}^{r} \tau\xi_{jk}(\tau)d\tau \tag{3.12}$$

where $r_{min} = d_{jk} - R_k$, d_{jk} is the distance between PAL base station j to the other PAL base station k.

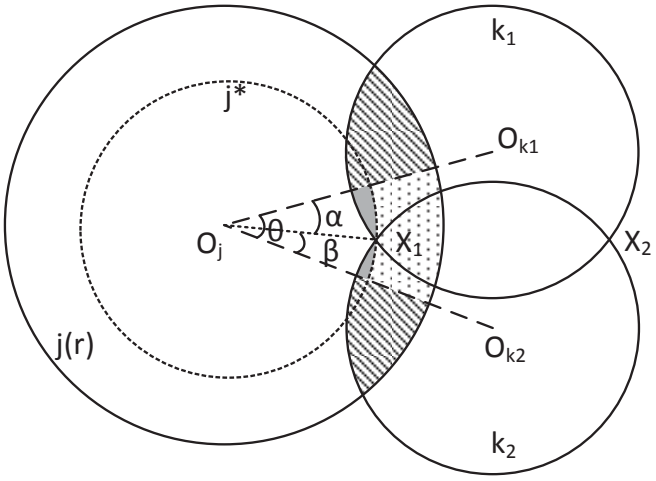

(a)

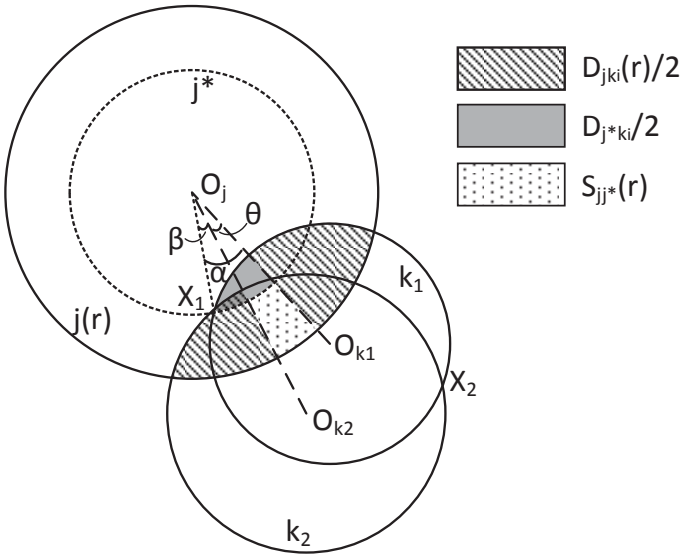

(b)

Figure 3.3: Illustration of two overlapping exclusion zone. When $\min\left(d_{jk}^{X}\right) < r < \max\left(d_{jk}^{X}\right)$, only one intersection point X_1 is covered by circle $j(r)$. (a): $c_1 = 1, \theta = \alpha + \beta$; (b):$c_1 = -1, \theta < \alpha + \beta$. Note: $D_{j^*k_2}$ area is overlapping with $D_{jk_2}(r)$ and D_{j^*k1} in (b).

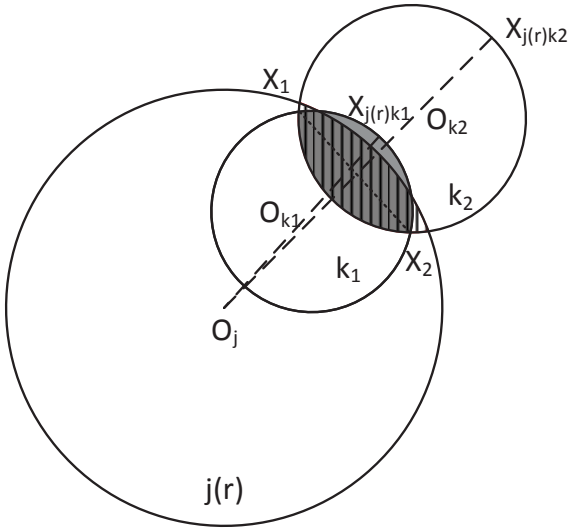

(a)

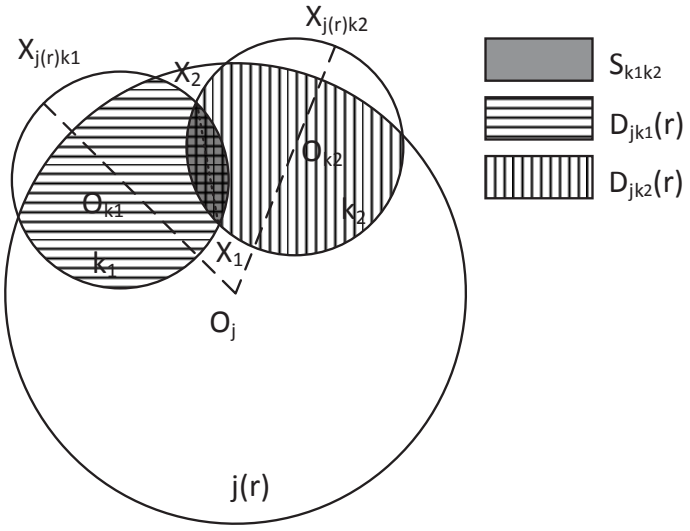

(b)

Figure 3.4: Illustration of two overlapping exclusion zones. $\max\left(d_{jk}^{X}\right) \leq r < \max\left(d_{jk_i}\right) + R_k$, both intersection points X_1 and X_2 are covered by circle $j(r)$. (a): $c_2 = 0$ $X_{j(r)k1}$ and $X_{j(r)k2}$ are on the same side of the line X_1,X_2; (b): $c_2 = 0$ $X_{j(r)k1}$ and $X_{j(r)k2}$ are on different sides of the line X_1,X_2. Note: $S_{k_1k_2}$ is overlapping with $D_{jk_2}(r)$ in (a); $S_{k_1k_2}$ is overlapping with $D_{jk_1}(r)$ and $D_{jk_2}(r)$ in (b).

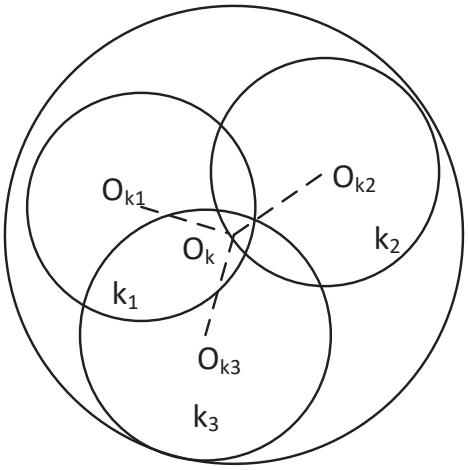

Figure 3.5: Illustration of three overlapping exclusion zones. O_{k1}, O_{k2} and O_{k3} are the centres of three overlapping exclusion zones. We assume that the sizes of the overlapping exclusion zones can be vaiours, but the differences are not large. We propose to use a new exclusion zone with the centre O_k that is the geometric centre of O_{k1}, O_{k2} and O_{k3}. The new exclusion zone radius is the maximum distance from O_k to O_{k1}, O_{k2} and O_{k3} plus the maximum size original exclusion radius.

If there are two PAL base stations in another exclusion zone k, we derive $D_k(r)$ as follows:

When two PAL exclusion zones are overlapping, we combine them into one exclusion zone k and denote the two individual PAL exclusion zones as k_1 and k_2. We define: 1) the location of two PAL base stations which are the centre of the exclusion zones k_1 and k_2 as O_{k1} and O_{k2}; 2) the intersection points of k_1 and k_2 as X_1 and X_2; 3) the circle with PAL base station j as the centre and distance r as the radius of circle $j(r)$; 4) location of PAL base station j as O_j and 5) the distance from O_j to X_1 and X_2 as set d_{jk}^X. We then calculate the intersection area $D_k(r)$ between circle $j(r)$ and exclusion zone k.

We divide this problem into three different cases according to the range of distance r:

1. $\min\left(d_{jk_i}\right) - R_k < r \leq \min\left(d_{jk}^X\right)$, neither X_1 or X_2 is covered by circle $j(r)$

   If the circle overlapping with $j(r)$ is k_1, k_2 or both, the intersection area is

equal to the summation of the intersection area with the individual exclusion zone. $D_k(r) = D_{jk_1}(r) + D_{jk_2}(r)$, where $D_{jk_i}(r)$ follows (3.12).

2. $\min\left(d_{jk}^X\right) < r < \max\left(d_{jk}^X\right)$, only one of X_1 or X_2 is inside of circle $j(r)$

As shown in Figure 3.3, we assume X_1 is inside of circle $j(r)$. We define the condition c_1 as:

$$c_1 = \begin{cases} 1 & \theta = \alpha + \beta \\ -1 & \theta < \alpha + \beta \end{cases} \tag{3.13}$$

where

$$\theta = O_{k_1}\hat{O}_j O_{k_2} \tag{3.14}$$

$$\alpha = O_{k_1}\hat{O}_j O_{X_1} \tag{3.15}$$

$$\beta = O_{k_2}\hat{O}_j O_{X_1} \tag{3.16}$$

(a) $c_1 = 1$

The overlapping area of $j(r)$ and exclusion zone k in Figure 3.3 (a) is given as

$$D_k(r) = \frac{D_{jk_1}(r)}{2} + \frac{D_{jk_2}(r)}{2} + \frac{D_{j^*k_1}}{2} + \frac{D_{j^*k_2}}{2} + S_{j^*j}(r) \tag{3.17}$$

(b) $c_1 = -1$

The overlapping area of A and exclusion zone k in Figure 3.3 (b) is given as

$$D_k(r) = \frac{D_{jk_1}(r)}{2} + \frac{D_{jk_2}(r)}{2} + \frac{D_{j^*k_1}}{2} - \frac{D_{j^*k_2}}{2} + S_{j^*j}(r) \tag{3.18}$$

where $D_{jk_1}(r)$ and $D_{jk_2}(r)$ is the intersection area of circle j and circle k_1 and k_2 respectively, follows (3.12). $D_{j^*k_1}$ and $D_{j^*k_2}$ are the intersection areas of circle j^* and circle k_1 and k_2 respectively. Circle j^* is the concentric circle with $j(r)$ and radius R_{j^*} which is the distance from O_j to X_1. $S_{j^*j}(r)$ is the area between circle j^* and circle $j(r)$ with the angle θ. $S_{j^*j}(r) = (r^2 - R_{j^*}^2)\theta$. $D_{j^*k_1}$, $D_{j^*k_2}$ and θ are constant to the change of r. The derivative of (3.17) and (3.18) is the same as

$$\frac{\partial D_k(r)}{\partial r} = r\xi_{jk_1}(r) + r\xi_{jk_2}(r) + 2r\theta \tag{3.19}$$

where $\xi_{jk_i}(r)$ follows (3.10).

3. $\max\left(d_{jk}^{X}\right) \leq r < \max\left(d_{jk_i}\right) + R_k$, both X_1 and X_2 are covered by circle $j(r)$

   As shown in Figure 3.4, we connect the centers of the two circles O_j and O_{k1} with a straight line and extend it to get the intersection point $X_{j(r)k1}$ at the exclusion zone k_1. Likewise, we can get the intersection point $X_{j(r)k2}$. We connect X_1 and X_2 with a straight line and define the function of the line as $g(\bullet) = 0$, $\bullet$ denotes the coordinates of the points on the line. We define the condition c_2 as

$$c_2 = \begin{cases} 0 & \text{sign}\left(g\left(X_{j(r)k1}\right)\right) = \text{sign}\left(g\left(X_{j(r)k2}\right)\right) \\ 1 & \text{sign}\left(g\left(X_{j(r)k1}\right)\right) \neq \text{sign}\left(g\left(X_{j(r)k2}\right)\right) \end{cases} \tag{3.20}$$

   which gives $c_2 = 0$ if $X_{j(r)k1}$ and $X_{j(r)k2}$ are on the same side of the line $g(\bullet) = 0$ and $c_2 = 1$ if $X_{j(r)k1}$ and $X_{j(r)k2}$ are on different sides of the line $g(\bullet) = 0$.

   (a) $c_2 = 0$

   As shown in Figure 3.4 (a), the overlapping area of circle $j(r)$ and exclusion zone k is given as

$$D_k(r) = |A_{k_1}| - S_{k_1k_2} + D_{jk_2}(r) \tag{3.21}$$

   where $|A_{k_1}|$ is the area of exclusion zone k_1, $S_{k_1k_2}$ is defined as the intersection area of exclusion zone k_1 and k_2. $D_{jk_2}(r)$ is defined as the intersection area of circle $j(r)$ and exclusion zone k_2. $|A_{k_1}|$ and $S_{k_1k_2}$ are constant to the change of r. The derivative of (3.21) is

$$\frac{\partial D_k(r)}{\partial r} = 2r\xi_{jk_2}(r) \tag{3.22}$$

   where $\xi_{jk_i}(r)$ follows (3.10).

   (b) $c_2 = 1$

   As shown in Figure 3.4 (b), the overlapping area of circle $j(r)$ and exclusion zone k is given as

$$D_k(r) = D_{jk_1}(r) + D_{jk_2}(r) - S_{k_1k_2} \tag{3.23}$$

where $D_{jk_1}(r)$ is defined as the intersection area of circle $j(r)$ and exclusion zone k_1 and $D_{jk_2}(r)$ is defined as the intersection area of circle $j(r)$ and exclusion zone k_2. The derivative of (3.23) is

$$\frac{\partial D_k(r)}{\partial r} = 2r\xi_{jk_1}(r) + 2r\xi_{jk_2}(r) \tag{3.24}$$

where $\xi_{jk_i}(r)$ follows (3.10).

In summary, when two PAL base stations are inside of exclusion zone k, $D_k(r)$ is given as (3.25), where $D_{jk_i}(r)$ is the intersection area of circle j and circle k_i. d_{jk}^X is the set of the distance from the centre of circle j to two intersection points X_1 and X_2 of the exclusion zone k. $\frac{\partial D_k(r)}{\partial r}$ is given as (3.26), where $\xi_{jk_i}(r)$ follows (3.10).

$$D_k(r) = \begin{cases} D_{jk_1}(r) + D_{jk_2}(r) & \min\left(d_{jk_i}\right) - R_k < r \leq \min\left(d_{jk}^X\right) \\ \dfrac{D_{jk_1}(r)}{2} + \dfrac{D_{jk_2}(r)}{2} & \\ \quad + \dfrac{D_{j^*k_1}}{2} + c_1\dfrac{D_{j^*k_2}}{2} + S_{j^*j}(r) & \min\left(d_{jk}^X\right) < r < \max\left(d_{jk}^X\right) \\ |A_{k_1}| - S_{k_1k_2} + D_{jk_2}(r) & \max\left(d_{jk}^X\right) \leq r < \max\left(d_{jk_i}\right) + R_k \text{ and } \overline{c_2} \\ D_{jk_1}(r) + D_{jk_2}(r) - S_{k_1k_2} & \max\left(d_{jk}^X\right) \leq r < \max\left(d_{jk_i}\right) + R_k \text{ and } c_2 \end{cases} \tag{3.25}$$

$$\frac{\partial D_k(r)}{\partial r} = \begin{cases} 2r\xi_{jk_1}(r) + 2r\xi_{jk_2}(r) & \min\left(d_{jk_i}\right) - R_k < r \leq \min\left(d_{jk}^X\right) \\ r\xi_{jk_1}(r) + r\xi_{jk_2}(r) + 2r\theta & \min\left(d_{jk}^X\right) < r < \max\left(d_{jk}^X\right) \\ c_2 \times 2r\xi_{jk_1}(r) + 2r\xi_{jk_2}(r) & \max\left(d_{jk}^X\right) \leq r < \max\left(d_{jk_i}\right) + R_k \end{cases} \tag{3.26}$$

If more than two PAL base stations are inside of exclusion zone k,

$$D_k(r) = 2\int_{r_{min}}^{r} \tau\xi_{jk}(r)d\tau \tag{3.27}$$

where $\xi_{jk}(r)$ follows (3.10), $r_{min} = d_{jk} - R_k$, d_{jk} is the distance between PAL base station j to the geometric centre of exclusion zone k.

Deriving (3.6), the PDF of distance r is given as

$$f_R(r) = \frac{2\pi r - \sum_l \frac{\partial B_l}{\partial r} + \sum_l \frac{\partial C_l}{\partial r} - \sum_{k=1}^{N_E} \frac{\partial D_k}{\partial r}}{|A^c| - \sum_{k=1}^{N_E} |A_k^e|} \tag{3.28}$$

where

$$\frac{\partial B_l(r)}{\partial r} = 2r \arccos\left(\frac{d_l}{r}\right) \tag{3.29}$$

$$\frac{\partial C_l(r)}{\partial r} = r\left(-\pi + \delta_l + \arccos\left(\frac{d_l}{r}\right) + \arccos\left(\frac{d_{l-1}}{r}\right)\right) \tag{3.30}$$

When $D_k(r)$ follows (3.9), (3.11), (3.12) and (3.27),

$$\frac{\partial D_k(r)}{\partial r} = 2r \arccos\left(\frac{r^2 + d_{jk}^2 - R_k^2}{2d_{jk}r}\right) = 2r\xi_{jk}(r) \tag{3.31}$$

where d_{jk}, R_k and the feasible range of r follows the parameter settings in (3.9), (3.11), (3.12) and (3.27) respectively.

When $D_k(r)$ follows (3.25), $\frac{\partial D_k(r)}{\partial r}$ is given as (3.26), where $\xi_{jk_i}(r)$ follows (3.10).

3.3 Distribution of aggregate interference from multiple GAA transmitters

We derive the PDF of interference from a transmitter to the receiver j using the transformation function in [89]

$$f_Y(y) = f_R\left(r(y)\right)\left|\frac{dr}{dy}\right| \tag{3.32}$$

where $r(y)$ is the inverse function of the path loss given as:

$$y(r) = P_t K\left(\frac{d_0}{r}\right)^{\beta} \tag{3.33}$$

Thus, we have

$$r(y) = (My)^{\lambda} \tag{3.34}$$

where $M = (d_0)^{-\beta}/(KP_t)$ and $\lambda = -1/\beta$. Thus the PDF of interference is given as:

$$f_Y(y) = f_R\left((My)^{\lambda}\right)\left|\lambda M(My)^{\lambda-1}\right| \tag{3.35}$$

where y represents a random variable of individual interference from transmitter i to receiver j, I_{ij}.

We assume the transmitters are independent and uniformly distributed inside of the census tract. Therefore the interference from the transmitters follows the

same and independent distribution. Thus, the PDF of the aggregate interference can be derived as [90]:

$$f_Z(z) = \underbrace{f_Y(y) * f_Y(y) * ... * f_Y(y)}_{N_{TX}} \tag{3.36}$$

where z represents a random variable of aggregate interference from multiple transmitters to receiver j, I_j, $*$ denotes convolution.

The convolution becomes complex and time consuming when the number of transmitters N_{TX} is large. Alternatively, we propose to use the Fourier Transform which is widely used in digital signal processing and communication systems. We use DFT to obtain the numerical approximation for future practical implementation.

The Characteristic Function (CF) of the aggregate interference is give as:

$$\Phi_Z(t) = \int e^{itz} f(z) dz \tag{3.37}$$

assign $t = 2\pi k$, (3.37) becomes

$$\Phi_Z(2\pi k) = \int e^{i2\pi kz} f(z) dz = \mathcal{F}^{-1}\left[f_Z(z)\right] \tag{3.38}$$

According to the CF property, the CF of the aggregate interference is the multiplication of the CF of the individual interferences [91].

$$\begin{aligned} \Phi_Z(2\pi k) &= \prod_{i=1}^{N_{TX}} \Phi_Y(2\pi k) = \left(\Phi_Y(2\pi k)\right)^{N_{TX}} \\ &= \left(\int e^{i2\pi ky} f_Y(y) dy \right)^{N_{TX}} \end{aligned} \tag{3.39}$$

where $f_Y(y)$ is obtained from (3.35). According to (3.38) the PDF of aggregate interference is given as:

$$\begin{aligned} f_Z(z) &= \mathcal{F}[\Phi_Z(2\pi k)] = \mathcal{F}\left[\left(\int e^{i2\pi ky} f_Y(y) dy \right)^{N_{TX}} \right] \\ &= \mathcal{F}\left[\left(\mathcal{F}^{-1}\left[f_Y(y)\right] \right)^{N_{TX}} \right] \end{aligned} \tag{3.40}$$

Thus we can calculate the CDF of the aggregate interference

$$F_Z(z) = \int_{-\infty}^{z} f_Z(t) dt = \int_{-\infty}^{z} \mathcal{F}\left[\left(\mathcal{F}^{-1}\left[f_Y(y)\right] \right)^{N_{TX}} \right] dt \tag{3.41}$$

We can calculate that the probability of aggregate interference to receiver j is less than or equal to I_0 by

$$P(I_j \leq I_0) = F_Z^j(I_0) \tag{3.42}$$

where $F_Z^j(I_0)$ follows (3.41).

3.4 Numerical approximation

In general, it is difficult to get a closed-form result for (3.41), thus we use DFT and Inverse Discrete Fourier Transform (IDFT) to approximate the Fourier transform in (3.41)

$$\begin{aligned} F_Z(z) &\approx \int_{-\infty}^{z} DFT\left[\left(IDFT\left[f_Y(y)\right]\right)^{N_{TX}}\right] dt \\ &= \int_{-\infty}^{z} \sum_{k=0}^{N_{\mathrm{DFT}}-1} \left[\left(\sum_{n=0}^{N_{\mathrm{IDFT}}-1} Y(n) e^{\frac{\mathrm{j}2\pi nk}{N_{\mathrm{IDFT}}}}\right)^{N_{TX}}\right] dt \end{aligned} \tag{3.43}$$

where $Y(n)$ is a digital sample sequence of $f_Y(y)$ with zero padding, given as:

$$Y(n) = \begin{cases} f_Y(nT_s) & \text{for } n = 0, 1, \cdots, N_s - 1 \\ 0 & \text{for } m = N_s, \cdots, N_{\mathrm{IDFT}} - 1 \end{cases} \tag{3.44}$$

where $N_{IDFT} = N_{TX} \times N_s$, N_s is the sample number and T_s is the sample interval. When the number of transmitters N_{TX} increases, the size of IDFT also increases, and so does the computational complexity. We propose to divide IDFT into groups of IFFT to decrease the computational complexity [92]. We assume the value of N_s is a power of two. Let $n = aM + b$ where $M \triangleq N_{\mathrm{IDFT}}/N_{\mathrm{IFFT}}$ is the total number of groups, $a = 0, 1, \cdots, N_{\mathrm{IFFT}} - 1$ is the data index in a group and $b = 0, 1, \cdots, M - 1$ is the group index. The b-th group can be rewritten as $Y(n) = Y(aM + b)$, thus the IDFT is given as:

$$\begin{aligned} \sum_{n=0}^{N_{\mathrm{IDFT}}-1} Y(n) e^{\frac{\mathrm{j}2\pi nk}{N_{\mathrm{IDFT}}}} &= \sum_{m=0}^{N_{\mathrm{IFFT}}-1} Y(aM+b) e^{\frac{\mathrm{j}2\pi am}{N_{\mathrm{IFFT}}}} \\ &= \sum_{m=0}^{N_{\mathrm{IFFT}}-1} \left[Y_1(m) \times Y_2(b, m)\right] e^{\frac{\mathrm{j}2\pi am}{N_{\mathrm{IFFT}}}} \end{aligned} \tag{3.45}$$

where

$$Y_1(m) = \begin{cases} f_Y(mT_s) & \text{for } m = 0, 1, \cdots, N_s - 1 \\ 0 & \text{for } m = N_s, \cdots, N_{\text{IFFT}} - 1 \end{cases} \tag{3.46}$$

$$Y_2(b, m) = e^{\frac{\text{j}2\pi bm}{N_{\text{IFFT}}}} \tag{3.47}$$

where $\text{j} = \sqrt{-1}$. Thus (3.43) becomes

$$F_Z(z) \approx \int_{-\infty}^{z} \sum_{k=0}^{N_{\text{DFT}}-1} \left[\left(\sum_{m=0}^{N_{\text{IFFT}}-1} \left[Y_1(m) \times Y_2(b, m) \right] e^{\frac{\text{j}2\pi am}{N_{\text{IFFT}}}} \right)^{N_{TX}} \right] dt \tag{3.48}$$

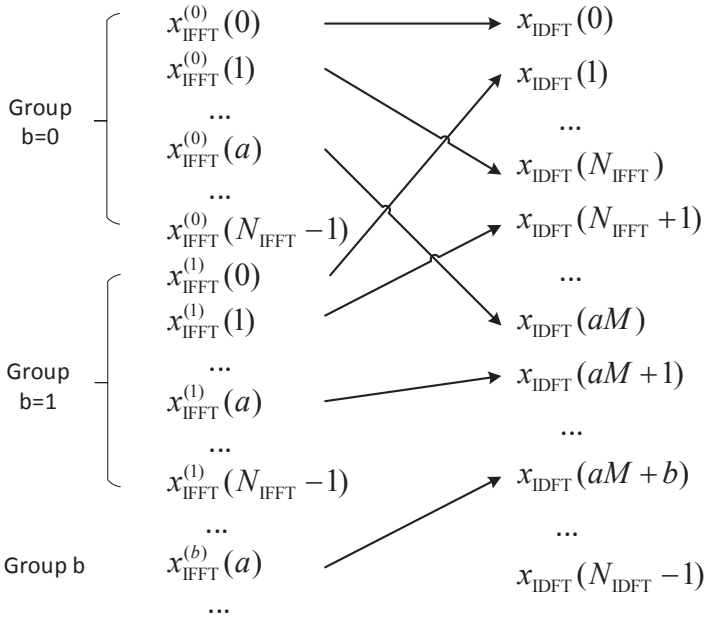

Figure 3.6: Illustration of the IDFT group mapping.

3.5 Optimisation of the exclusion zones

Given a certain exclusion zones' location and size, we can calculate the probability in (3.42). By increasing the size of the exclusion zones, the interference decreases, providing better interference protection for the PALs. However, GAA transmitters will be restricted to a smaller area within the census tract. To achieve a fair trade-off between the two networks, we seek an optimised exclusion zone pattern to meet the

interference requirement, as well as enlarging the GAA transmission area as much as possible. In other words, we want to find the smallest exclusion zone to keep the interference below the threshold.

3.5.1 Problem formulation

The optimisation problem is formulated as

$$\mathcal{P}: \begin{cases} \min & \sum_k \pi R_k^2 \\ \text{s.t.} & F_Z^j(I_0) > P_0 \\ \text{for} & 1 \le j \le N_{RX} \end{cases} \tag{3.49}$$

where $I_0 = -40dBm, P_0 = 0.99$ in the default case [7]. $F_Z^j(I_0)$ follows (3.42) and it is a function of $f_R(r)$ which is a function of R_k .

$F_Z^j(z)$ is a convex function of R_k if PAL receiver j is at the centre of its own exclusion zone k. The convexity of $F_Z^j(z)$ of R_k is proved as follows:

According to (3.41),

$$\frac{\partial^2 F_Z^j(z)}{\partial R_k^2} = \int_{-\infty}^{z} \frac{\partial^2 f_Z(t)}{\partial R_k^2} dt \tag{3.50}$$

Define $g(y) = \underbrace{f_Y(y) * f_Y(y) * ... * f_Y(y)}_{N_{TX}-1}$

$$\frac{\partial^2 f_Z(t)}{\partial R_k^2} = \frac{\partial^2 (f_Y(y) * g(y))}{\partial R_k^2} = \frac{\partial^2 f_Y(y)}{\partial R_k^2} * g(y) \tag{3.51}$$

where

$$\frac{\partial^2 f_Y(y)}{\partial R_k^2} = \left|\frac{dr}{dy}\right| \times \frac{\partial^2 f_R(r)}{\partial R_k^2} \tag{3.52}$$

$$\frac{\partial^2 f_R(r)}{\partial R_k^2} = C(r) \frac{\partial^2 g(R_k)}{\partial R_k^2} \tag{3.53}$$

where $C(r) = 2\pi r - \sum_l \frac{\partial B_l}{\partial r} + \sum_l \frac{\partial C_l}{\partial r} - \sum_{k=1}^{N_E} \frac{\partial D_k}{\partial r} > 0$ is a function of r only.

Define

$$g(R_k) = \frac{1}{|A^c| - \sum_{n=1}^{N_E} |A_n^e|} = \frac{1}{C - \pi R_k^2} \tag{3.54}$$

where $C = |A^c| - \sum_{n=1,n\neq k}^{N_E} |A_n^e|$ is constant with the change of R_k.

$$\frac{\partial^2 g(R_k)}{\partial R_k^2} = \frac{2\pi \left(C - \pi R_k^2 + 4\pi R_k\right)}{(C - \pi R_k^2)^3} \tag{3.55}$$

$\frac{\partial^2 g(R_k)}{\partial R_k^2} > 0$, $\frac{\partial^2 f_R(r)}{\partial R_k^2} > 0$, $\frac{\partial^2 f_Y(y)}{\partial R_k^2} > 0$ and $\frac{\partial^2 F_Z(z)}{\partial R_k^2} > 0$. Thus $F_Z(z)$ is convex of R_k.

3.5.2 Convex lower bound for the optimisation problem

The convexity of $F_Z^j(z)$ in the domain of: 1) R_k of its own exclusion when PAL receiver j is not at the centre of the exclusion zone and 2) R_k of other exclusion zones are difficult to prove. We define the exclusion zone as $\hat{k}$ with the radius $R_{\hat{k}}$ for those two cases. We propose to use a lower bound $f_R^-(r)$ for $f_R(r)$, given as (3.56) to tighten the constraint in (3.49).

$$\begin{aligned} f_R^-(r) =& \frac{2\pi r - \sum_l \frac{\partial B_l}{\partial r} + \sum_l \frac{\partial C_l}{\partial r} - \sum_{k=1,k\neq\hat{k}}^{N_E} \frac{\partial D_k}{\partial r} - \left(\frac{\partial D_{\hat{k}}}{\partial r} - C_4(r)\xi_{j\hat{k}}(r)\right)}{|A^c| - \sum_{k=1}^{N_E} |A_k^e|} \\ &+ \frac{h\left(R_{\hat{k}}\right)}{|A^c| - \sum_{k=1,k\neq\hat{k}}^{N_E} |A_k^e| - \max\left(\left|A_{\hat{k}}^e\right|\right)} \end{aligned} \tag{3.56}$$

where

$$h\left(R_{\hat{k}}\right) = -C_4(r) \times 2\arccos\left(\frac{r^2 + d_{j\hat{k}}^2 - w\left(R_{\hat{k}}\right)^2}{2d_{j\hat{k}}r}\right) \tag{3.57}$$

$$w\left(R_{\hat{k}}\right) = \left(R_{\hat{k}} - \left|r - d_{j\hat{k}}\right|\right) \frac{\sqrt{r^2 + d_{j\hat{k}}^2}}{r + d_{j\hat{k}}} + \left|r - d_{j\hat{k}}\right| \tag{3.58}$$

and $\max\left(\left|A_{\hat{k}}^e\right|\right) = \pi \max\left(R_{\hat{k}}\right)^2$. We consider the feasible range of $R_{\hat{k}}$ is finite according to the size of the census tract. $C_4(r) = r$, when $\frac{\partial D_k(r)}{\partial r}$ follows (3.26) and $\min\left(d_{jk}^X\right) < r < \max\left(d_{jk}^X\right)$; $C_4(r) = 2r$ for other cases.

We use $f_R^-(r)$ to replace $f_R(r)$ in the feasible range of r, $|d - R_{\hat{k}}| < r < |d + R_{\hat{k}}|$ to calculate $F_Z^j(z)$, defined as a lower bound $F_Z^{j-}(z)$. The convexity of $F_Z^{j-}(z)$ of $R_{\hat{k}}$ is proved as follows:

$$
\begin{aligned}
f_R(r) &= \frac{2\pi r - \sum_l \frac{\partial B_l}{\partial r} + \sum_l \frac{\partial C_l}{\partial r} - \sum_{k=1,k\neq\hat{k}}^{N_E} \frac{\partial D_k}{\partial r} - \frac{\partial D_{\hat{k}}}{\partial r}}{|A^c| - \sum_{k=1}^{N_{RX}} |A_k^e|} \\
&= \frac{2\pi r - \sum_l \frac{\partial B_l}{\partial r} + \sum_l \frac{\partial C_l}{\partial r} - \sum_{k=1,k\neq\hat{k}}^{N_E} \frac{\partial D_k}{\partial r}}{|A^c| - \sum_{k=1}^{N_E} |A_k^e|} \\
&+ \frac{-\left(C_4(r)\xi_{j\hat{k}}(r) + C_5(r)\right)}{|A^c| - \sum_{k=1}^{N_E} |A_k^e|} \\
&> \frac{2\pi r - \sum_l \frac{\partial B_l}{\partial r} + \sum_l \frac{\partial C_l}{\partial r} - \sum_{jk=1,k\neq\hat{k}}^{N_E} \frac{\partial D_k}{\partial r} - C_5(r)}{|A^c| - \sum_{k=1,k\neq\hat{k}}^{N_E} |A_k^e| - \left|A_{\hat{k}}^e\right|} \\
&+ \frac{-C_4(r)\xi_{j\hat{k}}(r)}{|A^c| - \sum_{k=1,k\neq\hat{k}}^{N_E} |A_k^e| - \max\left(\left|A_{\hat{k}}^e\right|\right)} \\
&= \frac{C_1(r)}{C_2 - \pi R_{\hat{k}}^2} + \frac{-C_4(r)\xi_{j\hat{k}}(r)}{C_3} > \frac{C_1(r)}{C_2 - \pi R_{\hat{k}}^2} + \frac{h\left(R_{\hat{k}}\right)}{C_3}
\end{aligned}
\tag{3.59}
$$

where $C_1(r)$, C_2, C_3, $C_4(r)$ and $C_5(r)$ are positive constants with the change of $R_{\hat{k}}$. $C_5(r) = \frac{\partial D_{\hat{k}}}{\partial r} - C_4(r)\xi_{j\hat{k}}(r)$. $\frac{C_1(r)}{C_2 - \pi R_{\hat{k}}^2}$ is convex, the proof follows the same process as Appendix A.

We focus on $-C_4(r)\xi_{j\hat{k}}(r)$ and we propose a lower bound as:

$$
h\left(R_{\hat{k}}\right) = -C_4(r) \times 2\arccos\left(\frac{r^2 + d_{j\hat{k}}^2 - w\left(R_{\hat{k}}\right)^2}{2d_{j\hat{k}}r}\right) \tag{3.60}
$$

$C_4(r)$ follows (3.31) and (3.26) depends on different exclusion zone settings,

$$
w\left(R_{\hat{k}}\right) = \left(R_{\hat{k}} - \left|r - d_{j\hat{k}}\right|\right)\frac{\sqrt{r^2 + d_{j\hat{k}}^2}}{r + d_{j\hat{k}}} + \left|r - d_{j\hat{k}}\right| < R_{\hat{k}} \tag{3.61}
$$

For $\left|r - d_{j\hat{k}}\right| \leq R_{\hat{k}} \leq \sqrt{r^2 + d_{j\hat{k}}^2}$, $-C_4(r)\xi_{j\hat{k}}(r)$ is convex. However, for $\sqrt{r^2 + d_{j\hat{k}}^2} \leq R_{\hat{k}} \leq r + d_{j\hat{k}}$, $-C_4(r)\xi_{j\hat{k}}(r)$ is concave. Thus we design a convex lower bound $h\left(R_{\hat{k}}\right)$ for $-C_4(r)\xi_{j\hat{k}}(r)$ by stretching the convex part. The lower bound proof is given as:

$$
h\left(R_{\hat{k}}\right) - \left(-C_4(r)\xi_{j\hat{k}}(r)\right) = -C_4(r) \times \left(2\arccos\left(\frac{r^2 + d_{j\hat{k}}^2 - w\left(R_{\hat{k}}\right)^2}{2d_{j\hat{k}}r}\right) - \xi_{j\hat{k}}(r)\right) \tag{3.62}
$$

Since the cosine function is decreasing in $\{0, \pi\}$, we turn the proof into:

$$\begin{aligned}
&2\left(\frac{r^2+d_{j\hat{k}}^2-w\left(R_{\hat{k}}\right)^2}{2d_{j\hat{k}}r}\right)^2-1-\left(\frac{r^2+d_{j\hat{k}}^2-R_{\hat{k}}^2}{2d_{j\hat{k}}r}\right)\\
&<2\left(\frac{r^2+d_{j\hat{k}}^2-w\left(R_{\hat{k}}\right)^2}{2d_{j\hat{k}}r}\right)^2-1-\left(\frac{r^2+d_{j\hat{k}}^2-w\left(R_{\hat{k}}\right)^2}{2d_{j\hat{k}}r}\right)\\
&=\left(\frac{r^2+d_{j\hat{k}}^2-w\left(R_{\hat{k}}\right)^2}{d_{j\hat{k}}r}+1\right)\left(\frac{r^2+d_{j\hat{k}}^2-w\left(R_{\hat{k}}\right)^2}{2d_{j\hat{k}}r}-1\right) \qquad (3.63)
\end{aligned}$$

Since $\left|r-d_{j\hat{k}}\right| \le w\left(R_{\hat{k}}\right) \le \sqrt{r^2+d_{j\hat{k}}^2}$, (3.63) < 0,

$$2\left(\frac{r^2+d_{j\hat{k}}^2-w\left(R_{\hat{k}}\right)^2}{2d_{j\hat{k}}r}\right)^2-1<\frac{r^2+d_{j\hat{k}}^2-R_{\hat{k}}^2}{2d_{j\hat{k}}r} \qquad (3.64)$$

$$2\left(\cos\left(\arccos\left(\frac{r^2+d_{j\hat{k}}^2-w\left(R_{\hat{k}}\right)^2}{2d_{j\hat{k}}r}\right)\right)\right)^2-1<\cos\left(\xi_{j\hat{k}}(r)\right) \qquad (3.65)$$

$$\cos\left(2\arccos\left(\frac{r^2+d_{j\hat{k}}^2-w\left(R_{\hat{k}}\right)^2}{2d_{j\hat{k}}r}\right)\right)<\cos\left(\xi_{j\hat{k}}(r)\right) \qquad (3.66)$$

$$2\arccos\left(\frac{r^2+d_{j\hat{k}}^2-w\left(R_{\hat{k}}\right)^2}{2d_{j\hat{k}}r}\right)>\xi_{j\hat{k}}(r) \qquad (3.67)$$

Thus (3.62) < 0, $h\left(R_{\hat{k}}\right) < -C_4(r)\xi_{j\hat{k}}(r)$ is a lower bound. Since $\left|r-d_{j\hat{k}}\right| \le w\left(R_{\hat{k}}\right) \le \sqrt{r^2+d_{j\hat{k}}^2}$, $h\left(R_{\hat{k}}\right)$ is convex. Our lower bound of $f_R(r)$ is

$$f_R^-(r)=\frac{C_1(r)}{C_2-\pi R_{\hat{k}}^2}+\frac{h\left(R_{\hat{k}}\right)}{C_3}<f_R(r) \qquad (3.68)$$

is convex, thus $F_Z^{j-}(z)$ is a convex function of $R_{\hat{k}}$.

The problem (3.49) is turned into a sub-optimal problem given as:

$$\mathcal{P}:\begin{cases}\min & \sum_k \pi R_k^2\\ \text{s.t.} & F_Z^{j-}(I_0)>P_0\\ \text{for} & 1\le j\le N_{RX}\end{cases} \qquad (3.69)$$

(3.69) can be numerically solved by using the MATLAB convex optimisation tool and the optimisation solver design is out of the scope of this chapter.

3.6 Numerical results

To verify our analytical results, we build numerical simulations using the following parameters: The census tract area: $S_1 = 1000m, S_2 = 707.11m, S_3 = S_4 = 500m$, $V_1 = V_4 = \pi/2, V_2 = \pi/4, V_3 = 3\pi/4$. The transmit power of GAA base stations is 47 dBm [39]. We place two PAL receivers in the census tract, the coordinates are $PAL_1 = \{250m, 250m\}$ and $PAL_2 = \{625m, 125m\}$ with V_1 as the reference point $\{0, 0\}$ as shown in Figure 3.1.

Figure 3.7 show the PDF of the distance from GAA transmitters to PAL receivers. We indicated four sections in the ranges of r, illustrated as $X_1, ..., X_4$. These four ranges are determined by the intersection between circle $\{PAL_j, r\}, j = 1, 2$, the census tract boundary and the exclusion zones. For PAL 1 and 2 the sections are shown in Table. 3.1 and 3.2 respectively.

The intersection area variables in (3.6) and (3.28) are valid in different ranges of r as: 1) $B_l = 0, C_l = 0, D_k = 0, r \in X_1$; 2) $B_l > 0, C_l = 0, r \in X_2$; 3) $B_l > 0, C_l > 0, r \in X_3$ and 4) $D_l > 0, r \in X_4$.

We use an LTE path loss model in [93], $L_{ij} = 133.5 + 37.6 \log_{10} d_{ij}$. We choose the central frequency $f_c = 3.6$ GHz within the range 3.55 - 3.7 GHz. The feasible range of the radius of exclusion zones of PAL 1 and 2 is 10 to 250 m and 10 to 125 m respectively.

Table 3.1: Sections of the distance from GAA transmitters to PAL 1

section	range	numerical value (m)
X_1	$R_1 < r \leq d_{S_1}$	$100 < r \leq 250$
X_2	$d_{S_1} < r \leq d_{V_1}$	$250 < r \leq 353.55$
X_3	$d_{V_1} < r < r_{max}$	$353.55 < r < 790.57$
X_4	$d_{PAL_2} - R_2 \geq r \leq d_{PAL_2} - R_2$	$295.28 < r \leq 495.28$

The simulation and analytical results of the PDF of the interference from one GAA transmitter to PAL receivers are shown in Figure 3.8 (a) and (b) for PAL 1 and 2 respectively. We compare the simulation and analytical results for the PDF of the aggregate interference when $N_{TX} = 2$ as shown in Figure 3.9 (a) and (b). Moreover,

Table 3.2: Sections of the distance from GAA transmitters to PAL 2

section	range	numerical value (m)
X_1	$R_1 < r \leq d_{S_1}$	$100 < r \leq 125$
X_2	$d_{S_1} < r \leq d_{V_2}$	$125 < r \leq 395.28$
X_3	$d_{V_2} < r < r_{max}$	$395.28 < r < 728.87$
X_4	$d_{PAL_1} - R_2 \geq r \leq d_{PAL_1} - R_1$	$295.28 < r \leq 495.28$

the CDF of the aggregate interference results are shown in Figure 3.10 (a) and (b). We focus on the CDF range close to 99%. We also include the original sample result which calculates $N_{TX} = 2$ and random GAA aggregate interference using Monte-Carlo simulation in comparison. Simulation and analytical results are integral from the PDF histogram data shown in Figure 3.9 (a) and (b). The gap between the simulation result from the PDF histogram and the original sample result is due to the MATLAB PDF histogram approximation. We can consider a certain margin in later design for this gap. From Figure 3.7 to 3.10, we can see that the analytical results are close to the simulation results.

We present the solution for the optimisation problem in (3.49) when $I_0 = -40$ dBm and $P_0 = 0.99$ in Figure 3.11. The results show that with the increase of the GAA transmitter number, the PAL exclusion zone size increases as well. Moreover, with a small number of GAA transmitters, (i.e. $N_{TX} \leq 8$ in this scenario), the exclusion zone size of PAL 1 and PAL 2 is the same. However, with more GAA transmitters, (i.e. $N_{TX} > 8$), PAL 1 needs a larger exclusion zone than PAL 2. As the location of PAL 1 is more central, there is a higher probability of PAL 1 suffering from interference. When the number of GAAs increases, this effect is more prominent, hence requiring a larger radius than PAL 2.

We also show the sub-optimal approach in (3.69) in Figure 3.11 for comparison. We assume that the exclusion zones do not exceed the census tract boundary and maximum exclusion zone radius for PAL 1 and PAL 2 is 250 m and 125 m respectively. For the same GAA transmitter number, the sub-optimal approach in (3.69) requires a larger exclusion zone size than the original problem in (3.49). In Figure 3.11, we can see the increase in the PAL 2 exclusion zone. Since, in the lower bound

equation (3.56) we use PAL 1 maximum exclusion zone size as a PAL 2 constraint, and PAL 1 maximum exclusion zone has a larger difference with the exclusion zone size range in the solution.

Moreover, we compare our results with the exclusion zones size when there is no information shared between two SASs. We focus on one PAL and assume that the distribution of the base stations of the other SAS is unknown. For a certain number of possible transmitters N_{TX}, the maximum interference occurs when all the GAA transmitters have the same distance to a PAL receiver. Thus, the exclusion zone radius which can guarantee that the aggregate interference is below I_0 can be calculated as:

$$R_k = d_0 \left(\frac{P_t N_{TX} K}{I_0} \right)^{1/\beta} \tag{3.70}$$

The result of (3.70) when no information is shared is shown Figure 3.12 for comparison. With the same number of GAA transmitters, our method reduces the exclusion zone size by 40.49%-64.32% that provides GAA network more opportunities to transmit. Note that PAL knowing all GAA locations is a less comparable scenario, as it results in a combinatorial problem to select the GAA users that can transmit. Exclusion zones cannot be defined in this scenario.

Furthermore, to show the difference between the optimum and sub-optimal solutions, we calculate the aggregate interference level when: 1) the input probability for the CDF of aggregate interference is 99% and at the same time 2) the optimum exclusion zone size solution of (3.49), as shown in Figure 3.11 labeled with original constraints. The results are shown in Figure 3.13. We can see that the interference level is still below -40 dBm and the gap is very narrow, approximately 0.005 dB. These results coincide with our analytical results. The gaps between the optimum and sub-optimal solutions are narrow enough that we can use the sub-optimal solutions as network design references.

3.7 Summary

In this chapter, we have proposed a method for inter-operator interference mitigation in Spectrum Access System between Priority Access and General Authorised

Access base stations. Our method does not require or expose the exact locations of any base stations. GAA base stations share their location distribution and the number of transmitters in a closed finite census tract area and the PAL network can derive and calculate the distribution of aggregate interference from the GAA base stations. Furthermore, we considered the practical implementation with the Inverse Fast Fourier Transform and Discrete Fourier Transform. Moreover, we proposed a novel way of using the exclusion zone to protect PAL base stations. According to the distribution of aggregate interference, PAL network can design and optimise their exclusion zone size. We proposed a convex lower bound to approximate the non-convex optimisation problem. Simulation results show that the lower bound provides a good approximation. Our approach reduces the exclusion zone size by over 40%, which gives significantly more spectral opportunities to GAA in the spatial domain. Our method meets the interference requirements of SAS, keeps the fairness between PAL and GAA networks and protects the location information of both networks. The spectrum access technologies and coexistence methods in LSA and SAS will be discussed in the next chapter.

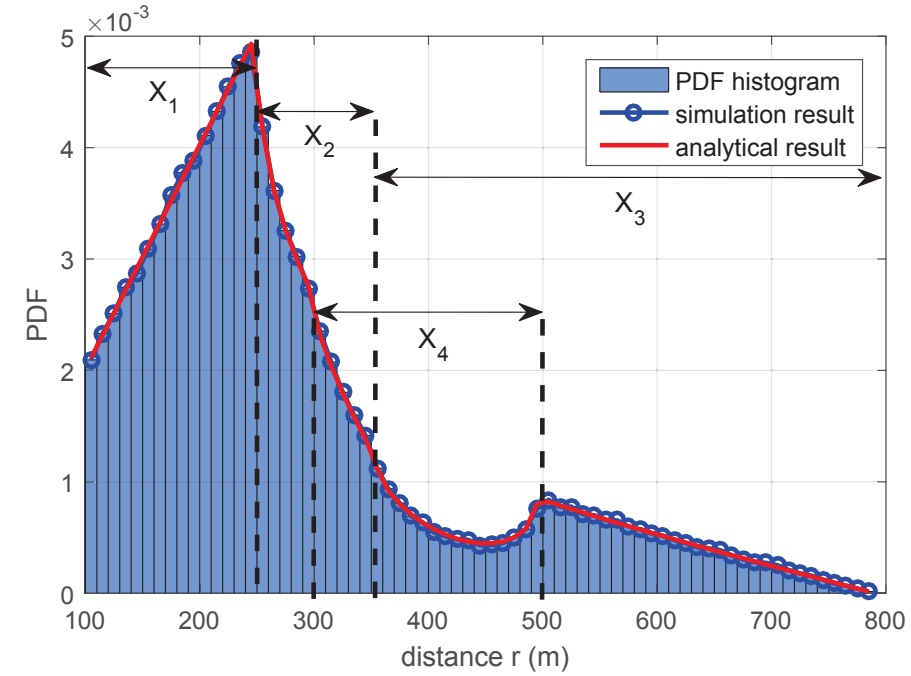

(a)

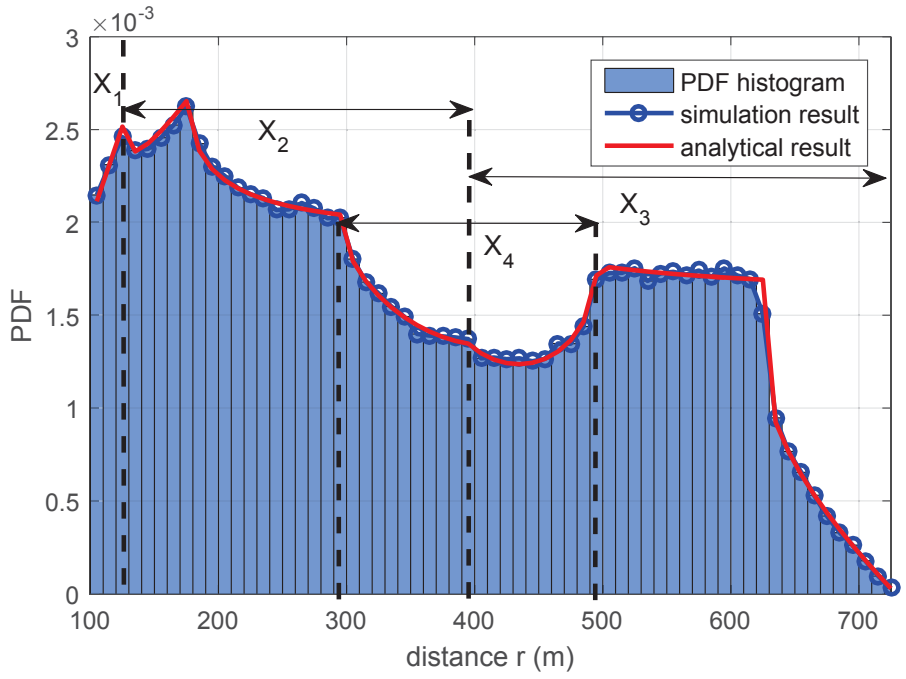

(b)

Figure 3.7: PDF of the distance from a random GAA transmitter to PAL base stations of Figure 3.1: (a) for PAL 1; (b) for PAL 2.

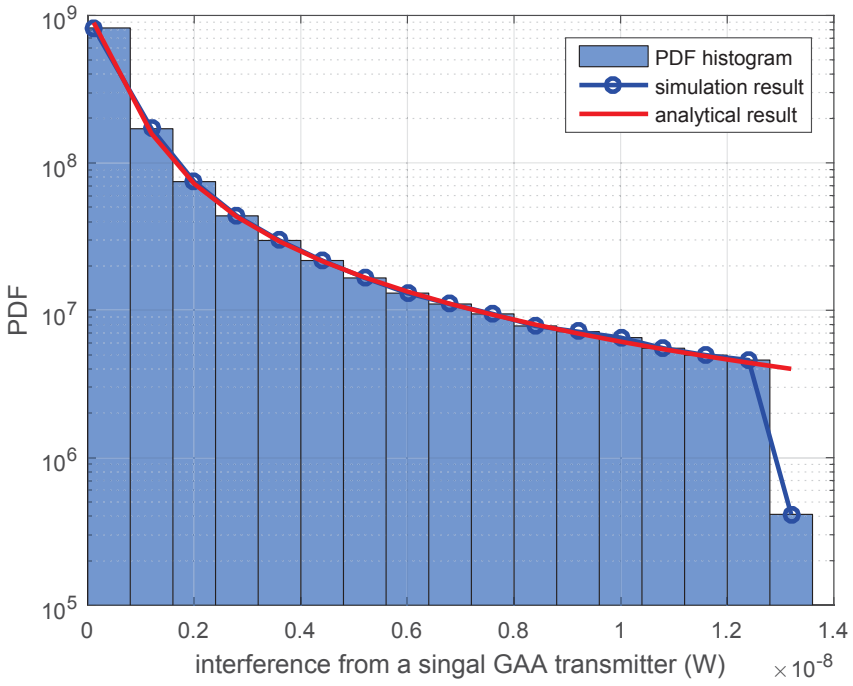

(a)

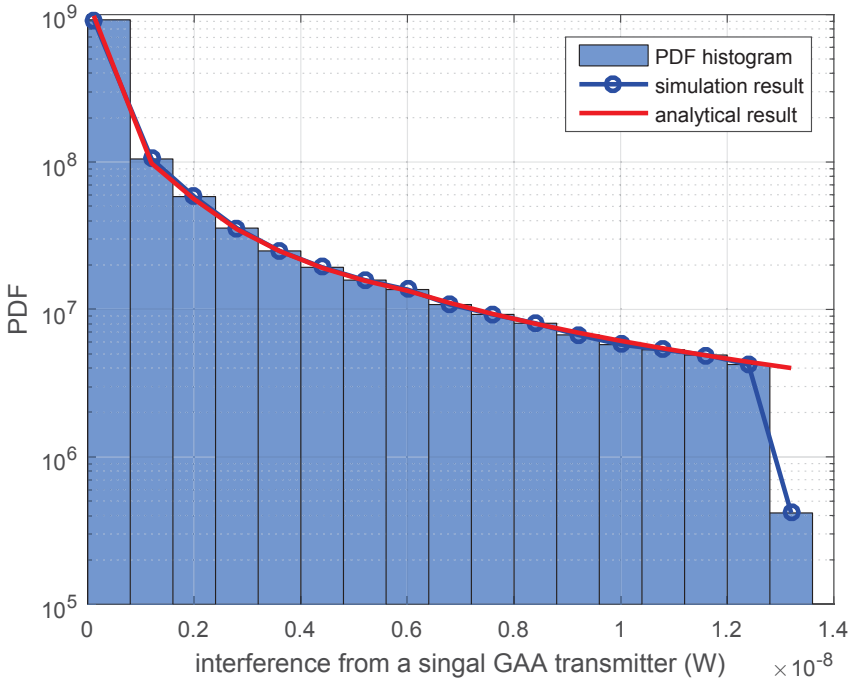

(b)

Figure 3.8: PDF of the interference from a GAA transmitter to PAL base stations: (a) for PAL 1; (b) for PAL 2.

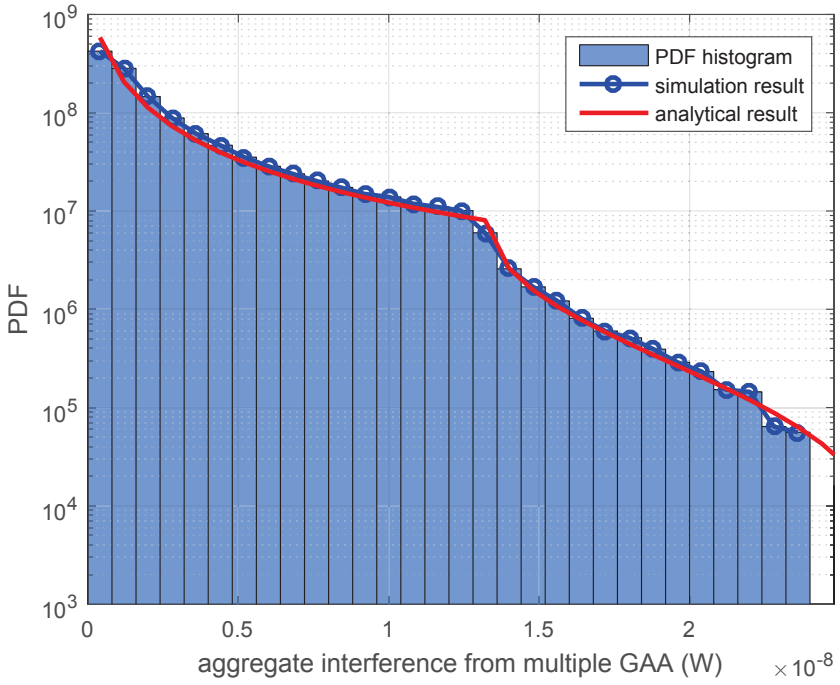

(a)

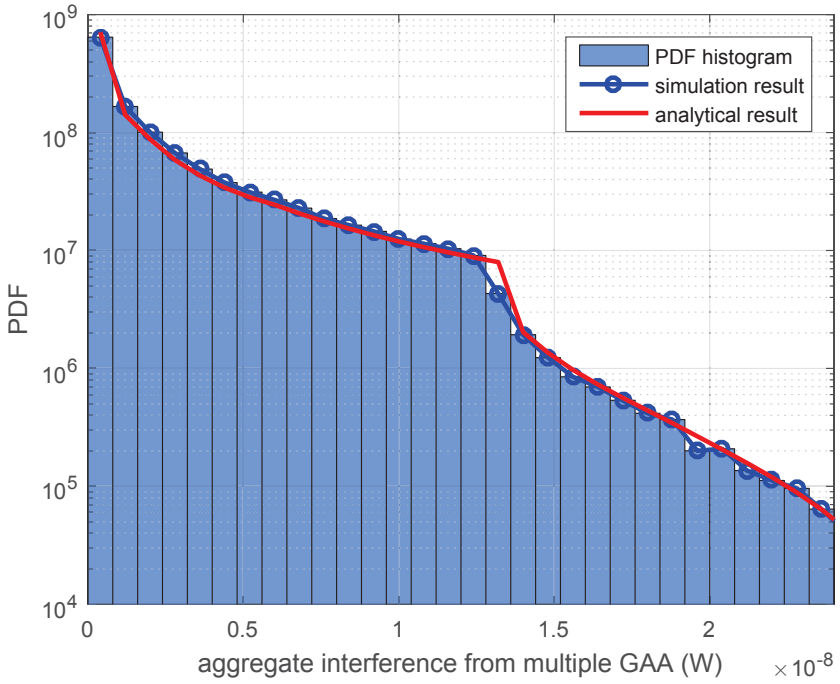

(b)

Figure 3.9: PDF of the aggregate interference from multiple GAA transmitters to PAL base stations: (a) for PAL 1; (b) for PAL 2.

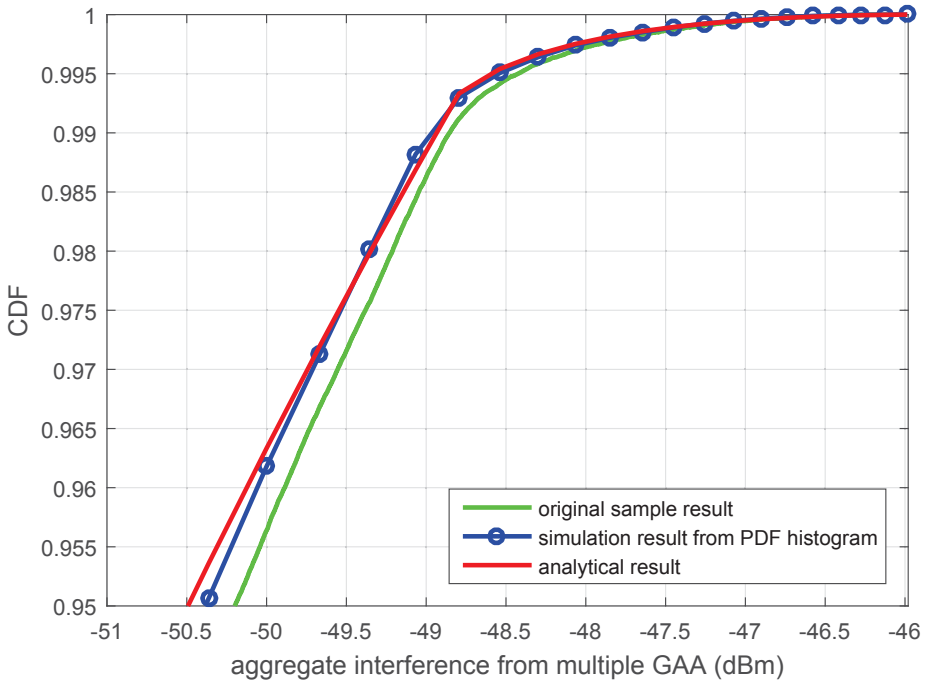

(a)

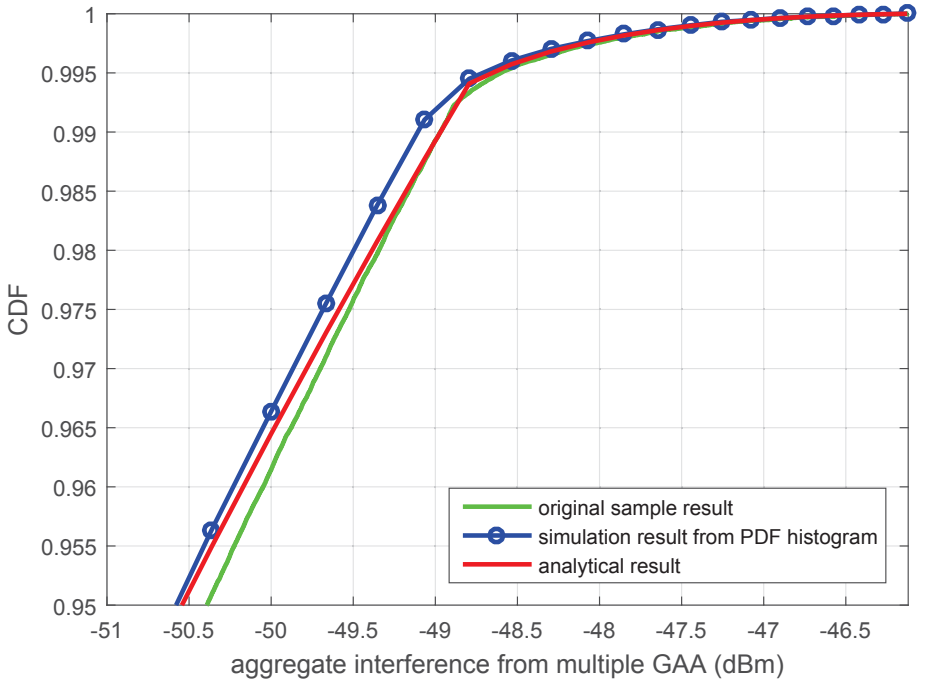

(b)

Figure 3.10: CDF of the aggregate interference from multiple GAA transmitters to PAL base stations: (a) for PAL 1; (b) for PAL 2.

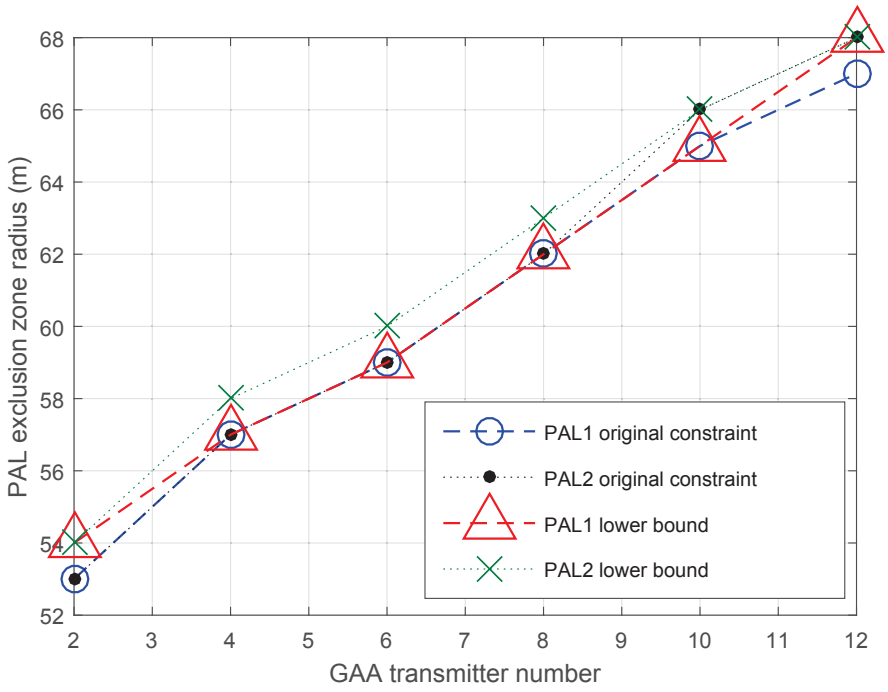

Figure 3.11: Exclusion zone radius solution for the optimisation problems (3.49) and (3.69), with $I_0 = -40$ dBm and $P_0 = 0.99$

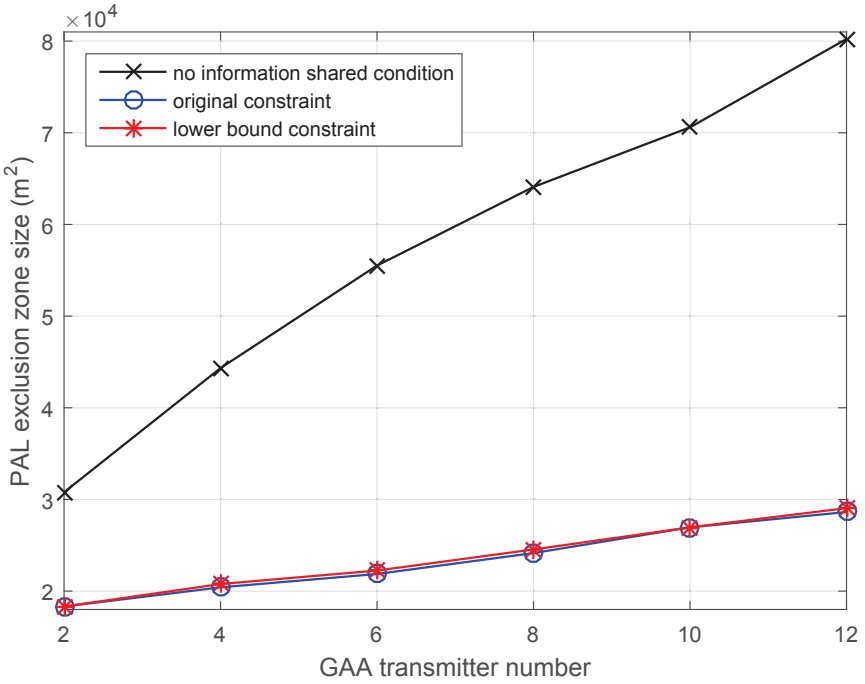

Figure 3.12: Comparison between the exclusion zone area when no information is shared and the exclusion zone area from the optimisation.

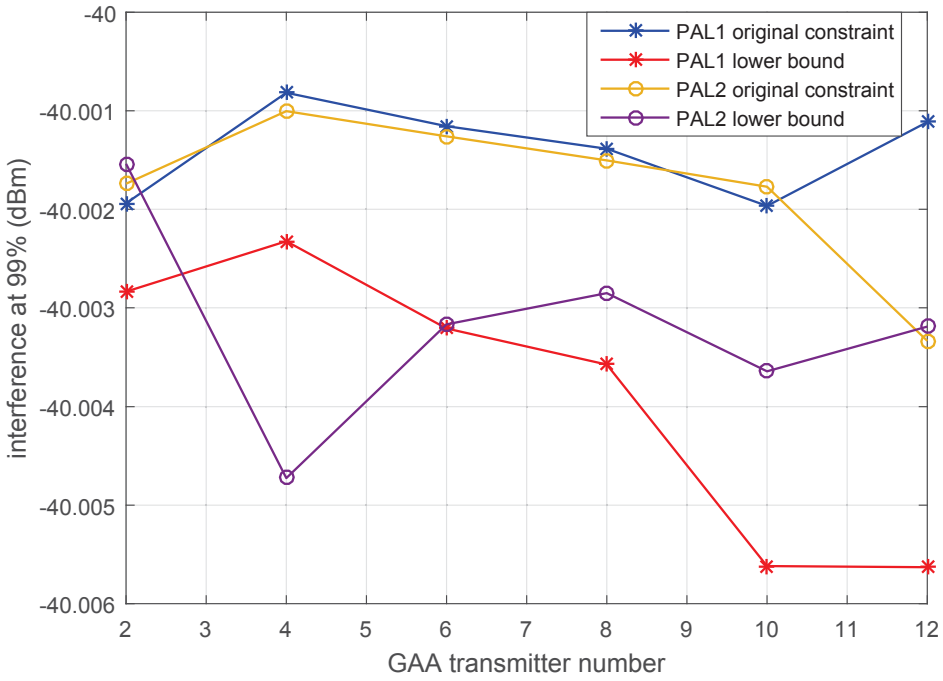

Figure 3.13: Aggregate interference for PAL 1 and 2, when the input probability for the CDF of aggregate interference is 0.99 and at the same time the optimal/sub-optimal exclusion zone size.

Chapter 4

Spectrum Access and Coexistence in LSA and SAS

Spectrum sharing frameworks, such as LSA and SAS, provide mobile operators opportunities to utilise extra spectrum resources as secondary users. In the previous chapter, we have investigated the PAL and GAA co-channel interference mitigation which is a key problem in SAS. The spectrum frameworks cover other aspects as well. In this chapter, the spectrum access and coexistence methods are analysed.

This chapter includes three sections that cover the top to bottom levels in the LSA and SAS frameworks. Firstly, access of all secondary users, such as LSA licensees, PAL and GAA in SAS, to the incumbents' bands is discussed in Section 4.1. Secondly, GAA users sensing the PAL bands in SAS is discussed in Section 4.2. When higher tier users, such as incumbents or PAL users reclaim their bands back, lower tier users, such as secondary users or GAA users have to quit the bands and offload to other bands. We propose WiFi and LTE coexistence for the offloading in Section 4.3.

4.1 Secondary users' access to the incumbents' bands in LSA and SAS

As explained in Section 2.2, secondary users share the spectrum with incumbents in time or spatial domains. Incumbents receive interference protection from secondary users. In LSA, exclusion zones, restriction zones and protection zones are defined to protect incumbents. In SAS, an exclusion zone with geo-location limits and with Environmental Sensing Capability (ESC) assistance are defined. In short, an exclusion zone is the area where secondary users cannot transmit except when authorised; a restriction zone is the area where the transmit power per secondary users is set; a protection zone is where the aggregate interference from secondary users has to be below a certain threshold. The requirements on the exclusion and restricted zones are very straightforward. The aggregate interference management to the protection zone is a key problem in the secondary users' access to the licensed bands. However, there is no available direct interface between incumbents and secondary users due to the privacy requirements of incumbents (e.g. shipborne radar in SAS) or the unpredictable transmission of incumbents (e.g. digital camera in LSA). The interference mitigation method we proposed in Chapter 3 that is based on the information sharing cannot be applied to this scenario. Therefore, we propose a method with measurements and user selection for secondary users to meet the protection zone requirements in LSA and SAS.

4.1.1 Measurement of the aggregate interference from secondary users to incumbents

The aggregate interference from secondary users to incumbents can come from uplink or downlink transmission, from UEs or base stations respectively. The downlink transmission can be controlled by the base stations through power and time allocation. However, the uplink transmission from the UEs is not easily controlled. One conservative method is to shut down sectors or cells. However, binary decisions as such are not flexible enough to adapt to the changes of incumbent activities.

Therefore, we propose to use the UEs in the cellular network to measure the interference. This can save the cost of installing dedicated sensor networks. We assume UEs are using LTE specifications. Thus, UEs know when they operate in downlink or uplink and they can demodulate the downlink reference signal, but they cannot demodulate other UEs' uplink signals. The measurement UEs can utilise the feature of the LTE downlink reference signal to separate the power of the LTE downlink reference signal and other signals including the incumbent signals and noise. The implementation is the cross-correlation between the receiving signal and the LTE downlink reference signal. Based on the measurement results, the base station can estimate the interference levels and identify a classification of UEs with respect to the uplink interference onto the incumbent. Finally, base stations can determine which UEs will be allowed/not allowed to use uplink in the LSA/SAS bands to maintain the maximum aggregate interference levels to incumbents.

We assume that the incumbents' signal power is constant on average across all the licensed bands. We consider the path loss as the main factor in channel fading. Cell edge UEs that are closer to incumbents cause more interference. Thus those UEs are more suitable for taking measurements. The measurement UEs will receive, instead of transmitting in the uplink bands, in order to measure the uplink interference. We assume that the LTE downlink reference signal and uplink signal are independent to the incumbents' signal or the noise. This means that the cross-correlation between the LTE downlink reference signal and incumbent signal or noise is equal to zero in theory or to a substantially small value in practice.

The procedure of the measurement is as follows: The base station assigns UEs to measure the incumbents' signal. As per the LTE specification, the UEs need to report their downlink channel conditions to the base station. UEs report the incumbent signal power to the base station. The base station assigns UEs with highest receiving incumbents' signal power to do uplink measurements and assigns UEs which receive the least of the incumbents' signal power to transmit uplink signals.

The time and frequency domain format of the downlink signal that is received

by the UEs is given as:

$$y_d(t) = h_{rs}(t)x_{rs}(t) + h_{inc}(t)x_{inc}(t) + n(t) \tag{4.1}$$

$$Y_d(f) = H_{rs}(f) * X_{rs}(f) + H_{inc}(f) * X_{inc}(f) + N(f) \tag{4.2}$$

where, in the time domain, $y_d(t)$ is the receiving signal, $h_{rs}(t)$ is the channel from the LTE base station to UE, $x_{rs}(t)$ is the downlink reference signal transmitted from the base station, $h_{inc}(t)$ is the channel from incumbents to UE, $x_{inc}(t)$ is the incumbent transmitted signal and $n(t)$ is the noise. In the frequency domain, $Y_d(f)$ is the receiving signal, $H_{rs}(f)$ is the channel from the LTE base station to UE, $X_{rs}(f)$ is the downlink signal transmitted from the base station, $H_{inc}(f)$ is the channel from incumbents to UE, $X_{inc}(f)$ is the incumbent transmitted signal and $N(f)$ is the noise. $*$ denotes convolution. We assume the LTE reference signal, incumbents' signal and noise are independent of each other. Thus, the average receiving downlink power is given as:

$$P_d = P_{rs} + P_{inc} + P_n \tag{4.3}$$

$$P_n = P_{rs} + P_{inc} - P_d \tag{4.4}$$

where P_d is the average receiving signal power during the downlink period, P_{rs} is the downlink reference signal receiving power, P_{inc} is the receiving power of incumbents' signal and P_n is the power of the noise.

We assume the measurement is taken both the incumbent and downlink of secondary user are transmitting at the same time. According to the CAZAC feature of Zad-off Chu sequence, we know that the correlation between the LTE reference signal and other signals is given as follows:

$$X_{rs}(f) \star X_{rs}(f) = \delta(f) \tag{4.5}$$

$$X_{rs}(f) \star X_{inc}(f) = 0 \tag{4.6}$$

$$X_{rs}(f) \star N(f) = 0 \tag{4.7}$$

where $\star$ denotes cross-correlation. Thus, we perform a cross-correlation to obtain the channel on downlink reference signal by :

$$H_{rs}(f) = Y_d(f) \star X_{rs}(f) \tag{4.8}$$

Then we can calculate the power of the downlink reference signal by:

$$P_{rs} = \frac{1}{N} \sum (H_{rs}(f) * X_{rs}(f)) = \frac{1}{N} \sum ((Y_d(f) \star X_{rs}(f)) * X_{rs}(f)) \tag{4.9}$$

The time and frequency domain of the uplink signal that is received by one measurement UE in is given as:

$$y_u(t) = \sum_{i=1}^{N_{ul}} h_{ul}^i(t) x_{ul}^i(t) + h_{inc}(t) x_{inc}(t) + n(t) \tag{4.10}$$

$$Y_u(f) = \sum_{i=1}^{N_{ul}} H_{ul}^i(f) * X_{ul}^i(f) + H_{inc}(f) * X_{inc}(f) + N(f) \tag{4.11}$$

where, in the time domain, $y_u(t)$ is the receiving signal of one measurement UE during the uplink duration. $y_u(t)$ is an aggregated signal from all the uplink transmissions. N_{ul} is the number of the uplink users. We assume the uplink transmit power is the same. $h_{ul}^i(t)$ is the channel from the i th uplink UE to the measurement UE and $x_{ul}^i(t)$ is the transmitted signal from the i th uplink UE. In the frequency domain, $Y_u(f)$ is the receiving signal of one measurement UE during the uplink duration, $H_{ul}^i(f)$ is the channel from the i th uplink UE to the measurement UE and $X_{ul}^i(f)$ is the transmitted signal from the i th uplink UE.

We assume the LTE uplink signal, incumbents' signal and noise are independent of each other. Thus, the average uplink receiving signal power is given as:

$$P_u = P_{ul} + P_{inc} + P_n \tag{4.12}$$

where P_u is the average receiving signal power during uplink period, P_{ul} is the power of the uplink signal that reached the measurement UE, P_{inc} is the receiving power of the incumbents' signal and P_n is the power of the noise. We assume that the noise power level is the same between two measurements. Therefore, we substitute P_n with (4.4). The power of the uplink signal that reached the measurement UE P_{ul} can be estimated as:

$$P_{ul}* = P_u - P_{inc} + P_n = P_u + P_{rs} - P_d \tag{4.13}$$

We define G_{all} as the set of all UEs in the cell, S_{inc} as the ordered set of all UEs, G_{all}, sorted in the descending order of P_{inc}, S_{inc}^{-1} as the ordered set of all UEs,

G_{all}, sorted in the ascending order of P_{inc} and S_{rs} as the ordered set of all UEs, G_{all}, sorted in the ascending order of P_{rs}.

We propose to select the UEs, with the highest receiving power from the incumbents' signal, and the lowest power from the LTE base station's downlink signal, to take measurements. The selected measurement UEs are closest to the incumbent at the cell boundary. All the UEs need to measure the downlink reference signal power, according to the LTE specification [94]. In our approach, all UEs need to measure the incumbents' signal once at the beginning of the measurement process. Only the selected measurement UEs need to measure the uplink signal power. The selection of the measurement UE is given as:

$$G_{ms} = S_{inc} \cap S_{rs} \tag{4.14}$$

where G_{ms} is the set of the selected measurement UEs, S_{inc} is the ordered set of all the UEs sorted as per the descending order of the receiving power from the incumbents' signal, and S_{rs} is the ordered set of all the UEs sorted as per the the ascending order of the downlink reference signal received by the base station.

Because the measurement UEs are at the boundary of the MNO cell, they are not inside of the incumbent's coverage. Thus, the uplink interference measurement will always be greater than or equal to the real interference happening inside of the incumbent cell. We can set the threshold according to the measurement to control the interference inside of the incumbent cell.

4.1.2 Selection of secondary users for transmission

After the measurement UEs are selected and the estimation of the uplink interference is obtained and sent back to the base station, the base station can select the UEs that can transmit accordingly. We propose to pick the cell boundary UEs that are far away from incumbents which will cause the least interference. Those UEs are with the lowest receiving incumbent signal power excluding the measurement UEs. The set of the selected UEs for the uplink transmission is given as:

$$G_{ul} = S_{inc}^{-1} \cap \{G_{all} - G_{ms}\} \tag{4.15}$$

$$|G_{ul}| = N_{ul} \tag{4.16}$$

where G_{ul} is the set of UEs that can transmit and S_{inc}^{-1} is the set of all the UEs sorted with the ascending order of the receiving power from the incumbents' signal.

Simulation results

We use Monte-Carlo simulations to evaluate the performance of our access approach. We set an MNO cell that has 100 uniformly distributed UEs, out of which, 9 UEs are selected as the measurement UEs and 50 UEs are selected as the UEs for uplink transmission. The base station transmit power is 43 dBm. We set the incumbent area that has 200 users and the incumbent base station's transmit power as 53 dBm. Both cells have a disk shape with the cell radius of 200 m.

We compare our uplink UE selection method with random uplink UEs' transmission. We select an equal number of UEs randomly from the UEs that have not been selected as the measurement UEs. The set of random UEs that are allowed to transmit is given as:

$$G_{rand} = rand\{G_{all} - G_{ms}\} \tag{4.17}$$

$$|G_{rand}| = N_{ul} \tag{4.18}$$

where G_{rand} is the set of randomly selected UEs for uplink transmission. We numerically calculated the average interference received by each incumbent user. The results are shown in Figure 4.2 and Figure 4.3. The interference received by the incumbent users is shown as a heat map. The results show a snapshot of the system that, the random selected UEs' uplink transmission will cause more uplink interference to the incumbent users than the selected UEs.

We then simulated on average, the interference received by the incumbent users with a different number of UEs transmitting. The results are shown in Figure 4.4. We can see from the graph that the method using selected UEs always causes less average interference to incumbents. When the number of transmitting UEs are close to the total number of UEs, the locations of the selected UEs are similar to the random UEs. With the increase of the number of transmitting UEs, the gap between two methods decreases.

We numerically calculated the gap between the measurement and actual in-

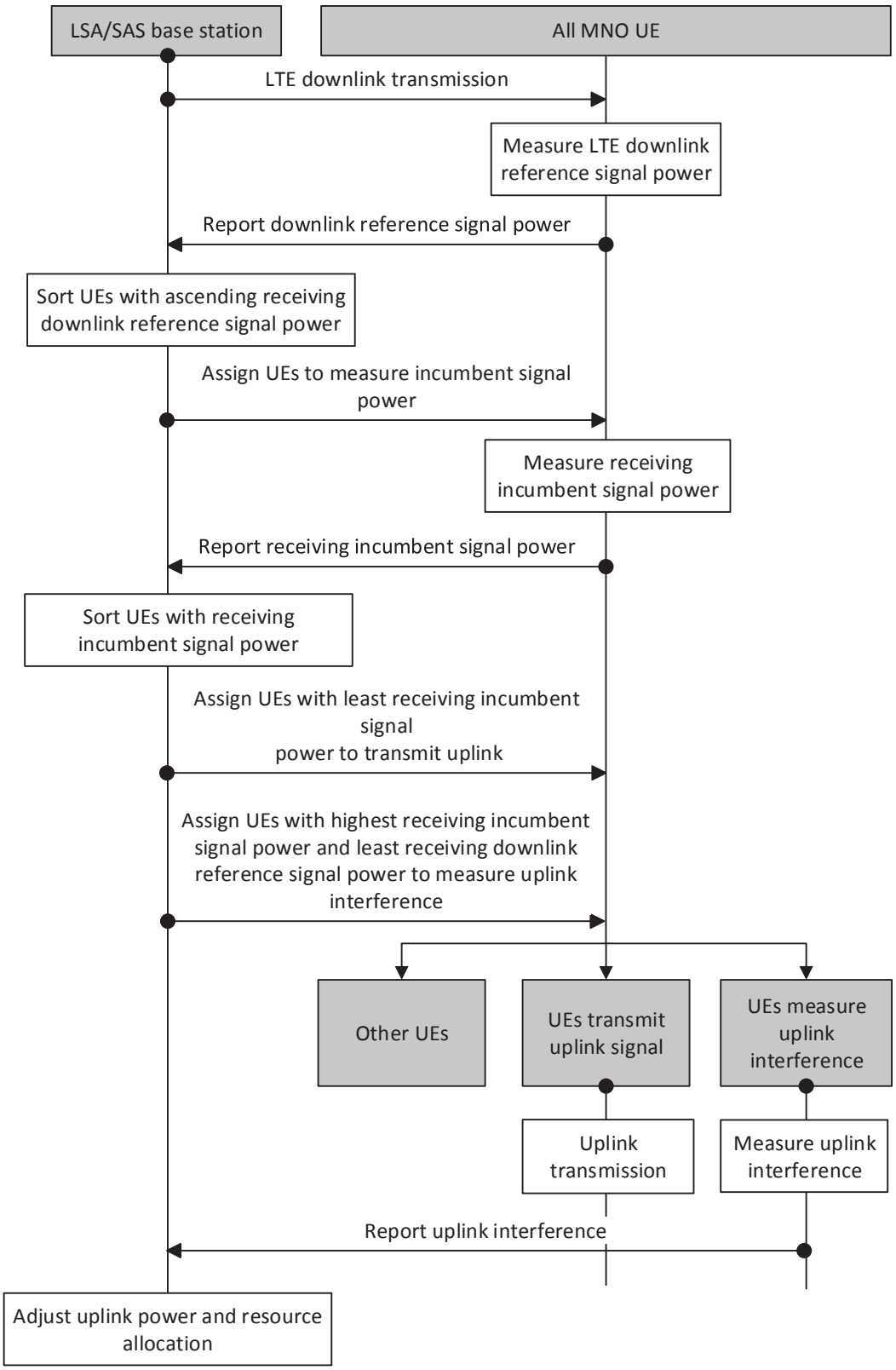

Figure 4.1: Uplink interference mitigation procedure.

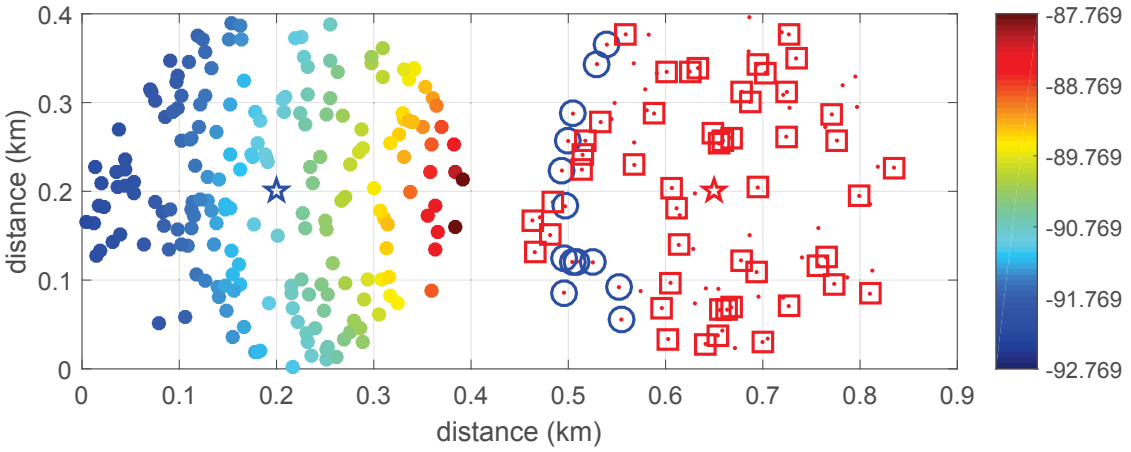

Figure 4.2: Uplink interference signal power (dB) received in the incumbents' area, with random MNO UEs transmission. One the left is the incumbent area and the right cell is operated by the MNO. The ★ in the centre represents the base station location. In the incumbent area, the scattering colour represents the level of uplink interference at the incumbent users. In the MNO cell, all UEs' locations are represented by red dots. The blue ◯ illustrates the location of measurement UEs and the red □ illustrates the random uplink transmission UEs.

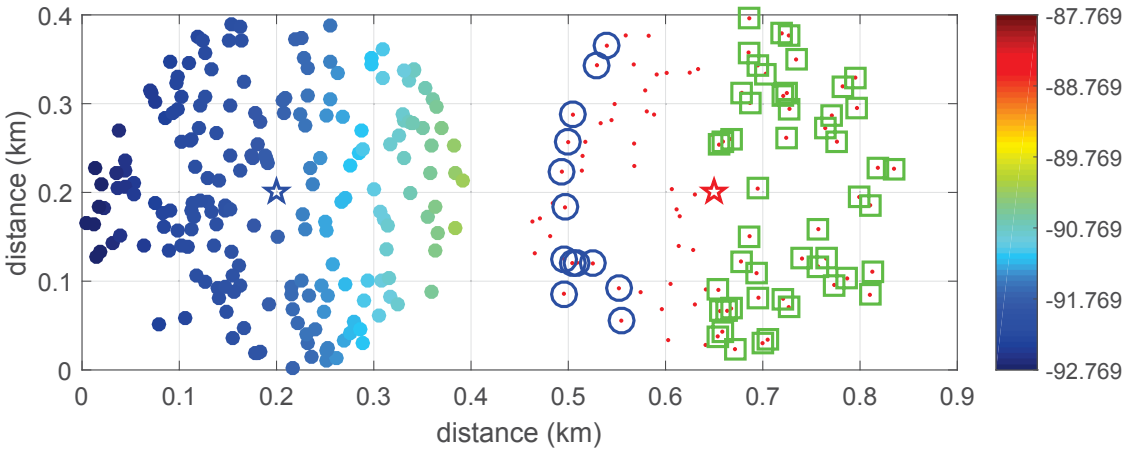

Figure 4.3: Uplink interference signal power (dB) received in the incumbents' area, with selected MNO UEs transmission. The illustration follows Figure 4.2, except that the green squares illustrate the selected UEs for uplink transmission.

terference to the incumbent users on average with random UE transmission. The results are shown in Figure 4.5. We can see from the graph that the measurement value is higher than the actual interference. There is a nearly constant offset between the measurement and the actual interference. This offset is due to the distance from

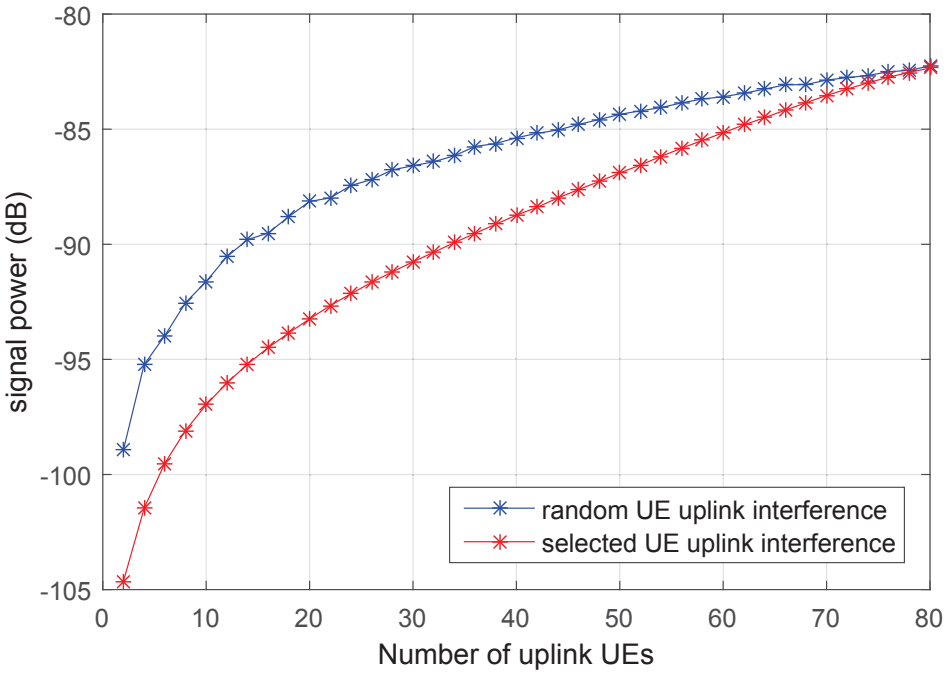

Figure 4.4: Average uplink interference received signal power of the incumbent users with random and selected UEs' transmission.

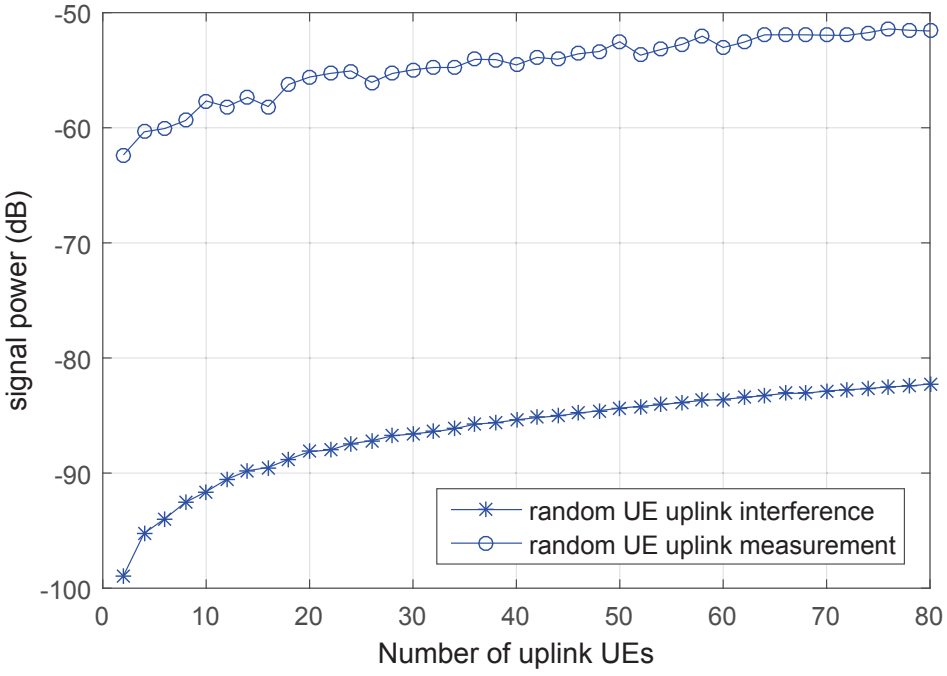

Figure 4.5: Measurement of the interference and the actual interference of uplink transmission from random UEs

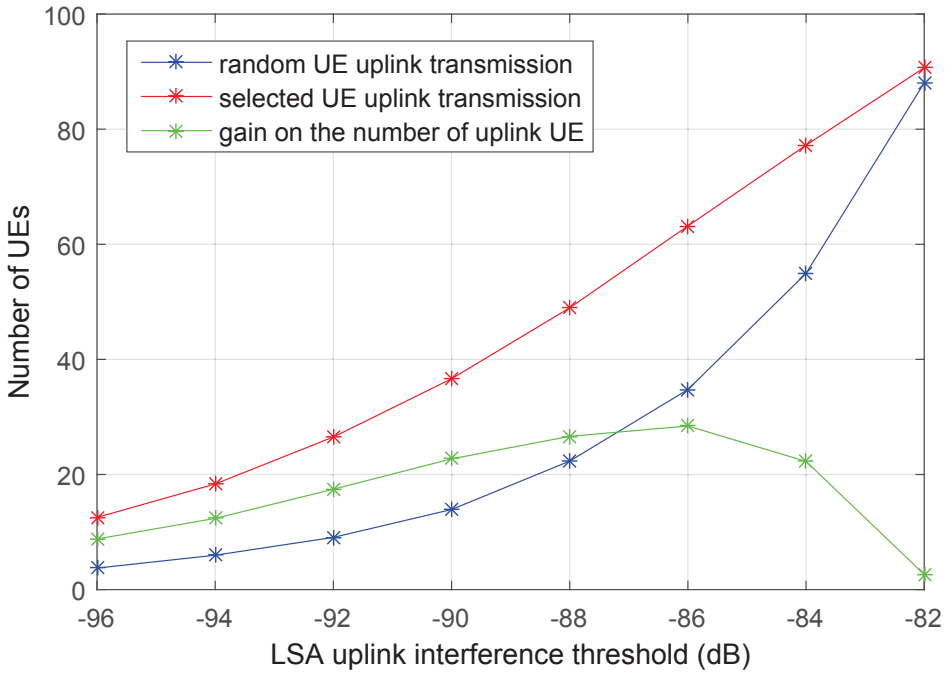

Figure 4.6: Number UEs that can transmit with different average interference threshold and the gain on the number of UEs between using selected and random UEs.

the measurement UEs to incumbents. Even if the measurement UEs detect that the interference is over a certain threshold, the secondary user network will receive a warning and the interference to incumbents is still below the threshold. This will prevent secondary users causing too much interference to incumbents.

We also calculated the maximum number of UEs that are allowed to transmit under a certain threshold. The results are shown in Figure 4.6. We calculated the gain of the number of UEs as the difference between the number of UEs allowed to transmit in our proposed approach and the number of UEs allowed if they were selected randomly, under the same interference threshold. The gain starts to increase with the increase of the number of uplink transmission UEs to a maximum number, then it starts to decrease since the number of uplink transmission UEs is close to total number of UEs, the selected UEs are approaching to be at the same locations at the randomly selected UEs.

In summary, by using measurement UEs, the secondary networks can monitor the interference to the incumbent. Moreover, by selecting the UEs that cause less

interference to the incumbent, the secondary networks can allow more UEs to access the uplink channel.

4.2 PAL detection using sub-sampling in SAS

In Spectrum Access Systems (SAS), the GAA users are able to (1) access a database with information about incumbents' locations and frequency and (2) access the results of PAL auctions and subsequent PAL frequency assignments. In the previous section, we discussed the interference from secondary users (tier two and/or three) to incumbents (tier-one) and the first type of access using selected UEs for uplink transmission. In this section, we focus on the second type of access that is the access of the GAA users (tier-three) to the PAL (tier-two) bands in SAS. Both GAA and PAL are secondary users.

GAA users need to check if the SAS band is clear and that neither the PAL nor the incumbent is active before starting the transmission. In such a context, we propose a sub-sampling method for GAA users to detect the PAL usage when the incumbent is not using the channel. In SAS, there are multiple PAL channels,

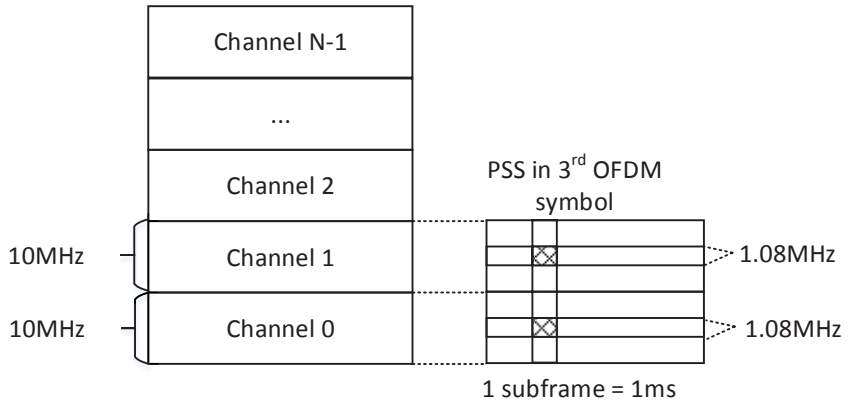

Figure 4.7: PAL channels and the LTE PSS allocation.

as illustrated in Figure 4.7. Each channel has 10 MHz bandwidth. The maximum number of channels is currently $N = 7$. GAA users can use existing spectrum sensing technologies to detect the PAL signals. Nevertheless, to improve the efficiency, we propose to use the feature of PAL signals in the detection. We assume that the PAL

network is using the LTE specifications. In the LTE specification [95], the Primary Synchronisation Sequence (PSS) is used in cell search and synchronisation. It is allocated in the third OFDM symbol of subframe 1 and 6. The PSS is generated from a Zadoff-Chu sequence with index 25, 29 and 34 for the base 63. The bandwidth of the PSS signal is 1.08 MHz which is substantially narrower compared to the PAL bandwidth 10 MHz. Thus, we propose to use sub-sampling to capture the PSS, as well as, reduce the complexity of the sampling unit in the GAA.

In our method, we choose the PSS in the LTE as the characterisation sequence for the detection. We assume, that if the GAA network detects a PSS signal in a channel, a PAL base station is regarded as active in the channel. We assume that no incumbent users are transmitting when GAA is sensing, given that if the incumbent is present, no secondary users (PAL or GAA) can access the SAS bands. According to the requirements in [7], the GAA users transmit power is substantially less than the PAL users transmit power.

The detection procedure is given as follows:

1. GAA users will synchronise to at least one PAL channel before detection.

2. After synchronisation, the GAA users will receive time domain signals $y(t)$ from multiple PAL channels in bandwidth of $10 \times N$ MHz, e.g. bandwidth is 30 MHz if $N = 3$.

3. The GAA will sub-sample the signal in the time domain, by one sampling rate α for the receiving signal $y(t)$, where α is equal or lower than the Nyquist sample rate, and obtains the sub-sampled signal in time domain $y(t')$. The sub-sampling rate α needs to be i) positive integer and ii) such that the sub-sampling can be performed through the selection of a sub-set of time domain samples (i.e., the number of OFDM carriers per symbol divided through the sub-sampling rate must result in an integer value e.g. assume that an OFDM symbol has 64 carriers, a sub-sampling rate of 4 is possible since the corresponding symbol can be created by choosing one out of 4 time domain OFDM samples. A sub-sampling rate of 5 is not possible, since 64/5 is not integer).

4. The GAA will use FFT to turn the time domain signal to the frequency domain, $y(k), k = 0, ..., N_{FFT} - 1$, N_{FFT} is the size of FFT for the sub-sampled signal, it is equal or less than the FFT size of $10 \times N$ MHz, so the complexity of FFT can be decreased.

5. The GAA will identify the frequency domain carriers relevant for the different characterisation sequences and perform cross-correlation of the sub-carriers corresponding to the target characterisation sequence cross-correlation with $r_{ud}(k)$. $r_{ud}(k)$ is generated from original characterisation sequence $r(k)$. Allocate $r(k)$ in the resource for the characterisation sequence in 10 MHz bandwidth, use IFFT of size for $10 \times N$ MHz bandwidth to turn it into the time domain, then use same sample rate α to sub-sample the sequence to obtain $r_{ud}(k)$. To improve the efficiency, we propose to detect multiple indices in parallel using the orthogonal features of the Zad-off Chu sequence. $r(k)$ is given as $r(k) = r_1(k + \Delta k_1^r) + r_2(k + \Delta k_2^r) + r_3(k + \Delta k_3^r), k = 0, ..., N_{ZC} - 1$, where $r_1(k)$, $r_2(k)$ and $r_3(k)$ are the PSS sequence with index 25, 29 and 34 respectively. $\Delta k_1^r \neq \Delta k_2^r \neq \Delta k_3^r$ and $0 \leq \Delta k_i^r < N_{ZC}$.

6. Finally, the GAA will use pulse detection to determine PAL's existence. The positions of possible pulses have a one-to-one mapping to the positions of PAL in the frequency domain. If any pulses detected in the particular position $\Delta k_i^r, i = 1, 2, 3$ in the sequence, a PAL exists respectively.

To further improve the efficiency, we propose to detect multiple PALs using parallel aggregation with cyclic shifting each PAL characterisation sequence and adding the shifted sequences together.

$$a(n) = \sum_{i=0}^{M-1} y_j((k + \Delta k_j) \bmod N_{ZC}), j = 0, ..., N_{ZC} - 1, k = 0, ..., N_{ZC} - 1 \tag{4.19}$$

where mod represents the modulo operation, M is the number of aggregated sequences, $M \leq N$, typical value is $M = 2$. Δk_j is the cyclic shift of the ith PAL's characterisation sequence. The expected pulse position is $\Delta k_i^r + \Delta k_j$.

We propose two implementations for the PAL detection method. Depending on different GAA receiver's architectures, the implementations are: sequential aggregation and parallel aggregation. For GAA receivers with the Application-Specific Integrated Circuit (ASIC) design, we aggregate multiple PAL sequences consecutively. For GAA receivers with the Digital Signal Processor (DSP) design, we combine multiple PAL sequences with parallel signal aggregation, following (4.19). The implementation is shown in Figure 4.8.

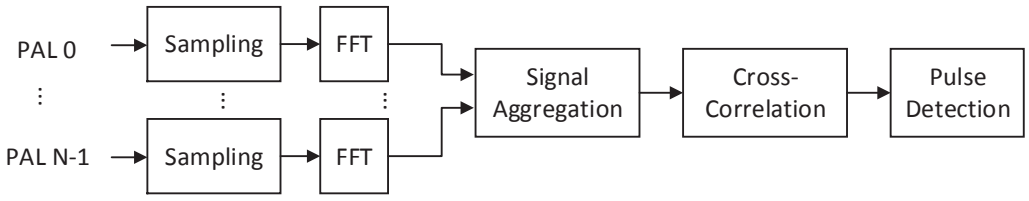

Figure 4.8: PAL detection with sequential or parallel aggregation.

4.3 WiFi and LTE coexistence for LSA and SAS in the unlicensed band

The previous section discusses the detection of PAL signals. After a GAA successfully detects a clear PAL band, the GAA will start to transmit. Since GAA operates on a cognitive basis, it is highly possible that multiple GAA will request to access the same channel which will lead to collisions between GAAs. Therefore, we propose coexistence methods to solve the collision problems between GAAs. This problem will also exist in the future LSA/SAS system between the licensees. Two mainstream transmission schemes i.e. WiFi and LTE, are considered for secondary users. If incumbents require the spectrum back, the MNO has to offload the LSA/SAS users from the licensed spectrum to another available spectrum. The unlicensed spectrum is one of possible candidates. Therefore, the secondary users coexistence in the unlicensed band is also an important problem in spectrum sharing systems. In this section, we propose coexistence schemes for WiFi and LTE in the unlicensed band. We use the term LTE-LAA [37] to denote the LTE in the

unlicensed band.

4.3.1 Offloading procedure of LSA/SAS users

The overall procedure that MNO offloads secondary users to the unlicensed band is given as follows, as illustrated in Figure 4.9.

Step 1: MNO operates LTE in the MNO band

Sense the licensed band or receive the spectrum information from LSA/SAS controller to obtain the geolocation area, available time and transmit power constraints, if the licensed band is available, go to Step 2.

Step 2: MNO operates LTE in the MNO band and licensed bands

If part of the licensed band is lost (e.g. incumbents start to reclaim the licensed band), the corresponding UEs have to vacate the reclaimed licensed band, and the MNO will offload those UEs to the unlicensed band, go to Step 3.

Step 3: MNO operates LTE in the MNO and licensed bands during the "band moving time"

The defined incumbents allow the MNO to offload the UEs in a certain time starting from reclaiming notification which is known as the "band moving time", marked as t_2 in Figure 4.10 and Figure 4.11. After the MNO receives the reclaiming notification from LSA/SAS controller, MNO base station starts to sense the unlicensed band. If the unlicensed band is available, go to Step 4.

Step 4: MNO operates LTE in the MNO band, part of licensed bands and operates LTE-LAA in the unlicensed band

If the licensed band is available again, go to Step 2.

4.3.2 LTE-LAA sensing and access solutions

We provide two solutions for the LTE-LAA sensing and access. The transmission time for the LTE-LAA t_a needs to be smaller or equal to the maximum

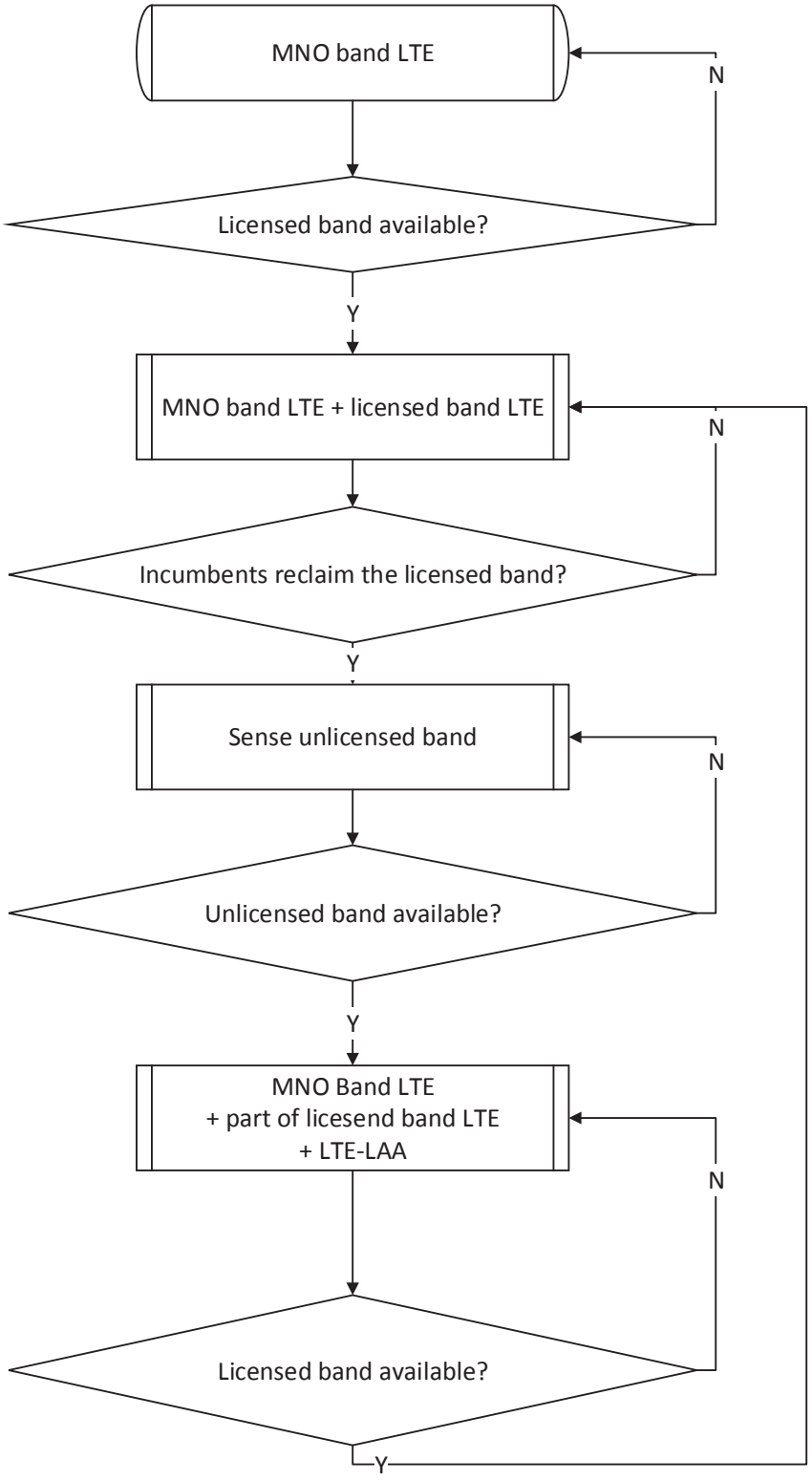

Figure 4.9: Flowchart of the LSA offloading method.

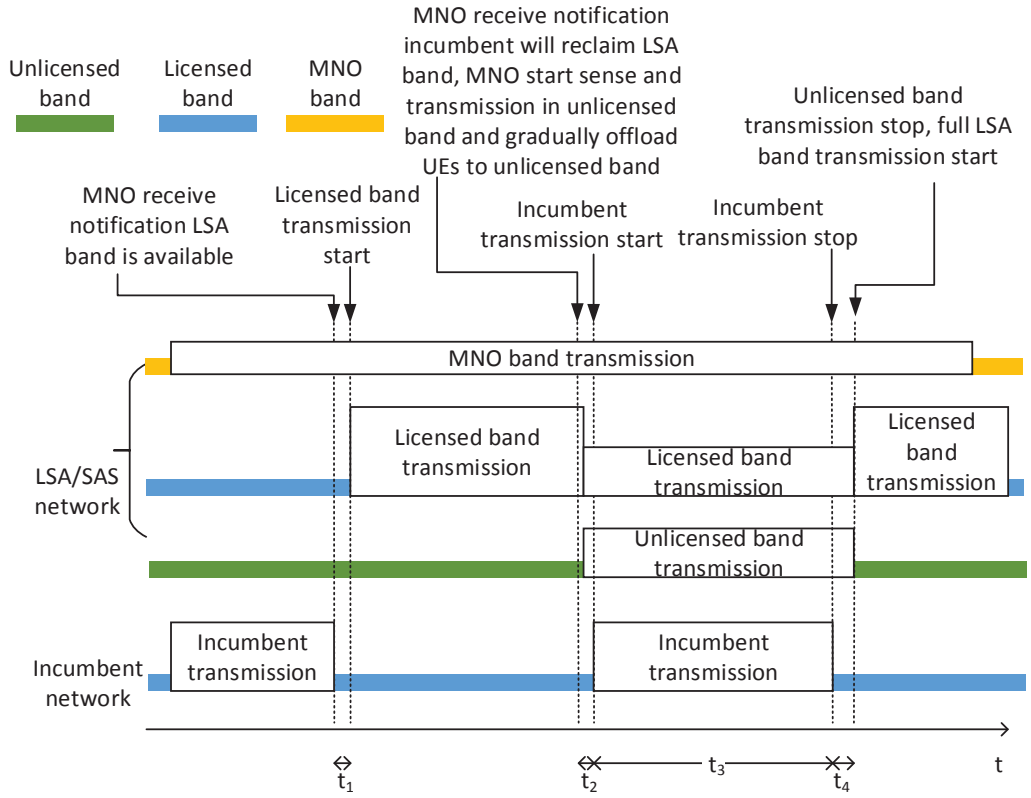

Figure 4.10: LSA offloading procedure.

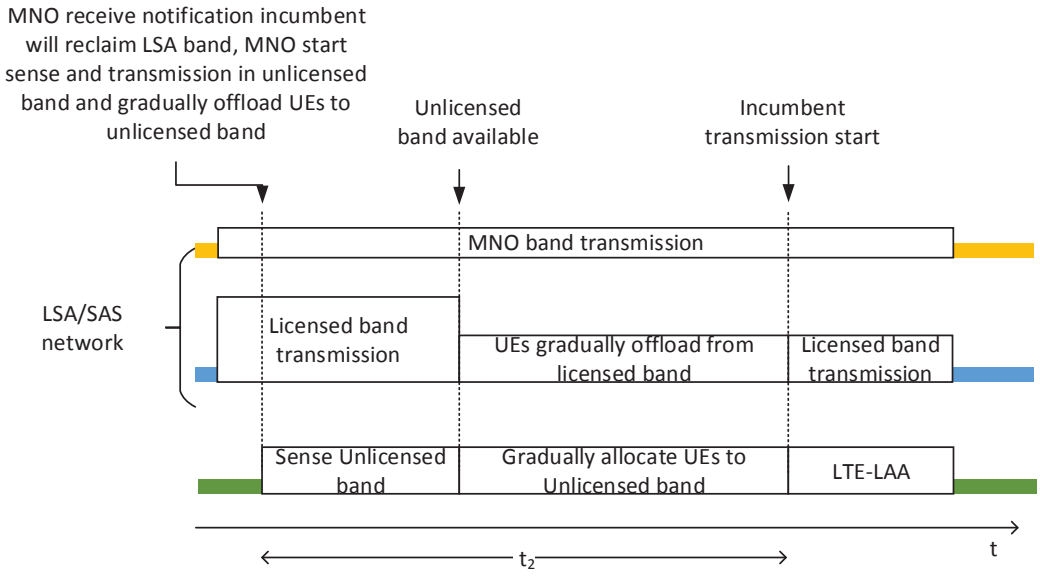

Figure 4.11: Illustration of the band moving time.

	APPDUMaxTime = 5.484ms	APPDUMaxTime = 10ms
TDD-LTE	SDL depending on the UL/DL configuration	UL and DL depending on the UL/DL configuration
FDD-LTE	UL and DL	UL and DL

Table 4.1: LTE transmission schemes

transmission time defined in 802.11 spec. (APPDUMaxTime = 5.484 ms, for very high throughput (VHT) or 10 ms for high throughput greenfield (HT-GF) [96]). The starting time of t_a needs to be aligned with the start of an LTE subframe. According to the parameters in the WiFi and LTE specification, different transmission schemes are listed as Table. 4.1. SDL is supplymentary downlink in the LTE, if t_a needs to be smaller than 5.848ms, there will be not enough time to schedule a uplink subframe [94].

Solution A: Clear Channel Assessment (CCA) only

In this solution, we assume the WiFi AP is not using Hybrid Automatic Repeat reQuest (HARQ). The LTE base station will process the sensing, if the channel is clear, the base station will start transmission. There will be collision and interference between the LTE and WiFi. One way to prevent other WiFi nodes from transmitting is to transmit a blocking signal, so if other WiFi nodes start CCA they will detect the channel as busy and stop transmitting and start backoff. This blocking signal has to start from the channel available after CCA and continue until the next LTE subframe starts. The time, illustrated as t_w in Figure 4.12 can go up to {one LTE subframe time - CCA time} which is nearly 1 ms. The transmission of only the blocking signal will underutilise the resources. When the base station knows the channel is clear after CCA, the base station will start to transmit a WiFi signal to an LTE-LAA UE. Here we assume, the LTE-LAA UE already has access to the base station via WiFi, which is reasonable because most current UEs are equipped with both the LTE and WiFi. WiFi transmission is already defined in [96], the signal will be masked with the UE identifier. The WiFi signal will last until next LTE

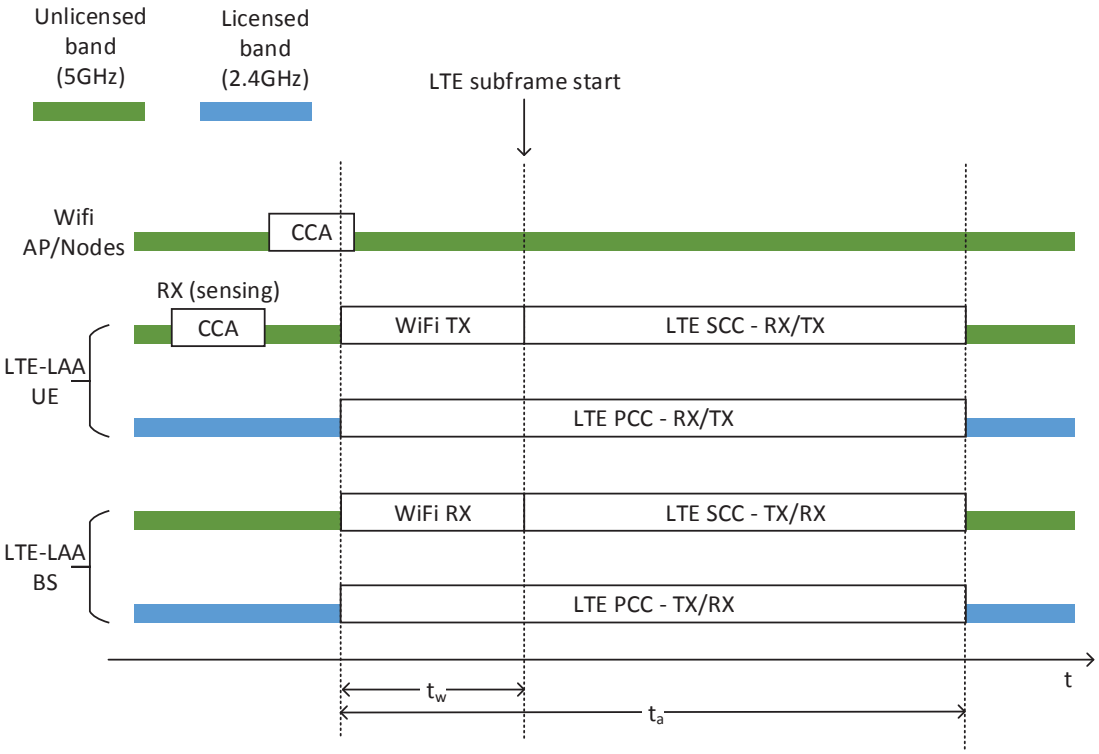

Figure 4.12: CCA only.

subframe starts. The base station will start transmitting an LTE subframe right after the WiFi signal finishes. This will not trigger any RF switch at UE, because WiFi and LTE-LAA run in the same band. If time t_w in Figure 4.12 is smaller than a valid WiFi packet transmission then a blocking signal will be transmitted.

Solution B: CCA and Request to Send / Clear to Send (RTS/CTS)

In this solution, we use the RTS/CTS to prevent interference between the LTE-LAA and WiFi. Three different settings are given as:

- The LTE-LAA base station does the CCA, after which it will transmit a dummy CTS if the channel is clear, as shown in Figure 4.13. The WiFi AP, WiFi nodes and LTE UEs will receive the dummy CTS. Thus the WiFi network will stop transmission, no interference from WiFi will happen when the LTE-LAA begins transmission.

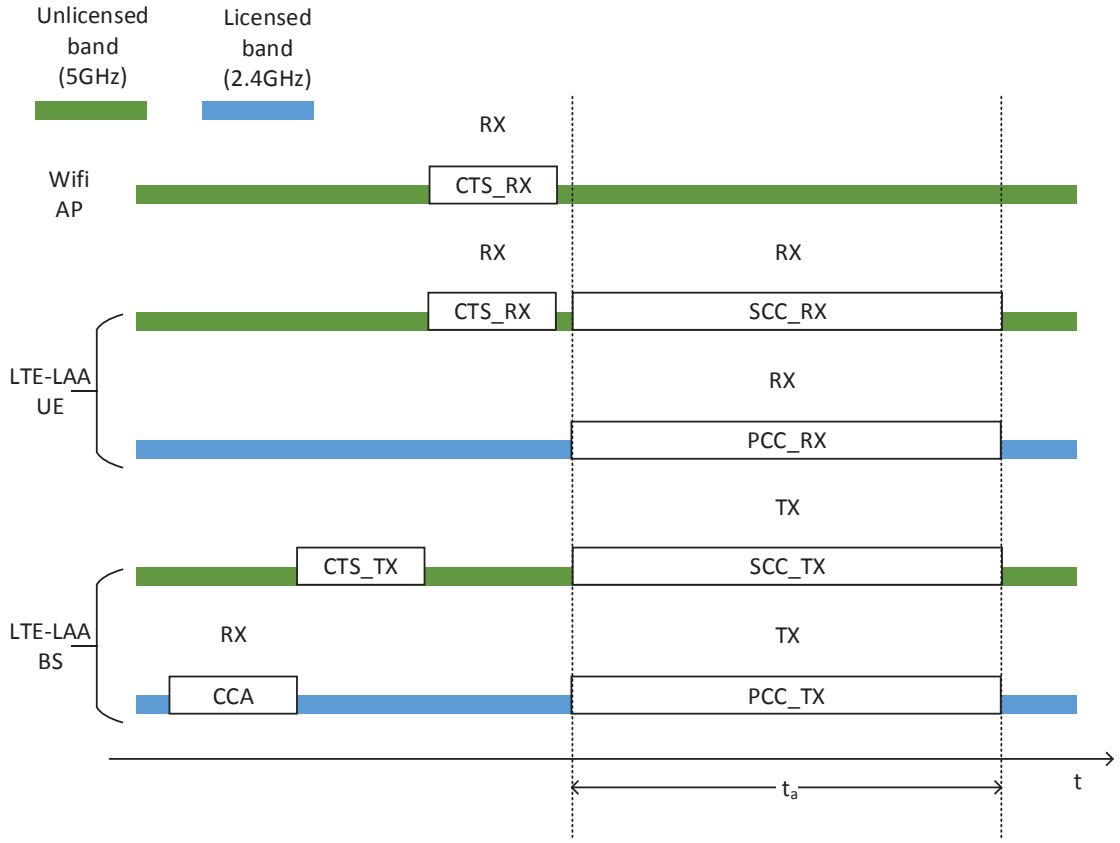

Figure 4.13: Base station does CCA.

- The LTE-LAA UE does CCA and transmits RTS to get CTS from the LTE-LAA base station, because UEs are distributed in different geolocations and have more visibility. There are two ways to start UE CCA:
  - The LTE-LAA base station assigns UEs to start CCA in the WiFi band or a specific WiFi channel, as shown in Figure 4.14. The LTE-LAA base station will know when to wait for RTS from the UEs. An indication needs to be added to the downlink control channel of the LTE specification, e.g. PDCCH.
  - The LTE-LAA UE always listens to the WiFi band. No modification to the LTE specification is needed.

In this solution, there will be no collisions between the LTE-LAA and WiFi Nodes, from the WiFi networks point of view, the LTE-LAA is the same as a WiFi node in another network.

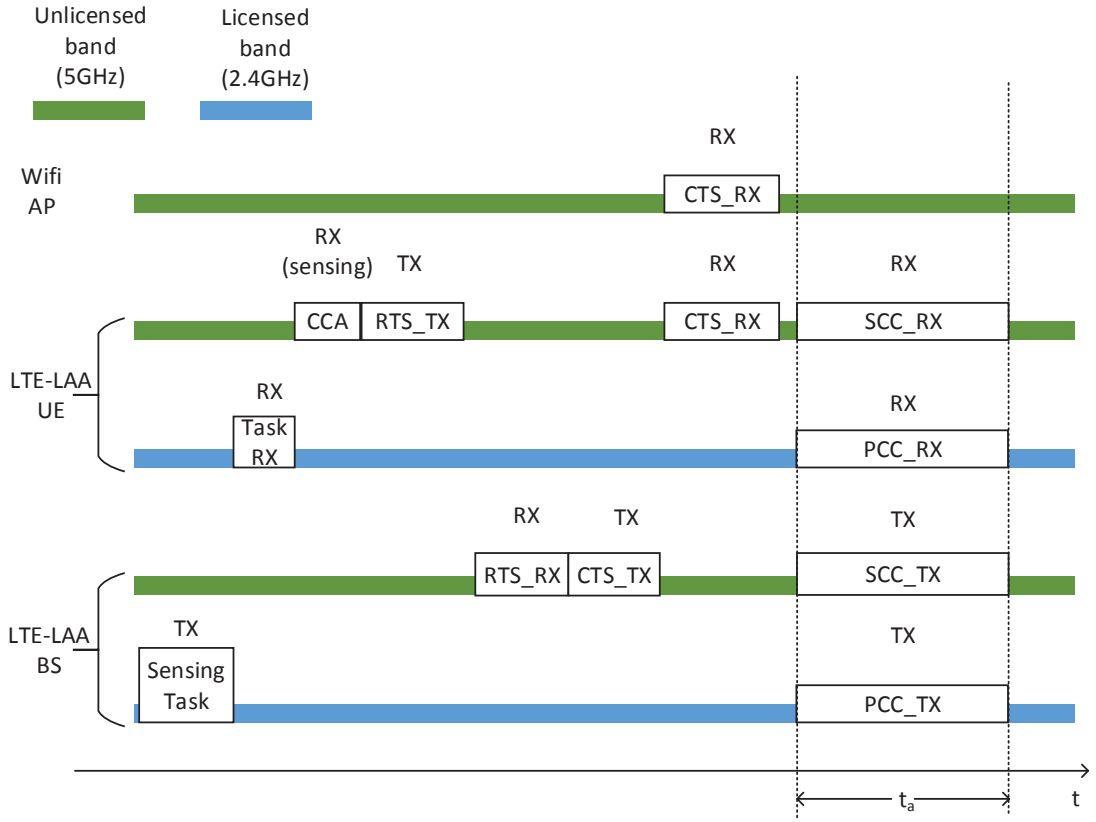

Figure 4.14: LTE-LAA base station assigns the UE to do CCA.

4.4 Summary

In this chapter we proposed spectrum access and coexistence methods for users in different tiers in LSA and SAS. Our methods cover problems in all levels of LSA and SAS frameworks. For the access of all secondary users, such as LSA licensees, PAL and GAA in SAS, to the incumbents' bands, we proposed interference measurement and user selection methods that can guarantee that the interference to incumbents remains below a certain threshold as well as enable more uplink transmission of the secondary network. For the access of the third-tier user GAA to the second-tier user PAL in SAS, we proposed an efficient PAL detection method with sub-sampling. For the access and coexistence between cognitive basis secondary users, we propose WiFi and LTE coexistence in the unlicensed band for offloading secondary users to avoid collisions and to maintain fairness.

In Chapter 3 and Chapter 4, we have discussed interference mitigation, spec-

trum access and coexistence in the spectrum sharing framework. The frameworks involve incumbents, third-party entities and MNOs. The overall target is to provide the MNOs with more spectrum resources given that incumbents are well protected. How to leverage spectrum sharing to further enhance the capacity performance, even after MNOs have obtained extra spectrum, or even with their currently allocated spectrum is also a key problem. This will be discussed in the next chapters.

Chapter 5

Capacity Analysis of Cloud Radio Access Networks with Coordinated Multi-Point and Fractional Frequency Reuse

To achieve better capacity performance in the cellular network, MNOs need to utilise the given spectrum resources efficiently. In the previous chapters, we have proposed methods to solve the problem in spectrum sharing frameworks to provide MNOs with extra spectrum. In this chapter, we investigate how to use spectrum sharing techniques in the cellular network to increase capacity.

We choose the Cloud Radio Access Networks (C-RAN) to be the network architecture and introduce Coordinated Multi-Point (CoMP) and Fractional Frequency Reuse (FFR) to further enhance coordination and mitigate interference. The system model is given in Section 5.1. We first analyse the differential capacity of C-RAN with multiple coordinated antennas in Section 5.2. Multiple-Input-Multiple-Output (MIMO) techniques are introduced to the system and the performance is analysed in Section 5.3. Lastly, we analyse the capacity of C-RAN with one of the spectrum sharing frameworks discussed in the previous chapters, i.e. LSA, in Section 5.4.

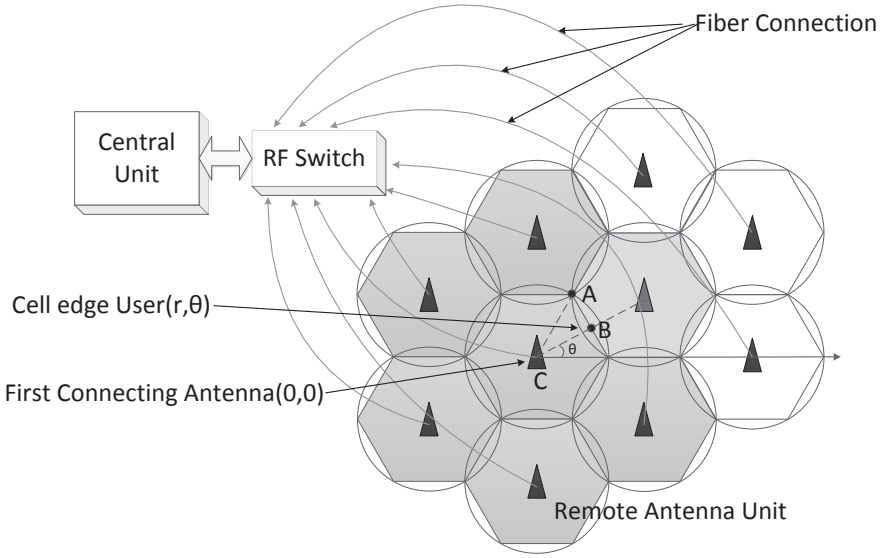

Figure 5.1: Cloud Radio Access Network architecture.

5.1 System model

Consider a C-RAN multicellular and multiuser system including hexagonal shaped cells with one antenna in the centre of each cell and mobile users in each cell. All the antennas are geographically distributed and connected through fiber to a remote central unit, as illustrated in Figure 5.1.

5.1.1 SU-MISO using Joint Transmission

We consider a Single-User Multiple-Input-Single-Output (SU-MISO) transmission. We use Cooperative Joint Transmission (CJT), as a form of MISO transmission. We assume the use of the Maximum Ratio Transmission (MRT) precoding technique, the received signal by a user k is given by [97]:

$$y_k = \sum_{j \in B_S} \sqrt{P_t} h_{jk} x_k + \sum_{i \in B_I} \sqrt{P_t} h_{ik} x_{im} + n_k \tag{5.1}$$

where n_k is the Additive White Gaussian Noise (AWGN) of which the power density is N_0 and x_k is the original transmitting signal to user k. The transmitting antenna set is B_S and the interfering antenna set is B_I, h_{jk} is the channel gain from transmitting antenna j to user k, i is the index of the interfering antenna, h_{ik} is

the channel gain from interfering antenna i to user k and x_{im} is the transmit signal from antenna i to the user m it is serving.

Thus, the downlink capacity of user k is given as:

$$C_k = BW_k \log_2(1 + \gamma_k) \tag{5.2}$$

where the signal-to-interference-plus-noise ratio (SINR) is given as:

$$\gamma_k = \frac{\sum_{j \in B_S} P_t |h_{jk}|^2}{\sum_{i \in B_I} P_t |h_{ik}|^2 + P_n} \tag{5.3}$$

where

$$P_n = N_0 \times BW \tag{5.4}$$

where N_0 is the noise power density and BW is the bandwidth.

A special simplified case is when the co-channel interference is equal to zero, the signal-to-noise-ratio (SNR) is given as:

$$\gamma_k = \frac{\sum_{j \in B_S} P_t |h_{jk}|^2}{P_n} \tag{5.5}$$

We assume γ follows a distribution with Probability Density Function (PDF) $f_{\Gamma_N}(\gamma)$. We consider a UE at the coordinates (r, θ) of the polar coordinate system, and a base station at the centre with coordinates $(0, 0)$, as the point C illustrated in Figure 5.1. The capacity is given as:

$$C(r, \theta) = \int_0^\infty \log_2(1 + \gamma) f_{\Gamma_N(r,\theta)}(\gamma) d\gamma \tag{5.6}$$

The ergodic capacity for a user at the cell boundary is given by:

$$\begin{aligned} C_{edge,N} &= \frac{1}{2\pi} \int_0^{2\pi} \int_0^\infty \log_2(1 + \gamma) f_{\Gamma_N(r_e,\theta_e)}(\gamma) d\gamma d\theta_e \\ &= \frac{1}{\pi/6} \int_0^{\pi/6} \int_0^\infty \log_2(1 + \gamma) f_{\Gamma_N(r_e,\theta_0)}(\gamma) d\gamma d\theta_0 \end{aligned} \tag{5.7}$$

where $r_e = \frac{\sqrt{3}}{2} R_0 \cos^{-1}(\theta_0 - \frac{\pi}{6}))$, where (r_e, θ_e) is the coordinate of cell edge user. To simplify the calculation, we consider 1/6 of the cell edge with the coordinate (r_e, θ_0).

5.1.2 MU-MIMO using Coordinated Beamforming

We consider MU-MIMO transmission. Two antennas are transmitting to two users with different beams. We use CoMP-CB to accomplish MU-MIMO transmission, thus the received signal matrix for a pair of coodinated users is given by:

$$\mathbf{y} = \sqrt{P_t}\mathbf{H}\mathbf{x} + \sum_{i \in B_I} \sqrt{P_t}\mathbf{H}_i\mathbf{x}_i + \mathbf{n} \tag{5.8}$$

where $\mathbf{x} \in \mathbb{C}_{2\times1}^T$ is the transmitting signal from the remote antenna units, $\mathbf{H} \in \mathbb{C}_{2\times2}$ is the channel fading matrix, $\mathbf{x}_i \in \mathbb{C}_{2\times1}^T$ is the transmitting signal from the other remote antenna units to interfering users, $\mathbf{H}_i \in \mathbb{C}_{2\times2}$ is the channel fading matrix to interfering users, $\mathbf{n} \in \mathbb{C}_{2\times1}^T$ is the AWGN of power density equal to N_0 and $\mathbf{y} \in \mathbb{C}_{2\times1}^T$ is the received signal of two users at the sectors of neighbour cells. B_I denotes the interfering antenna set. We use zero-forcing beamforming precoding to obtain MIMO multiplexing gain and the precoding matrix is:

$$\mathbf{M} = \mathbf{H}^\dagger \tag{5.9}$$

where $\mathbf{H}^\dagger$ denotes the pseudo-inverse matrix of square matrix $\mathbf{H}$. Then the transmitting signal from the remote antenna units becomes:

$$\mathbf{x} = \mathbf{M}\mathbf{s} \tag{5.10}$$

where $\mathbf{s} \in \mathbb{C}_{2\times1}^T$ is the source transmitting data from the antenna units. However, in order to achieve a fair comparison with SU-MISO case, equal transmit powers should be used in comparison, hence we set the precoding matrix to satisfy the power constraint as:

$$\mathbf{M}_S = \frac{\mathbf{H}^\dagger}{\|\mathbf{H}^\dagger\|} \tag{5.11}$$

Thus, the received signal is given by:

$$\mathbf{y} = \sqrt{P_t}\mathbf{H}\mathbf{M}_S\mathbf{s} + \sum_{i \in B_I} \sqrt{P_t}\mathbf{H}_i\mathbf{M}_{Si}\mathbf{s}_i + \mathbf{n} \tag{5.12}$$

and the MU-MIMO CoMP-Coordinated Beamforming (CB) capacity is:

$$C = BW \log_2 \left| \mathbf{I} + \frac{P_t\mathbf{H}\mathbf{M}_S\mathbf{M}_S^*\mathbf{H}^*}{\sum_{i \in B_I} P_t\mathbf{H}\mathbf{M}_S\mathbf{M}_S^*\mathbf{H}^* + P_n} \right| \tag{5.13}$$

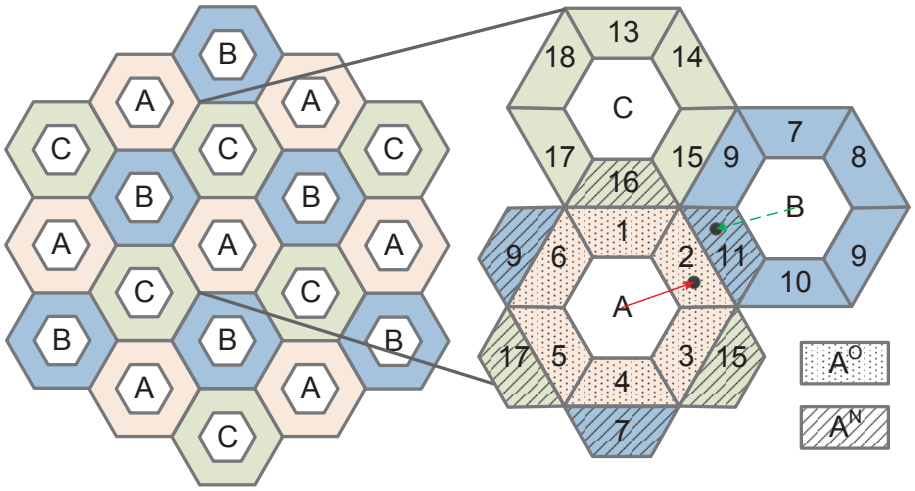

Figure 5.2: Two-tier three-cell cluster deployment with FFR. A^O denotes sectors in the reference cell. A^N denotes sectors in the neighbour cells.

where $\mathbf{H}^*$ denotes the conjugate transpose of square matrix $\mathbf{H}$. We assume that the receiver has perfect channel information, we can use the block diagonalisation (BD) algorithm to demodulate the signal by:

$$[\mathbf{S}\ \mathbf{V}\ \mathbf{D}] = \text{svd}(P_t \mathbf{H}\mathbf{M}_S\mathbf{M}_S^*\mathbf{H}^*) \tag{5.14}$$

and select the diagonal value of the matrix $\mathbf{V}$ as:

$$\lambda_j = \text{diag}(\mathbf{V}) \tag{5.15}$$

Thus, the downlink capacity of MU-MIMO CB user k is given as:

$$C_k = BW_k \log_2 |1 + \gamma_k^{CB}| \tag{5.16}$$

where

$$\gamma_k^{CB} = \frac{\prod_j \lambda_j}{\prod_i \lambda_i + \delta_n^2} \tag{5.17}$$

5.1.3 Fractional Frequency Reuse

We assume that users are uniformly distributed in each cell, the user number is the same for each cell. Our idea of spectrum sharing in this section is by dividing the

bandwidth into frequency slices using FFR. We assume that each slice has the same bandwidth and for each user there is another user occupying the same bandwidth in the interfering cell. The bandwidth of each frequency slice is given as :

$$\frac{BW_{edge}}{N_f} = \frac{BW_{all} - BW_{centre}}{N_f} \tag{5.18}$$

where BW_{edge} is the bandwidth at the cell edge, BW_{centre} is the bandwidth in the cell centre and N_f is the frequency division number. We assume that the size of the cell centre is 2/3 of the cell radius.

We use a cell cluster to construct the cellular model. We assume that N_c cells in a cluster and denote a cell in a cluster as $A_k, k = 1, ..., N_c$. We choose a typical 3-cell cluster model as illustrated in Figure 5.2. Cell A, B, C in a cluster is denoted as $A_k, k = 1, 2, 3$. We divide each cell edge into six sectors. Denote each sector in A_k as $a_i^k, i = 1, ..., 6$. Each sector will be allocated with one frequency slice $f_n, n = 1, ..., N_f$. The bandwidth of a frequency slice is $|f_n| = \frac{BW_{edge}}{N_f}$. The frequency slices f_n will be allocated to sectors a_i.

The downlink average capacity of the cell boundary users with the noise power P_n is given as:

$$E[C(N_f, P_n)] = \frac{1}{N_{ue}} \sum_{1}^{N_{ue}} C(N_f, P_n) \tag{5.19}$$

where N_{ue} is the number of downlink UEs.

5.2 Differential capacity analysis of C-RAN

In this section, we investigate a baseline case in C-RAN of multiple transmitting base stations and a single receiving user under low SNR conditions. We derive closed-form upper and lower bounds in efficiently computable expressions for differential capacity (DCAP) using the moment generating function (MGF) of SNR. Bounds accuracy is evaluated and compared to results in the current literature. Numerical results corroborate our analysis and the analytic bounds on DCAP are tight in the low SNR regime. Furthermore, the upper bound performs better compared with the approximation obtained in [69] under two different channel models. These lower

and upper bounds provide more accurate capacity measures, which can be used in the evaluation of DAS performance and C-RAN design.

In this section, we assume that $N_f = 1$ and $BW = 1$ Hz. We also assume that the channel gain h_i is Rayleigh distributed, according to [98], the power of channel gain h_i^2 is exponentially distributed. Thus, SNR γ_i, which is the summation of exponentially distributed variables, becomes Erlang distributed obeying the probability density function (PDF) of $f_{\Gamma_N}(\gamma)$ and mean of λ_i^{-1}.

Considering the impact of path loss, the longer the distance between the antenna and UE, the higher the loss experienced by the signal resulting in the lower SNR regime. Therefore, the sequence of connecting the antennas follows the nearest first rule. The connecting antenna when $i = 1$ is the same as in the traditional cellular network which has the shortest distance to UE.

5.2.1 Differential capacity bounds

DCAP is the capacity increment obtained by adding one additional transmitting antenna. It is well known that increasing the number of transmitters improves capacity. Therefore our primary interest is how much can capacity be increased by providing an additional antenna. The upper and lower bounds provide limits on the changes of DCAP with the increasing number of antennas. Knowledge of the bounds can help make antenna choices, allocate transmit power and design efficient transmission schemes for C-RAN communication.

As defined above, DCAP is given as:

$$\Delta C_N^{N-1} = C_N - C_{N-1} = I_N \lambda_N^{-1} \tag{5.20}$$

where, N is the number of antennas transmitting jointly to a user and λ_N^{-1} is the mean of distribution of SNR with N antennas transmitting:

$$I_N = \int_0^\infty \frac{f_{\Gamma_N}(\gamma)}{1+\gamma} d\gamma \tag{5.21}$$

The upper bound for high SNR has been proposed in [99] by:

$$\Delta C_N^{N-1} \leq \frac{1}{N-1} \tag{5.22}$$

However, this bound may not be suitable for low SNR and a tighter bound can be obtained by using the Moment Generating Function (MGF) approach [69]:

$$\frac{\varphi_{\Gamma_N}(-1)}{\lambda_N} \leq \Delta C_{N-1}^{N} \leq \frac{\varphi_{\Gamma_N}(-1)}{\lambda_N} + \frac{M_d}{\lambda_N} \tag{5.23}$$

where $\phi_{\Gamma_N}(s)$ is the MGF of the distribution Γ_N and M_d is a constant obtained numerically, according to [69].

According to the definition of the MGF:

$$\varphi_{\Gamma_N}(t) = E(e^{t\gamma}) = \int_0^{+\infty} e^{t\gamma} f_{\Gamma_N}(\gamma) d\gamma \tag{5.24}$$

when $t = -1$,

$$\varphi_{\Gamma_N}(-1) = E(e^{-\gamma}) = \int_0^{+\infty} e^{-\gamma} f_{\Gamma_N}(\gamma) d\gamma. \tag{5.25}$$

Since $f_{\Gamma_N}(\gamma)$ is the PDF of Γ_N, $f_{\Gamma_N}(0) = \lambda_1$ when $N = 1$ and $f_{\Gamma_N}(0) = 0$ for any $N > 1$ and (5.25) can be written as:

$$\int_0^{+\infty} e^{-\gamma} f_{\Gamma_N}(\gamma) d\gamma = \int_0^{+\infty} e^{-\gamma} f'_{\Gamma_N}(\gamma) d\gamma. \tag{5.26}$$

Furthermore, as proposed in [99], the derivative of $f_{\Gamma_N}(\gamma)$ with respect to γ can be written as a recursion expression:

$$-\frac{df_{\Gamma_N}(\gamma)}{d\gamma} = \lambda_N [f_{\Gamma_N}(\gamma) - f_{\Gamma_{N-1}}(\gamma)]. \tag{5.27}$$

Substitute (5.27) into (5.26) leads to:

$$\begin{aligned} \int_0^{+\infty} e^{-\gamma} f_{\Gamma_N}(\gamma) d\gamma &= \int_0^{+\infty} e^{-\gamma} \lambda_N [f_{\Gamma_{N-1}}(\gamma) - f_{\Gamma_N}(\gamma)] d\gamma) \\ &= \lambda_N \int_0^{+\infty} e^{-\gamma} f_{\Gamma_{N-1}}(\gamma) - \lambda_N \int_0^{+\infty} e^{-\gamma} f_{\Gamma_N}(\gamma). \end{aligned} \tag{5.28}$$

Thus, the recursive expression of $\varphi_{\Gamma_N}(-1)$ can be written as:

$$\varphi_{\Gamma_N}(-1) = \lambda_N \varphi_{\Gamma_{N-1}}(-1) - \lambda_N \varphi_{\Gamma_N}(-1). \tag{5.29}$$

Substitute (5.29) into (5.23), the recursive upper bound for DCAP can be obtained as:

$$\Delta C_N^{N-1} \leq \frac{\varphi_{\Gamma_{N-1}}(-1)}{\lambda_N + 1} + \frac{M_d}{\lambda_N} \leq \frac{\lambda_{N-1} \Delta C_{N-1}^{N-2}}{\lambda_N + 1} + \frac{M_d}{\lambda_N} < \frac{\lambda_{N-1} \Delta C_{N-1}^{N-2}}{\lambda_N} + \frac{M_d}{\lambda_N} \tag{5.30}$$

and the recursive lower bound for DCAP can be obtained as:

$$\Delta C_N^{N-1} \geq \frac{\varphi_{\Gamma_{N-1}}(-1)}{\lambda_N + 1} \geq \frac{\lambda_{N-1}\Delta C_{N-1}^{N-2}}{\lambda_N} - \frac{M_d}{\lambda_N} \tag{5.31}$$

(5.30) and (5.31) can be helpful when deciding whether to add another remote unit antenna in C-RAN to transmit to the UE, by evaluating the expression with current DCAP ΔC_{N-1}^{N-2}, current SNR λ_{N-1} and next stage SNR λ_N.

From (5.30) and (5.31), the bounds are given as:

$$\lambda_N \Delta C_N^{N-1} \gtrless \lambda_{N-1}\Delta C_{N-1}^{N-2} \pm M_d \tag{5.32}$$

From (5.32), we can see that M_d represents the difference between $\lambda_N \Delta C_N^{N-1}$ and $\lambda_{N-1}\Delta C_{N-1}^{N-2}$. (5.32) can be used to roughly predict the next stage DCAP.

For more accurate bounds, the closed-form expressions can be derived from (5.29) as:

$$\varphi_{\Gamma_N}(-1) = \frac{\lambda_N \varphi_{\Gamma_{N-1}}(-1)}{\lambda_N + 1} = \prod_{i=2}^{N} \frac{\lambda_i}{\lambda_i + 1} \varphi_{\Gamma_1}(-1) \tag{5.33}$$

where

$$\begin{aligned} \varphi_{\Gamma_1}(-1) = &\int_0^{+\infty} e^{-\gamma} f_{\Gamma_1}(\gamma) d\gamma = \int_0^{+\infty} e^{-\gamma} \lambda_1 e^{-\lambda_1 \gamma} d\gamma \\ = &\lambda_1 (-\frac{1}{\lambda_1 + 1} e^{-(\lambda_1+1)\gamma}|_0^{+\infty}) = \frac{\lambda_1}{\lambda_1 + 1} \end{aligned} \tag{5.34}$$

We assume that $\lambda_i \leq \lambda_N$ for $i = 1, ..., N-1$, substituting (5.34) into (5.33) gives:

$$\prod_{i=1}^{N} \frac{\lambda_1}{\lambda_1 + 1} \leq \varphi_{\Gamma_N}(-1) = \prod_{i=1}^{N} \frac{\lambda_i}{\lambda_i + 1} \leq \prod_{i=1}^{N} \frac{\lambda_N}{\lambda_N + 1} \tag{5.35}$$

In summary, the lower bound is given as:

$$\Delta C_N^{N-1} \geq \frac{(\frac{\lambda_1}{\lambda_1+1})^N}{\lambda_N} \tag{5.36}$$

with equality if $\lambda_i = \lambda_1$, and the upper bound is given as:

$$\Delta C_N^{N-1} < \frac{(\frac{A\lambda_N}{\lambda_N+1})^N}{\lambda_N} + \frac{M_d}{\lambda_N} \tag{5.37}$$

for $\lambda_N \leq 1$, where A and M_d are positive constants.

(5.36) and (5.37) indicate that in the limiting case under low SNR, DCAP for C-RAN downlink depends on SNR and the number of antennas. This differs from the conclusion drawn under high SNR in [69] where DCAP is independent of SNR and only replies on the number of antennas.

To calculate these bounds, SNR values from different links need to be collected and processed together which may be a problem for the traditional cellular network. However, in C-RAN, all the signals and data will be gathered at the central unit enabling better cooperative processing with no backhaul.

Capacity at cell boundaries

Ergodic capacity has been analysed in the previous section for an UE at a given location under low SNR. This section provides a more general view on the capacity of an UE located at the edge of a cell.

We assume that the UE is at the location (r, θ) of the polar coordinate system, and consider the first connected antenna as the centre at location $(0, 0)$, as the point C illustrated in Figure 5.1. The conditional capacity is an integration of the capacity at the location on the edge of two neighbouring cells as given by (5.6). Therefore ergodic capacity for a user at the cell boundary is given by (5.7).

Thus, the DCAP for a user at the cell boundary is given by:

$$\Delta C_{edge,N}^{N-1} = C_{edge,N} - C_{edge,N-1} \tag{5.38}$$

that represents the capacity increment for a user at the cell boundary served by between N antennas and $N-1$ antennas.

As analysed above, the upper bound obtained from the MGF analysis should be tighter than the one obtained in [69]. This subsection compares the new bounds, bound from [69] and simulation data under low SNR. The accuracy of the bounds is discussed in the following subsections.

5.2.2 Simulation results

In order to evaluate the accuracy of the bounds, the bounds obtained from the derived expressions have been compared to Monte-Carlo (MC) simulations con-

ducted on (5.38). Upper and lower bounds and the simulation results have been illustrated in Figure 5.3 to Figure 5.6.

The channel model in the simulations includes the small scale fading channel and the large scale fading channel which is the path loss. Shadow fading is not considered because it is assumed that for a cellular network shadow fading from antenna to UE is a constant value. The channel gain is given by $h_i = g_i * \sqrt{\Omega_i}$ [62], where g_i is the small-scale channel gain which is modelled as a Rayleigh channel and Ω_i is the multiplication of path loss and shadow fading from antenna i to the UE in which only path loss L_i has been taken into consideration in this section. Two different simulation channel models have been included in the simulation.

One is the classical wireless path loss model proposed by Goldsmith in [88] given as $L_i = K(\frac{d_i}{d_0})^{-\beta}$, where K is a constant parameter related to the antenna features and channel attenuation, d_i is the distance between antenna i and UE, d_0 is the reference distance, β is the path loss exponent. The scenario considered in this section is the cellular network C-RAN, thus Non-line-of-sight (NLOS) path loss parameters are configured for the simulation, including $d_0 = 10$ m and $\beta = 4.5$ dB [88].

The other model used in the simulations is the LTE path loss model proposed by 3GPP in [93]. The NLOS path loss model is used in the simulation, given as $L_i = 103.4 + 24.2 \log_{10}(d_i)$, where d_i is the distance from antenna i to UE in units of km.

It is apparent that the upper bound obtained from (5.36) is lower than the one from [69] for the considered cases. The lower bound obtained from (5.37) is also shown in those figures.

Monte Carlo simulations under both channel models, where the constant values $A = 1.5$ and $M_d = 0.01$ according to [69], have been carried out and they coincide with the analytical ones, hence verifying the accuracy of our analytical results.

Accuracy of proposed closed-form bounds

Figure 5.3 to Figure 5.6 show graphically the accuracy of the closed-form bounds that have been proposed. For further quantification of (5.36) and (5.37) and to assess

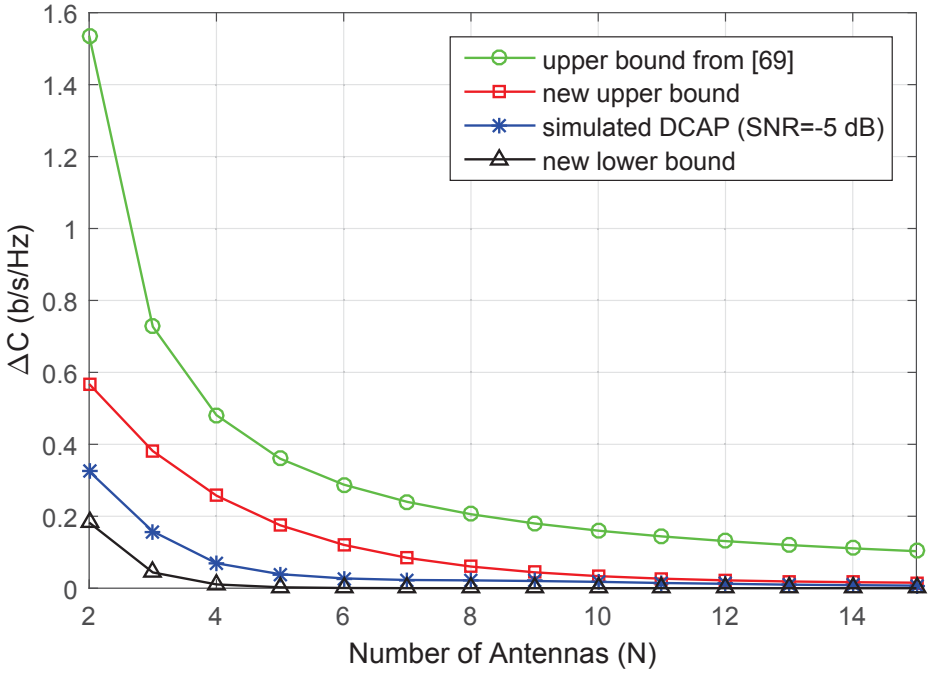

Figure 5.3: DCAP under Goldsmith path loss model, SNR = -5 dB.

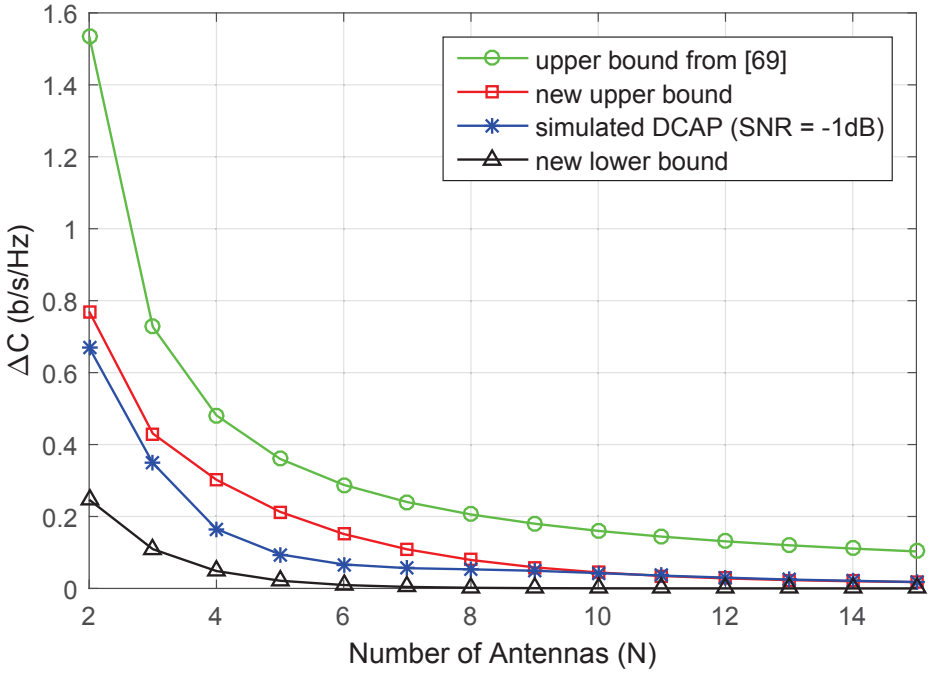

Figure 5.4: DCAP under Goldsmith path loss model, SNR = -1 dB.

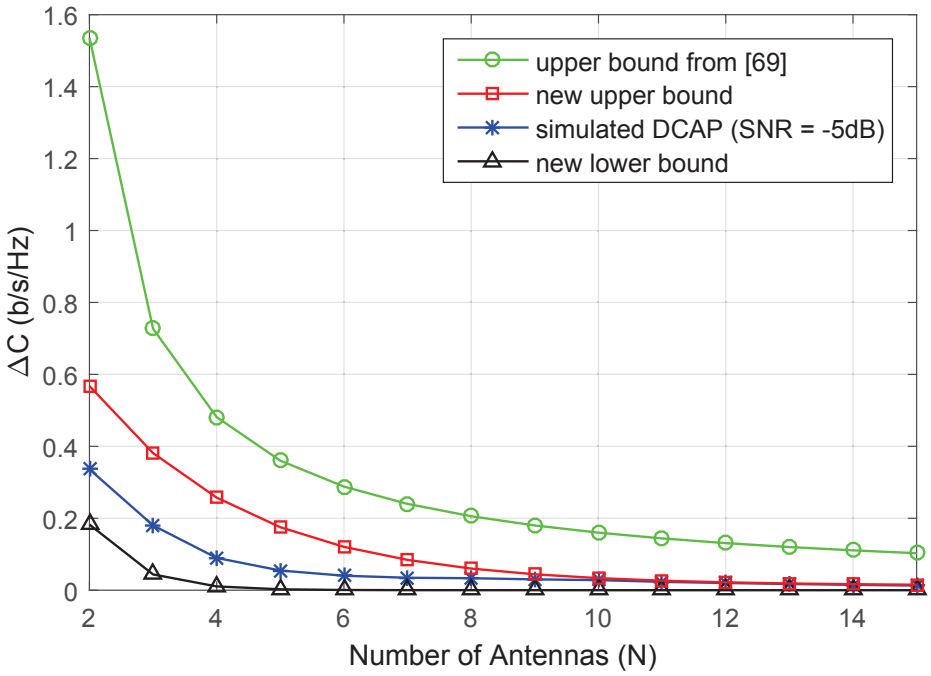

Figure 5.5: DCAP under LTE path loss model, SNR = -5 dB.

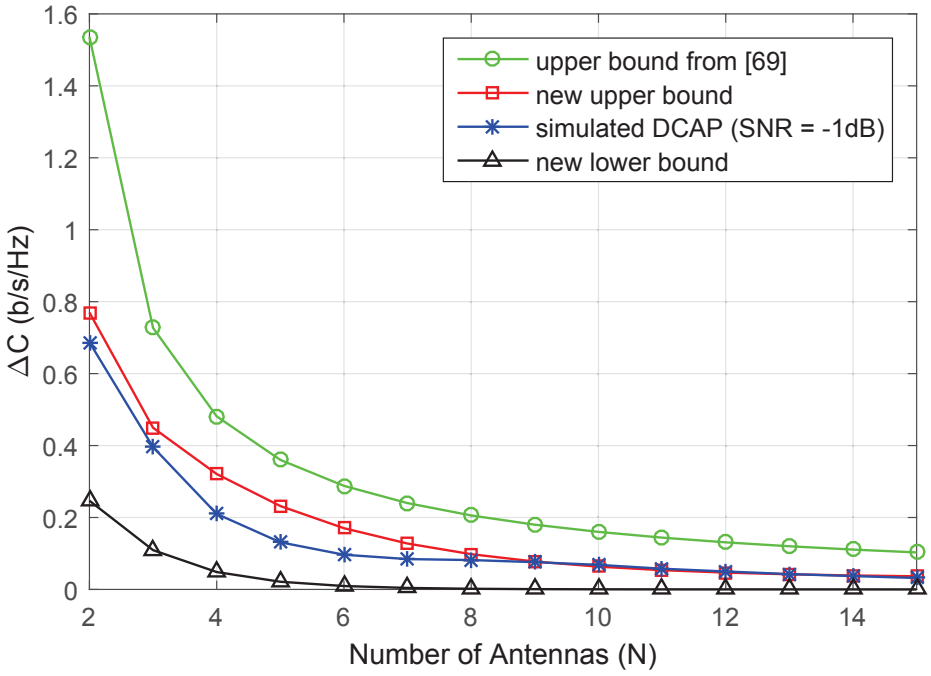

Figure 5.6: DCAP under LTE path loss model, SNR = -1 dB.

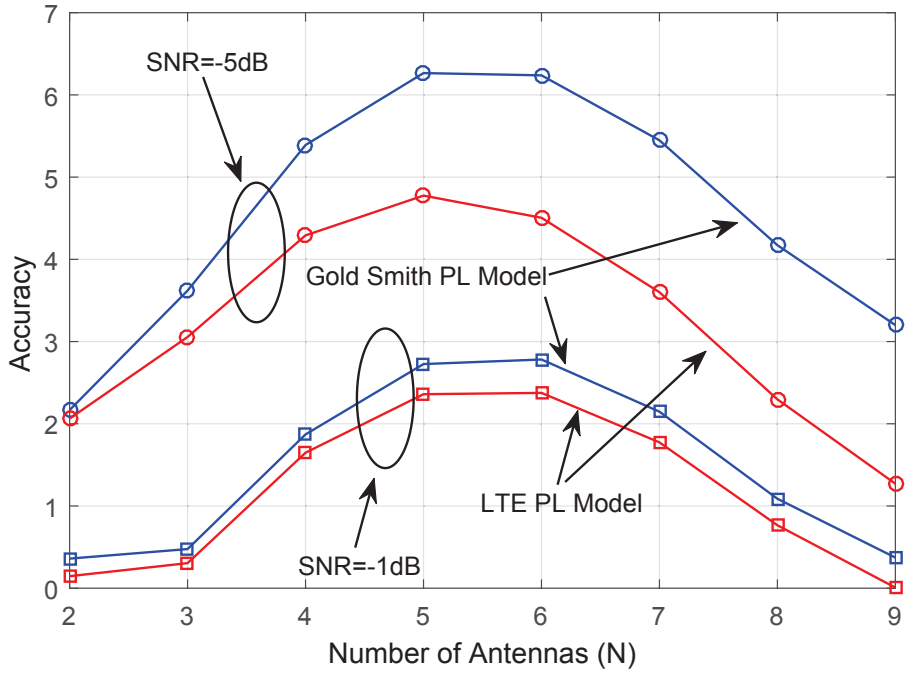

Figure 5.7: Accuracy of new upper bound.

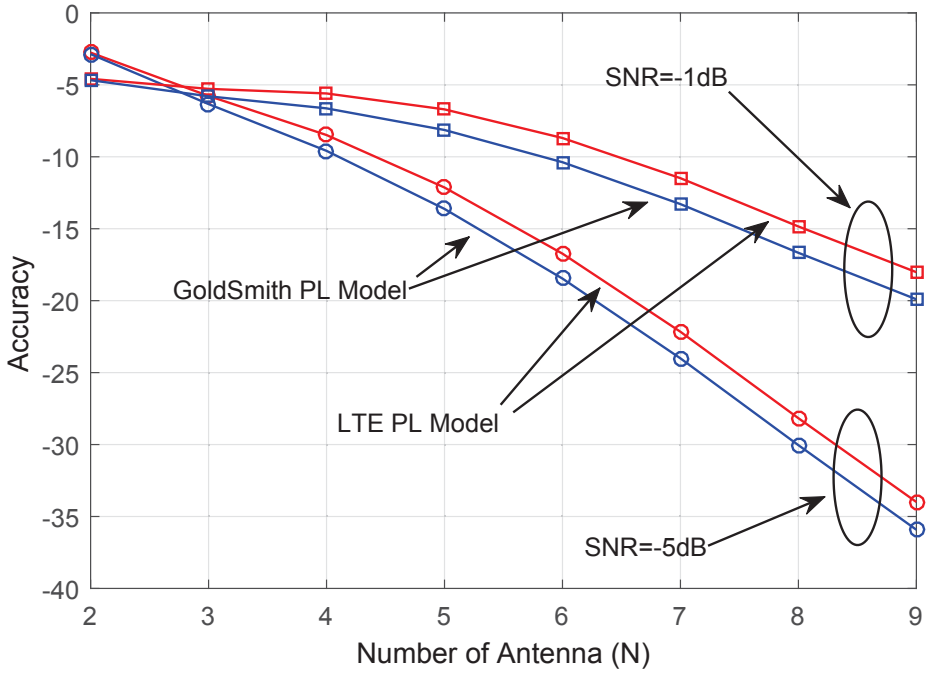

Figure 5.8: Accuracy of new lower bound.

their dependency on the number of antennas N, the following metric is used [100]:

$$\text{Accuracy} = 10\log_{10}\left(\frac{DCAP_{BD}(N)}{DCAP_{MC}(N)}\right) \tag{5.39}$$

$$= DCAP_{BD}(N)(dB) - DCAP_{MC}(N)(dB) \tag{5.40}$$

where $DCAP_{BD}$ is the analytical result with the bounds we derived and $DCAP_{MC}$ is the numerical result with the MC simulation. The accuracy results are shown in Figure 5.7 and Figure 5.8. The figures indicate that the bounds are much tighter for SNR = -1 dB than for SNR = -5 dB and under the LTE path loss model than under the Goldsmith path loss model. The upper bound in (5.36) has good accuracy with the varying number of antennas while the accuracy of the lower bound in (5.37) decreases with the increasing number of antennas which is mainly due to DCAP being quite low for a large number of antennas and due to the exponential nature of the expression.

Thus, the upper bound can be used for all antenna numbers and the lower bound can be more suitable when the number of antennas is low.

5.3 MIMO capacity analysis of C-RAN

In the previous section, we studied the differential capacity of C-RAN with SU-MISO scheme. In this section, we compare the C-RAN capacity between MU-MIMO and SU-MISO methods. As illustrated in Figure 5.9, to avoid neighbour sectors' interference, two neighbour sectors are allocated different frequency resources, $A_k^O \neq A_k^N$. To further avoid inter cluster interference, $N_f \geq 3N_c$ and $\forall N_f \geq 3N_c$, the interfering cells are the same and with the increase of N_f the bandwidth for each sector $\frac{BW_{all}}{N_f}$ will decrease, thus we pick $N_f = 3N_c = 18$.

The frequency allocation is different with that in the SU-MISO CoMP-JT case, because the two cooperating antenna units transmit the signal to two users in the neighbour sectors at the same time and same frequency $A_k^O = A_k^N$ as illustrated in Figure 5.10. To avoid intra-cell interference the six sectors in a cell are allocated different frequency resources $N_f >= 6$. We construct the cell topology with a 3-cell cluster consisting of 18 sectors. Considering the sectors and neighbour sectors of

cell A, they cover 12 sectors. 6 neighbour sectors are left which can be allocated 3 different frequency resources. Thus, to avoid intra-cluster interference $N_f >= 9$, we select $N_f = 9$.

5.3.1 Capacity comparison between MU-MIMO and SU-MISO

The performance improvement from MIMO over SISO is well known as the diversity SNR gain [101]. In this section, the capacity gain of MU-MIMO over SU-MISO comes from two factors: bandwidth gain from spectrum sharing and diversity gain from beamforming.

The bandwidth for each sector is different, according to our frequency allocation:

$$N_f^{MISO} > N_f^{MIMO} \tag{5.41}$$

The CoMP-CB SNR gain has been proposed by [102]:

$$\gamma_{MISO} < \gamma_{MIMO} \tag{5.42}$$

We compare the capacity as:

$$C_{MISO} = \frac{BW}{N_f^{MISO}} \log_2(1 + \gamma_{MISO}) \tag{5.43}$$

$$C_{MIMO} = \frac{BW}{N_f^{MIMO}} \log_2(1 + \gamma_{MIMO}) \tag{5.44}$$

Thus we have $C_{MIMO} > C_{MISO}$, and the performance gain is relevant to the difference of N_f.

We evaluate the capacity from two aspects, the capacity distribution over random uniformly located users, and the capacity changes with different transmitting SNRs.

Downlink capacity has been analysed in the previous section for an UE at a given location under low SNR. For all users in the cell edge of a cell, the CDF of capacity is investigated according to (5.7).

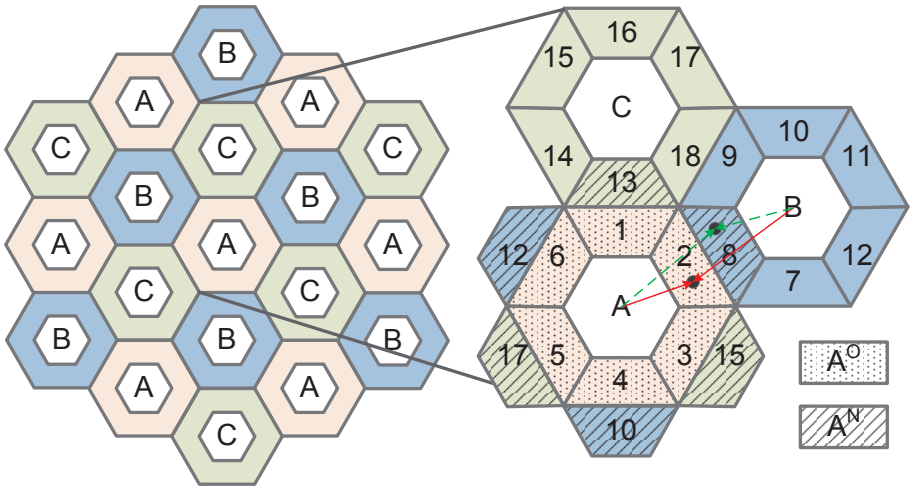

Figure 5.9: MISO Fractional Frequency Reuse pattern, $N_f = 18$.

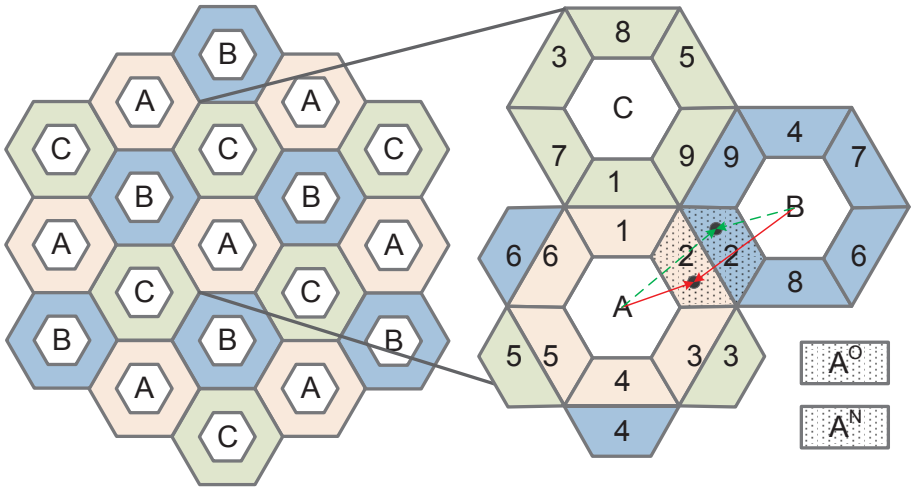

Figure 5.10: MU-MIMO Fractional Frequency Reuse pattern, $N_f = 9$.

Capacity with a transmitting SNR constraint

In [103], capacity is analysed with respect to the transmit power with a fixed noise power. We consider the performance for cell edge users, the constraints of transmitting SNR $\gamma_0 = \frac{P_t}{N_0}$ are more suitable than only considering the transmit power. The capacity with the transmitting SNR γ_0 is given as:

$$C_{edge,E} = E[C(r, \theta|\gamma_0)] = \frac{1}{N_{ue}} \sum_{e=1}^{N_{ue}} C(r_e, \theta_e|\gamma_0) \tag{5.45}$$

Costs and constraints from SU-MISO to MU-MIMO

We have analysed the capacity of SU-MISO and MU-MIMO, however, there are costs and constraints on upgrading from SU-MISO to MU-MIMO. The MU-MIMO CoMP-CB requires matrix diagonalisation. Yet, a $N \times N$ square matrix is diagonalisable if and only if the sum of the dimensions of its eigenspaces is equal to N. Thus, the user selection constraint for MU-MIMO is that, no co-located users should be paired as the CoMP-CB users, because they may have the same channel fading and the matrix will be not diagonalisable.

Therefore, to obtain better performance, more computational operations are required from SU-MISO than from MU-MIMO. This can be considered as a trade-off between performance and computational complexity. Moreover, not all users may be able to utilise MU-MIMO. Because we assumed there will be pairs of users for MU-MIMO, in reality the user distribution may not be even and user paring and selection will be constraints using MU-MIMO. If no suitable users could be paired for MU-MIMO, it will degrade into SU-MISO. The FFR allocation and capacity analysis depends on a snapshot of users evenly distributed and if the user distribution changes after a period of time the central unit of the C-RAN system is assumed to have adequate ability to do the allocation computation again.

5.3.2 Simulation results

The channel model considered in the simulations follows that in Section 5.2.2. The path loss model follows the classical wireless path loss model proposed by Goldsmith in [88] with $d_0 = 10$ m and $\beta = 4$ dB.

We use the Monte-Carlo method to simulate the capacity with and without considering inter-cell interference. The simulation results agree with our analysis in the previous section. The cell radius is 500 m and the user number in each cell is 120.

The simulation results of capacity CDF of the cell edge users is shown in Figure 5.11, and the capacity with different transmitting SNR γ_0 is shown in Figure 5.12. The schemes are compared under the same user distribution snapshot and capacity

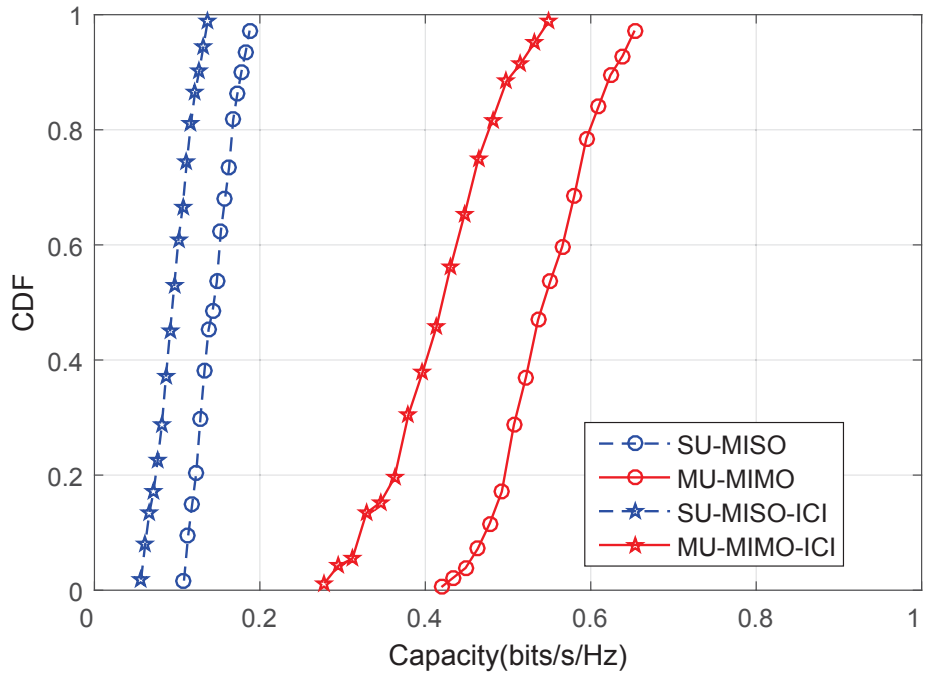

Figure 5.11: SU-MISO and MU-MIMO capacity CDF comparison.

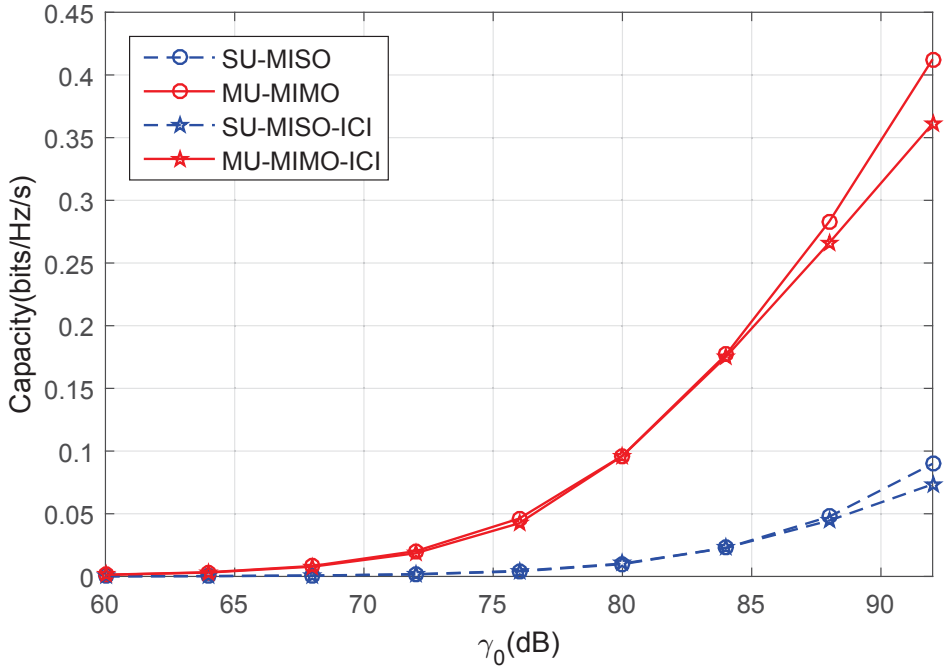

Figure 5.12: SU-MISO and MU-MIMO capacity with different transmitting SNR conditions.

CDF is evaluated under a certain transmitting SNR.

The simulation results agree with our previous analysis. MU-MIMO produces better performance than SU-MISO by approximately 6 dB with the performance improvement coming from the combination of spectrum sharing and diversity gain. ICI will cause a decrease in capacity and affect the MU-MIMO case more than the SU-MISO case.

5.4 Capacity analysis of C-RAN using LSA

As we mentioned in Section 2.2, in the next generation wireless communication networks, spectrum sharing frameworks will provide cellular networks more frequency resources. In the previous sections, we analysed the capacity of C-RAN standalone. In this section, we introduce LSA to C-RAN and investigate the performance of the combination. Due to the geolocation area limits of LSA, if we introduce LSA to the MU-MIMO CB C-RAN system for one particular cell, this cell will obtain more spectrum. However, the cell edge users have to quit from MU-MIMO CB and use SU-MISO JT in LSA band, since the neighbour cell users are not allowed to use LSA spectrum. Moreover, the previously paired and cooperated users in the neighbour cell will also have to quit from MU-MIMO CB and use SU-MISO JT in the MNO band. We compare the performance between using LSA and not using LSA by comparing the average downlink capacity of these two scenarios and use the comparison results for decision making on the usage of LSA. The comparison problem is divided into three parts:

1. Downlink capacity analysis of MNO users using MU-MIMO CB, LSA cell edge users using SU-MISO JT and previously paired MNO users using SU-MISO JT;

2. Average capacity comparison and threshold for using LSA or not;

3. Average capacity gain between using LSA or not.

5.4.1 Downlink capacity analysis for cell edge users

We assume that N_{LSA} users in the LSA cell, such as the central cell A in Figure 5.10, are switched from the previous band to the LSA band. We assume that all remote antenna units support both MNO band and LSA band. The number of paired users is equal to the number of LSA users according to our user paring assumption.

The average capacity of CB transmission is given as:

$$E\left[C^{CB}\right] = \frac{\sum_{k=1}^{N_{UE}} C_k^{CB}}{N_{UE}} = \frac{BW_{edge}}{9}\log_2\left(1 + E\left[\gamma^{CB}\right]\right) \tag{5.46}$$

The average capacity of LSA transmission is given as:

$$\begin{aligned} E\left[C^{LSA}\right] &= \frac{1}{N_{UE}}\sum_{k=1}^{N_{UE}} C_k \\ &= \frac{\sum_{k=1}^{N_{LSA}} C_k^{JT_0} + \sum_{k=1}^{N_{LSA}} C_k^{JT_1} + \sum_{k=1}^{N_{UE}-2N_{LSA}} C_k^{CB}}{N_{UE}} \\ &= \frac{N_{LSA}\left(E\left[C^{JT_0}\right] + E\left[C^{JT_1}\right]\right) + (N_{UE} - 2N_{LSA})E\left[C^{CB}\right]}{N_{UE}} \\ &= \alpha\left(E\left[C^{JT_0}\right] + E\left[C^{JT_1}\right]\right) + (1-2\alpha)E\left[C^{CB}\right] \end{aligned} \tag{5.47}$$

where C^{JT_0} is the average SU-MISO JT capacity of users in the LSA cell edge and C^{JT_1} is the average SU-MISO JT capacity of the previously paired users in the sectors of neighbour cells. We use $\alpha = \frac{N_{LSA}}{N_{UE}}$ to denote the ratio between the number of LSA users over the number of all users.

We consider a snapshot of the random located users, for one user k in the LSA cell edge, the downlink SU-MIMO JT capacity is given as:

$$C_k^{JT_0} = BW_k^{LSA}\log_2\left(1 + \gamma_k^{JT_0}\right) \tag{5.48}$$

where $BW_k^{LSA} = \frac{BW^{LSA}}{6}$. We assume only cell A is in the LSA zone and there are no other cells using the same frequency resource in the LSA band with cell A, thus there is no interference from other cells for LSA users in our model.

$$\gamma_k^{JT_0} = \frac{\sum_{j\in B_S} P_t|h_{jk}|^2}{P_n} \tag{5.49}$$

However, for one user k, there are interfering signals from other cells using the same frequency slices. Thus, the downlink SU-MISO capacity considering ICI is given as:

$$C_k^{JT_1} = BW_k^{JT_1} \log_2\left(1 + \gamma_k^{JT_1}\right) \tag{5.50}$$

where $BW_k^{JT_1} = BW_k^{CB} = \frac{BW_{edge}}{N_f}$, we select $N_f = 9$ and

$$\gamma_k^{JT_1} = \frac{\sum_{j \in B_S} P_t |h_{jk}|^2}{\sum_{i \in B_I} P_t |h_{ik}|^2 + P_n} \tag{5.51}$$

Thus, the average capacity of all the cell edge users with some users using LSA bandwidth is given as:

$$\begin{aligned} E[C^{LSA}] &= \alpha \left(\frac{BW_{LSA}}{6} \log_2\left(1 + E\left[\gamma^{JT_0}\right]\right) + \frac{BW_{edge}}{9} \log_2\left(1 + E\left[\gamma^{JT_1}\right]\right) \right) \\ &\quad + (1 - 2\alpha) \frac{BW_{edge}}{9} \log_2\left(1 + E\left[\gamma^{CB}\right]\right) \\ &= BW_{edge}\alpha \left(\frac{\eta}{6} \log_2\left(1 + E\left[\gamma^{JT_0}\right]\right) + \frac{1}{9} \log_2\left(1 + E\left[\gamma^{JT_1}\right]\right) \right) \\ &\quad + BW_{edge}(1 - 2\alpha) \frac{1}{9} \log_2\left(1 + E\left[\gamma^{CB}\right]\right) \end{aligned} \tag{5.52}$$

where $\eta = \frac{BW_{LSA}}{BW_{edge}}$ denotes the ratio between the LSA bandwidth and the MNO cell edge bandwidth. Moreover, the user ratio α and the bandwidth ratio η is independent with $E[\gamma^{JT_0}]$, $E[\gamma^{JT_1}]$ or $E[\gamma^{CB}]$.

Average downlink capacity comparison

Our target is using LSA to obtain an increase in capacity. Therefore, the problem is to find out when we can obtain higher average capacity with LSA bandwidth than the original MNO bandwidth, and then we can make the decision whether or not to use LSA bands and how much bandwidth we need to fulfil the capacity requirements. We compare (5.52) and (5.46) and it leads to:

$$\begin{aligned} &\alpha(3\eta \log_2(1 + E[\gamma^{JT_0}]) + 2\log_2(1 + E[\gamma^{JT_1}]) \geq 4\alpha \log_2(1 + E[\gamma^{CB}])) \\ &\quad 3\eta \log_2(1 + E[\gamma^{JT_0}]) + 2\log_2(1 + E[\gamma^{JT_1}] \geq 4\log_2(1 + E[\gamma^{CB}])) \end{aligned} \tag{5.53}$$

We assume that $E[\gamma^{JT_0}]$, $E[\gamma^{JT_1}]$ and $E[\gamma^{CB}]$ are all far greater than one, then we use $\log_2(1 + a) \approx \log_2(a), a \gg 1$ to obtain an approximation of (5.53) given as :

$$\eta \geq \frac{4\log_2(E[\gamma^{CB}]) - 2\log_2(E[\gamma^{JT_1}])}{3\log_2(E[\gamma^{JT_0}])} \tag{5.54}$$

Thus, the threshold of η is given as:

$$\eta* = \frac{4E[\gamma_{dB}^{CB}] - 2E[\gamma_{dB}^{JT_1}]}{3E[\gamma_{dB}^{JT_0}]} \tag{5.55}$$

Average downlink capacity gain

We assume that we have enough LSA bandwidth with $\eta > \eta*$, the performance gain on LSA over the original MU-MIMO MNO is given as :

$$\begin{aligned} G &= \frac{E[C^{LSA}]}{E[C^{CB}]} \\ &= \frac{BW_{edge}\left(\alpha\left(\frac{\eta}{6}\log_2(1+E[\gamma^{JT_0}]) + \frac{1}{9}\log_2(1+E[\gamma^{JT_1}])\right) + \frac{(1-2\alpha)}{9}\log_2(1+E[\gamma^{CB}])\right)}{\frac{BW_{edge}}{9}\log_2(1+E[\gamma^{CB}])} \\ &= \frac{\alpha(3\eta\log_2(1+E[\gamma^{JT_0}]) + 2\log_2(1+E[\gamma^{JT_1}])) + 2(1-2\alpha)\log_2(1+E[\gamma^{CB}])}{2\log_2(1+E[\gamma^{CB}])} \\ &\approx \alpha\eta\left(\frac{3E[\gamma_{dB}^{JT_0}]}{2E[\gamma_{dB}^{CB}]}\right) + (1-2\alpha) + \frac{E[\gamma_{dB}^{JT_1}]}{E[\gamma_{dB}^{CB}]} \end{aligned} \tag{5.56}$$

We use A to denote the ratio between the SNR of SU-MISO in LSA users over the SNR of the MU-MIMO users $A = \frac{E[\gamma_{dB}^{JT_0}]}{E[\gamma_{dB}^{CB}]}$; and B to denote the ratio between SNR of SU-MISO in MNO users over the SNR of the MU-MIMO users $B = \frac{E[\gamma_{dB}^{JT_1}]}{E[\gamma_{dB}^{CB}]}$. Due to $E[\gamma_{dB}^{JT_0}] > E[\gamma_{dB}^{CB}] > E[\gamma_{dB}^{JT_1}]$, we have $A > 1$ and $B < 1$, then (5.56) is given as

$$G \approx \left(\frac{3\eta A}{2} - 2\right)\alpha + B + 1 \tag{5.57}$$

Moreover

$$\frac{3\eta A}{2} \geq \frac{4E[\gamma_{dB}^{CB}] - 2E[\gamma_{dB}^{JT_1}]}{3E[\gamma_{dB}^{JT_0}]}\frac{3E[\gamma_{dB}^{JT_0}]}{2E[\gamma_{dB}^{CB}]} > 2 \tag{5.58}$$

Thus, for a fixed LSA bandwidth ratio $\eta > \eta*$ in our system model, the performance gain will have a linear increment with the increase of the LSA users' ratio. where $0 < \alpha <= \frac{N_{UE_{cell}}}{N_{UE}}$.

5.4.2 Simulation results

The channel model considered in the simulations follows that in Section 5.2.2. The path loss model follows the classical wireless path loss model proposed by Goldsmith in [88]. The path loss parameters configured for the simulation are: transmit power $P_t = 43$ dBm, $d_0 = 100$ m and $\beta = 4$.

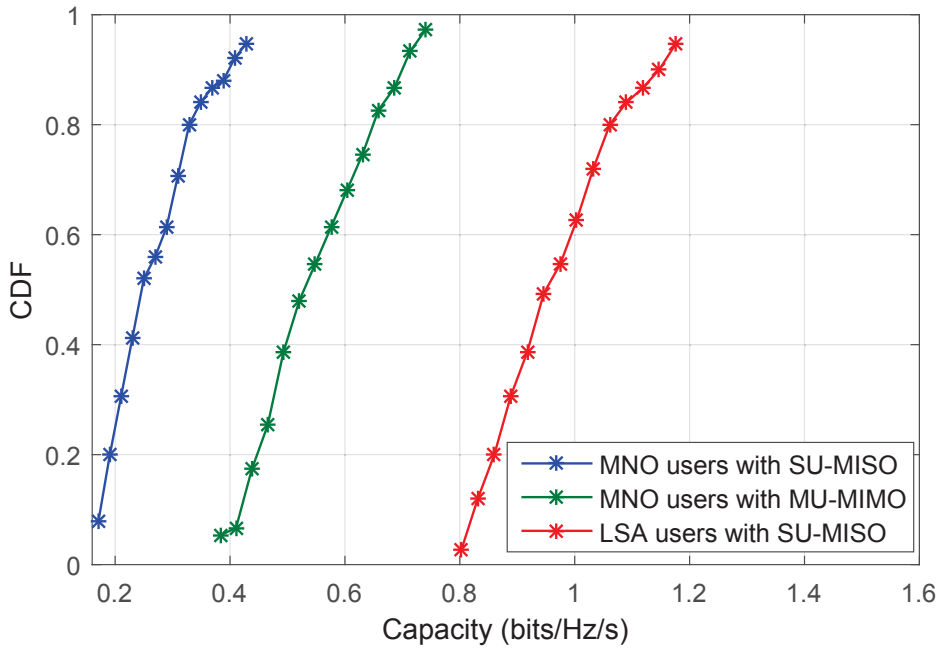

Figure 5.13: CDF of the capacity.

Cumulative Distribution Function of the capacity

In our previous work [104], we have showed that the noise power is a key factor for downlink capacity in FFR-DAS. Therefore, we consider non-zero AWGN noise power $P_n = -72.8$ dBm, which means the SNR is 115.8 dB. The downlink average capacity of the cell boundary users with the noise power P_n is given as (5.19). The capacity Cumulative Distribution Function (CDF) is investigated as follows. The average capacity for a user at the cell boundary is given as (5.7) and γ is equal to γ^{JT0}, γ^{JT1} and γ^{CB} in (5.49), (5.51) and (5.17) respectively.

We use Monte-Carlo simulations with $\eta = \eta*$ and the results are shown in Figure 5.13. The results indicate that LSA SU-MISO JT users' average capacity is higher than for the MNO MIMO-CB users and higher than for the MNO SU-MISO JT users. This validates our analysis that using LSA in MU-MIMO CB systems will cause a capacity decrease for the previously paired users in the sectors of the neighbouring cells.

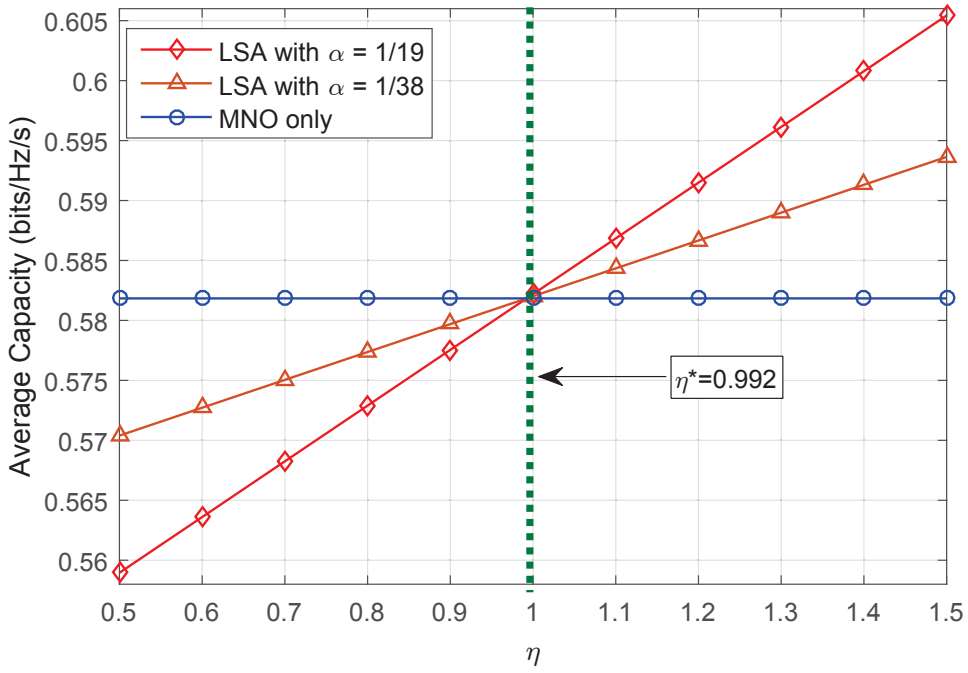

Figure 5.14: Average capacity comparison.

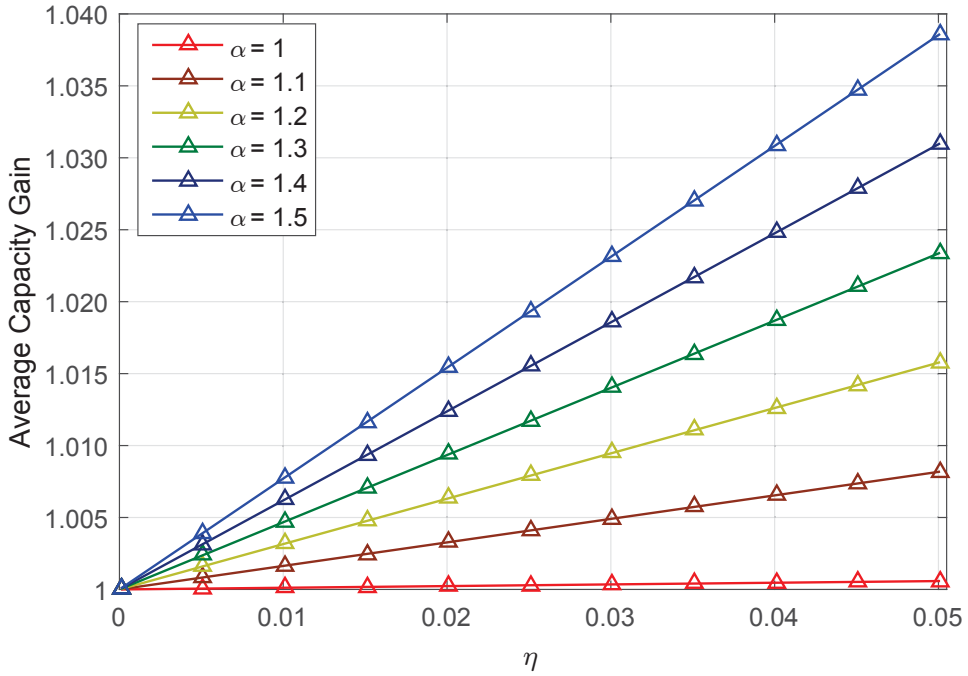

Figure 5.15: Average capacity gain with LSA users' ratio.

Bandwidth ratio threshold

We simulate the average capacity using LSA band and MNO bands with different values of η and two values of α using our system and channel model. The results in Figure 5.14 show that the threshold on $C^{LSA} \geq C^{CB}$ is dependent on η but independent with α. Moreover, the threshold is close to the analytical result we derived in (5.55).

Average downlink capacity gain

We derived the capacity gain between LSA and MNO with the numerical results shown in Figure 5.15. With the increase of η, the capacity gain will also increase. This shows that the MNOs use more LSA bandwidth, and hence the average LSA capacity is increased in the frequency domain. For a fixed value of η, the capacity gain has a linear increment with the increase of α. This shows that more users join the LSA band for a longer time, and hence the LSA capacity is increased in the time domain.

5.5 Summary

In this chapter, we presented a through analysis of the capacity of the Cloud Radio Access Network with Coodinated Multi-Point and Fractional Frequency Reuse techniques.

First of all, we considered the problem of deriving analytical bounds for the differential capacity of the cell edge users in Cloud Radio Access Networks (C-RAN) under low Signal-Noise-Ratio (SNR) conditions. We derived new closed-form upper and lower bounds by using the Moment Generating Function of SNR. Simulation results corroborate the analysis of the bounds under two different channel models. The numerical results show that the proposed upper bound is much tighter than the one in [69] and that the proposed bounds perform well under a realistic LTE channel model.

Secondly, we analysed downlink capacity of the cell edge users in the C-RAN with the Distributed Antenna Systems model. Two transmitting schemes were com-

pared: SU-MISO with CoMP Joint Transmission and MU-MIMO with CoMP Coordinated Beamforming. Capacity with inter-cell interference was also considered. Monte-Carlo simulations corroborate the analysis of the capacity CDF and capacity with transmitting SNR constraints. The MU-MIMO scheme obtains approximately 6 dB gain over the SU-MISO case with the extra cost of more computational operations and constraints imposed by user paring and selection.

Lastly, we use the Licensed Shared Access concept discussed in the previous chapters in the analysis of the downlink capacity of cell edge users in C-RAN using Fractional Frequency Reuse scheme for resource allocation. We analysed and compared the capacity of using LSA with SU-MISO joint transmission with original MNO MU-MIMO coordinated beamforming. A threshold of the LSA bandwidth ratio for the average capacity and the average capacity gain were derived. Numerical results validate the analytical results. The analytical results provide a merit for the desicion making of using LSA in C-RAN without the need for simulation.

Having a reference of the capacity of C-RAN, we will further investigate some details on spectrum sharing methods in the cellular networks in the next chapter, including the resource optimisation and decision making on the SNR threshold for the C-RAN networks.

Chapter 6

Fractional Frequency Reuse Resource Allocation and SNR Threshold in Cloud Radio Access Networks

In the previous chapter, we analysed the capacity of the Cloud Radio Access Network (C-RAN) from different angles. Knowing that the C-RAN architecture can provide cellular networks better performance with coordination, we study in more detail about spectrum sharing techniques in C-RAN in this chapter.

We investigate an optimum way to allocate the resource in C-RAN with Fractional Frequency Reuse in order to maximise capacity. We model the optimisation problem using Multiset and find the optimum frequency division number for the resource allocation. This part is discussed in Section 6.1. We also find that the SNR condition has an important impact on the coordination performance. Therefore, we derive a new threshold for the transmitting SNR to decide whether or not to use Coordinated Joint Transmission in FFR aided C-RAN. This is discussed in Section 6.2. This chapter provides key insights of spectrum sharing techniques in C-RAN.

6.1 Multiset based Fractional Frequency Reuse resource allocation optimisation in C-RAN

In this section, we investigate the effects of different FFR resource allocation schemes on the downlink cell edge users' capacity in C-RAN. We propose to use a Multiset approach to model resource allocation and interference. The system model follows that in Section 5.1.

6.1.1 Problem formulation

The C-RAN FFR resource allocation optimisation problem is divided into two steps.

1. Find the maximum capacity with a fixed frequency division number N_f;

2. Compare the maximum capacity with different N_f to obtain the optimum N_f.

We use a cell cluster to construct the cellular model. We assume that N_c cells are in a cluster and denote a cell in a cluster as $A_k, k = 1, ..., N_c$. We choose a typical 3-cell cluster model as illustrated in Figure 5.2. Cells A, B, C in a cluster are denoted as $A_k, k = 1, 2, 3$. We divide each cell edge into six sectors. Denote each sector in A_k as $a_i^k, i = 1, ..., 6$. Each sector will be allocated with one frequency slice $f_n, n = 1, ..., N_f$. The bandwidth of a frequency slice is $|f_n| = \frac{BW_{edge}}{N_f}$. The frequency slice f_n will be allocated to sectors a_i.

We now present the problem of finding the optimum frequency division number of N_f as:

$$\hat{N_f} = \arg\max\ (E[C(N_f)]), N_f > 0 \tag{6.1}$$

where

$$E[C(N_f)] = \frac{1}{N_{ue}} \sum_{1}^{N_{ue}} \left(\frac{BW}{N_f} \times \log_2(1+\gamma) \right) \tag{6.2}$$

where N_{ue} is the number of users and γ follows (5.3).

For each given value of N_f in this problem, there are different possible resource allocations. Thus, we divide the original problem into two steps: first, we fix the

value of N_f and find the resource allocation for the maximum capacity; second, we compare performance between all the different N_f and determine the optimum value of N_f that can reach the highest capacity.

For a fixed N_f, a different allocation will result in a different SNR, then the problem of $\mathcal{P}$: max $E[C(N_f)]$ becomes $\mathcal{P}$: max $E[\gamma(N_f)]$. We assume that transmit powers are equal, there is no inter-band interference and the noise power is the same in all the cells. Thus, the problem becomes that of minimising the interference:

$$\mathcal{P} : \begin{cases} \min\ E[P_I] = \ E[\sum\limits_{j \in B_I(N_f)} P_t |h_j|^2] \\ \\ \text{for fixed } N_f \end{cases} \tag{6.3}$$

where P_I is the average power of interference.

Since we use the cell cluster model, taking cell A in Figure 5.2 as an example, there are three types of interference :

1. Interference between the central cell A and cell A in tier two. This interference is caused by the layout of the cell cluster model and is dependant on the radius of the cell;

2. Interference between one sector of cell A and other sectors of cell B or C in the same cluster, if the sectors are allocated with the same frequency slice. This interference appears when $N_f < N_{max}$, where $N_{max} = N_c * 6$;

3. Interference between one sector of cell A and other sectors of the same cell A if the sectors are allocated with the same frequency slice. This interference appears when $N_f <= 6 < N_{max}$.

If $N_f > N_{max}$, there will be unused frequency slices which means spectrum efficiency is lower than in the case of $N_f = N_{max}$. Moreover, the interference is the same with $N_f = N_{max}$ and the capacity is lower than $N_f = N_{max}$. Thus we focus on $N_f <= N_{max}$. If N_f decreases, the spectrum efficiency and interference increase. Hence, the capacity does not monotonically increase with the decrease of N_f. If $N_f < N_{max}$, there will be overlaps in the frequency allocation and the traditional partial frequency reuse [105] does not work in our system model.

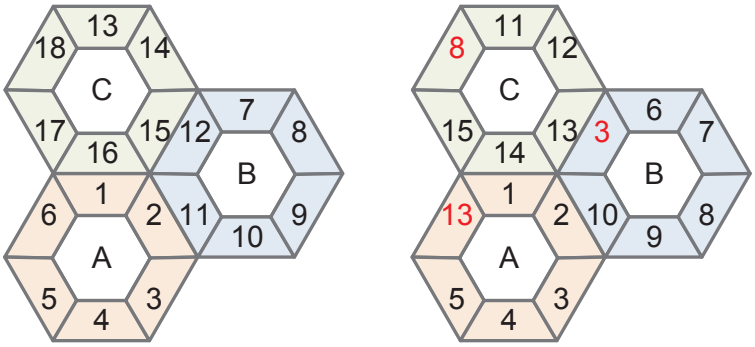

(a) $N_f = 18$

(b) $N_f = 15$

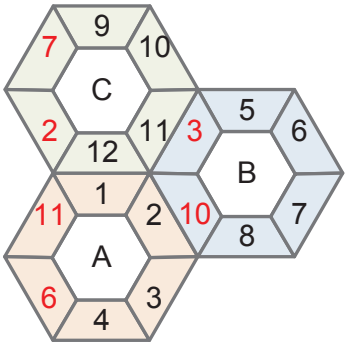

(c) $N_f = 12$

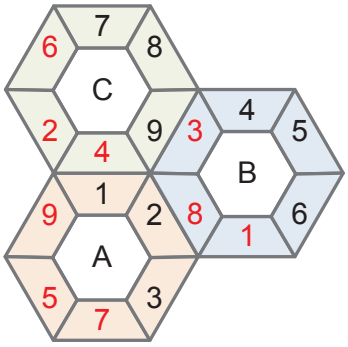

(d) $N_f = 9$

Figure 6.1: Fractional Frequency Reuse allocation in a three-cell cluster, $N_f = 9, 12, 15, 18$.

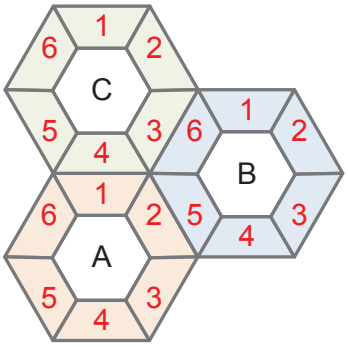

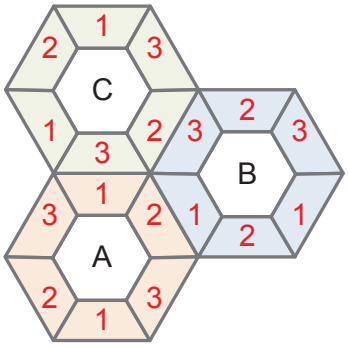

Figure 6.2: Fractional Frequency Reuse allocation in a three-cell cluster, $N_f = 6$ and $N_f = 3$.

6.1.2 Multiset based modelling

We use the Multiset concept [106], where a set has multiplicities associated with its elements in the form of natural numbers, where multiplicities denote the quantity of an element in the set. A frequency slice will be chosen from N_f different frequency slices and allocated into a cluster with three cells $A_k, k = 1, ..., N_c$, denoted as $A_k \rightarrow \mathbb{N}_{N_f} = 1, 2, .., N_f, k = 1, ..., N_c$. $|A_k|$ is the number of total elements in set A_k. Each sector in A_k is characterised with an element a_i^k with its multiplicity $m(a_i^k)$, denoted as $(a_i^k; m(a_i^k)) : a_i^k \in A_k, i = 1, ..., N_{sec}$, where N_{sec} denotes the sectors number in a cell. Thus we have $\sum_{k=1}^{3} |A_k| = N_f$.

We assume three cells in a cluster and six sectors covered by a cell, thus $N_c = 3, N_{sec} = 6$. We define the sectors in the cell edge of cell A_k as A_k^O and the neighbour sectors of cell A_k as A_k^N as illustrated in Figure 5.2. Using the Multiset model, the problem to minimise the power of interference is cast into:

$$\mathcal{P} : \begin{cases} \min\ E[P_I] = E[\sum\limits_{j \in B_I(N_f)} P_t |h_j|^2] \\ \text{s.t. } \sum\limits_{k=1}^{3} |A_k| = N_f \\ \text{for } \ a_i \in \{f_1, ..., f_{N_f}\} \end{cases} \tag{6.4}$$

where P_I is the interference power and we divide the interference from the different tiers as

$$P_I = P_I^{t_0} + P_I^{t_1} + P_I^{t_2} \tag{6.5}$$

where $P_I^{t_0}$ denotes the power of the interference from the current cell. $P_I^{t_1}$ and $P_I^{t_2}$ denotes the power of interference from tier one and tier two respectively.

Taking the central cell marked as A in Figure 5.2 as an example, we use Multiset to model the power of interference as:

$$P_I^{t_0} = (m(a_i \rightarrow A) - 1) P_t |h_j|^2 \tag{6.6}$$

where $m(a_i \rightarrow A)$ denotes the multiplicity of a_i in the set of A therefore $m(a_i \rightarrow A) - 1$ represents the number of sectors that have been allocated the same frequency

slice as sector a_i. Following this model, the interference is given as:

$$P_I^{t_1} = 3(m(a_i \to C))P_t|h_j|^2 + 3(m(a_i \to B))P_t|h_j|^2 \tag{6.7}$$

$$P_I^{t_2} = 6(m(a_i \to A))P_t|h_j|^2 + 3(m(a_i \to C))P_t|h_j|^2 + 3(m(a_i \to B))P_t|h_j|^2 \tag{6.8}$$

Due to the random channel fading property, we consider the average capacity, which reduces the problem into minimising the average power of interference as:

$$\mathcal{P}: \begin{cases} \min\ E[P_I] = E[\sum\limits_{j \in B_I(N_f)} P_t|h_j|^2] \\ \text{s.t. } \sum\limits_{k=1}^{3} |A_k| = N_f \\ \text{for } a_i \in \{f_1, ..., f_{N_f}\} \end{cases} \tag{6.9}$$

where $E[h_j] = E[g_j]\sqrt{E[\Omega_j]} = G\sqrt{E[L_j]}$. $G = E[g_j]$ is the expectation value of the small scale fading and we only consider path loss for the large scale fading. We use the Goldsmith path loss model $L_j = K(\frac{d_j}{d_0})^{-\beta}$ [88].

D_t is the distance between the central reference antenna unit and the antenna unit in tier t, $t = 0, 1, 2$. Since $E[d_j] \leq D_t$, thus (6.6), (6.7) and (6.8) are given as:

$$\begin{cases} P_I^{t_0} \geq P_t L_{D_0}((m(a_i \to A) - 1) \\ P_I^{t_1} \geq P_t L_{D_1} 3((m(a_i \to C)) + (m(a_i \to B))) \\ P_I^{t_2} \geq P_t L_{D_2}(6(m(a_i \to A)) + 3(m(a_i \to C)) + 3(m(a_i \to B))) \end{cases} \tag{6.10}$$

where $L_{D_i} = K\left(\frac{D_i}{d_0}\right)^{-\beta}, i = 0, 1, 2$. Consider the cellular network topology is symmetric, (6.10) is given as a general form by:

$$\begin{cases} P_I^{t_0} \geq P_t L_{D_0}((m(a_i^k \to A^k) - 1) \\ P_I^{t_1} \geq P_t L_{D_1} 3((m(a_i^k \to A^{(k+1) \bmod 3})) + (m(a_i^k \to A^{(k+2) \bmod 3}))) \\ P_I^{t_2} \geq P_t K L_{D_2}(6(m(a_i^k \to A^k)) + 3(m(a_i^k \to A^{(k+1) \bmod 3})) + 3(m(a_i^k \to A^{(k+2) \bmod 3}))) \end{cases} \tag{6.11}$$

where $L_{D_i} = K\left(\frac{D_i}{d_0}\right)^{-\beta}, i = 0, 1, 2$, $a_i^k \in \{f_1, ..., f_{N_f}\}$, $k = 1, 2, 3$ and mod is the modulus operator. Due to the symmetry of the three cell cluster layout and the linear

programming property, the minimum value of $E[P_I]$ in (6.9) will be reached when $E[m(a_i^k \to A^k)]$ is minimum and equal for all $k = 1, 2, 3$, thus $\sum_{m(a_i^k)=1} m(a_i^k \to A^k)$ is minimum and equal for $k = 1, 2, 3$.

6.1.3 FFR resource allocation algorithm for a fixed N_f

For simplicity, we consider $N_f = 3, 6, 9, 12, 15, 18$. Following the Multiset based analysis, for $9 \leq N_f \leq 18$, we have $\sum_{m(a_i^k)\neq 1}(m(a_i^k) - 1) = 6 - \frac{N_f}{3}$ for the sectors that have interference from their three-cell clusters; $\sum_{m(a_i^k)=1} m(a_i^k) = \frac{N_f}{3}$ for the sectors that have no interference from their three-cell clusters. For $N_f = 3$ and $N_f = 6$, there will always be interference from their three-cell cluster.

Algorithm 6.1: Table I - Multiset based FFR Allocation for fixed N_f

1 **for** $k = 1, ..., 3$ **do**
2 **for** $i = 1, ..., N_f/3$ **do**
3 $f_n = ((c-1)\left(\frac{N_f}{3}\right) + [n-1:n])\frac{BW_{edge}}{N_f}$;
4 set $a_i^k = f_n$;
5 **for** $i = N_f/3, ..., 6$ **do**
6 **for** $n = N_f/3, ..., N_f$ **do**
7 d_i = interfering distance of a_i^m;
8 **if** $d_i = \min(\{d_{N_f/3}, ..., d_6\})$ **then**
9 set $a_i^k = f_n$;

We propose our algorithm in Table I. We first allocate $\frac{N_f}{3}$ sectors until all the frequency slices are used, then we choose a frequency slice that has already been used to assign to unallocated sectors. Since we try to decrease the interference as much as possible, we consider path loss as the judging factor when choosing the frequency slice.

The allocations results are shown in Figure 6.1 and Figure 6.2. The number marked in each sector illustrates the frequency slice a_i^k. The number colored as black denotes that the frequency slice has been allocated in Step 3 in the algorithm where

$m(a_i^k) = 1$ and the number colored as red denotes that the frequency slice has been allocated in Step 11 in the algorithm where $m(a_i^k) \neq 1$. According to the algorithm, a closed-form lower bound of the maximum average capacity for a fixed N_f is given as:

$$E[C(N_f)] = \frac{1}{N_f} \log_2(1 + \gamma(N_f)) \tag{6.12}$$

where $\gamma(N_f)$ is given as:

$$\gamma(N_f) = \begin{cases} \frac{\frac{2N_f}{3} - 6}{6} \frac{D_0^{-\beta}}{6D_2^{-\beta} + P'_n} + \frac{2\left(6 - \frac{N_f}{3}\right)}{6} \frac{D_0^{-\beta}}{6D_1^{-\beta} + 12D_2^{-\beta} + P'_n} & 9 \leq N_f \leq 18 \\ \frac{D_0^{-\beta}}{6D_1^{-\beta} + 12D_2^{-\beta} + P'_n} & N_f = 6 \\ \frac{D_0^{-\beta}}{3D_0^{-\beta} + 12D_1^{-\beta} + 24D_2^{-\beta} + P'_n} & N_f = 3 \end{cases} \tag{6.13}$$

where

$$P'_n = \frac{P_n d_0^{-\beta}}{P_t K G} \tag{6.14}$$

The problem (6.1) can be solved by comparing $E[C(N_f)]$ in (6.12) with different N_f using (6.13) and find the maximum average capacity and the respective N_f.

6.1.4 Simulation results

The channel model considered in the simulations follows that in Section 5.2.2. The path loss model follows the classical wireless path loss model proposed by Goldsmith in [88]. The path loss parameters configured for the simulation are transmit power $P_t = 43$ dBm, $d_0 = 100$ m and $\beta = 4$.

Cumulative Distribution Function of the capacity

In Section 5.2, we have shown that the noise power is a key factor for downlink capacity in FFR-DAS. Therefore, we consider two different values of the AWGN

noise power $P_n = 0$ Watts and $P_n = -73$ dBm. The downlink average capacity of the cell boundary users with the noise power P_n is given as (5.19).

Figure 6.3 and Figure 6.4 show the CDF of capacity with different N_f when the noise power $P_n = 0$ Watts and $P_n = -73$ dBm. These figures show the capacity difference with various values of N_f. We can observe from both figures that $N_f = 3$ has the lowest capacity. However, the value of N_f that can reach the highest capacity changes with different values of noise power. The difference in the highest capacity CDF is not distinguished enough to be used as a figure of determining the optimum number of N_f.

Average capacity with different N_f

We simulate the average capacity with different values of N_f and with two noise power configurations using a Monte-Carlo simulation. The lower bound we obtain from (6.12) is also shown in Figure 6.5 and Figure 6.6. The optimum value of N_f is $N_f = 12$ when the noise power $P_n = 0$ Watts and the optimum value of N_f is $N_f = 6$ when the noise power $P_n = -73$ dBm. In comparison, the scheme where $N_f = 3$ in [86] and $N_f = 6$ in [87] are also shown in the figures. We can clearly observe the optimum value of the average capacity and the respective value of N_f. In Figure 6.5 and Figure 6.6, the capacity for $N_f = 9$ is low compared to when $N_f = 6$ and $N_f = 12$ is due to that this method is a discrete fraction allocation. The bandwidth is linearly decreasing from $N_f = 6$, $N_f = 9$ to $N_f = 12$, however, the interference is not linearly decreasing.

Moreover, the figures show that our lower bound has the same optimum result as the Monte-Carlo simulation, which illustrates that our lower bound can be used to calculate the optimum value of N_f and the maximum average capacity without the need to carry out simulations.

Optimum N_f with different levels of noise power

From the previous sections, the optimum value of N_f differs between the two configurations. We simulate the average capacity with two FFR resource allocations $N_f = 6$ and $N_f = 12$ with different levels of noise power. The simulation results

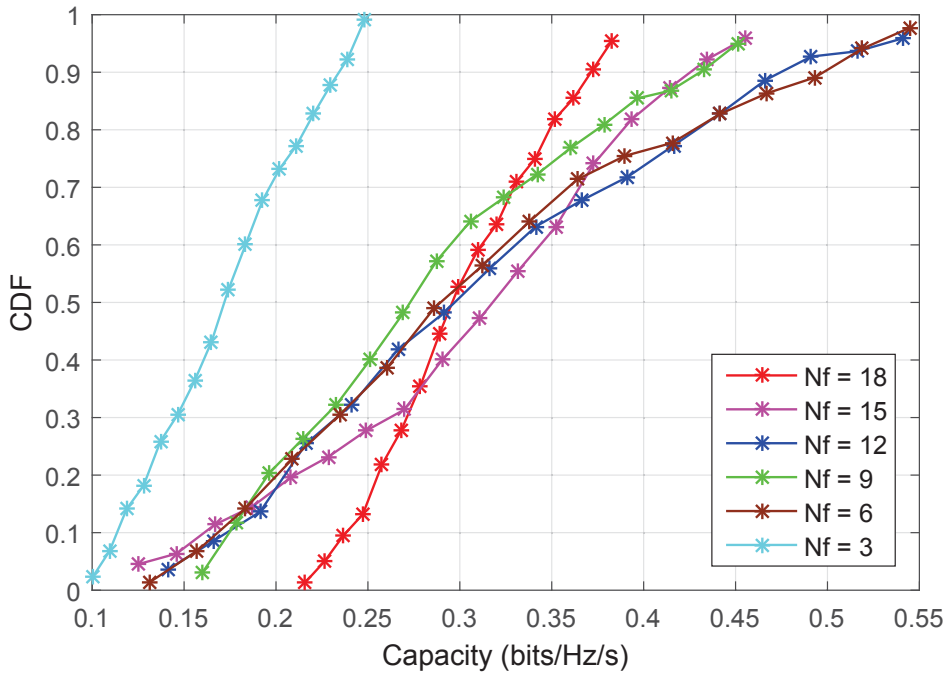

Figure 6.3: Capacity CDF comparison with $P_n = 0$ Watts.

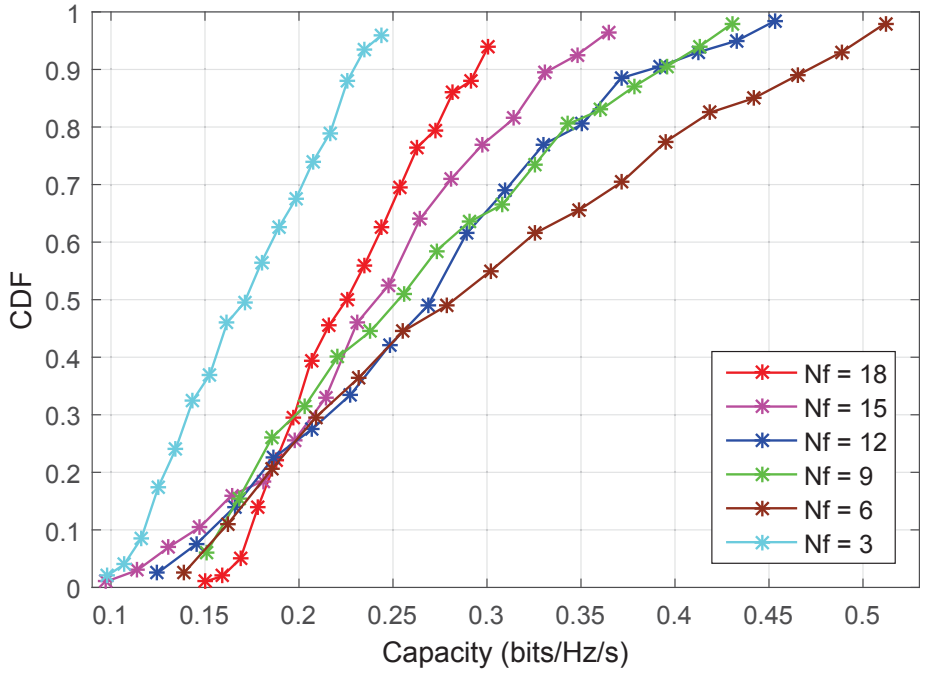

Figure 6.4: Capacity CDF comparison with $P_n = -73$ dBm.

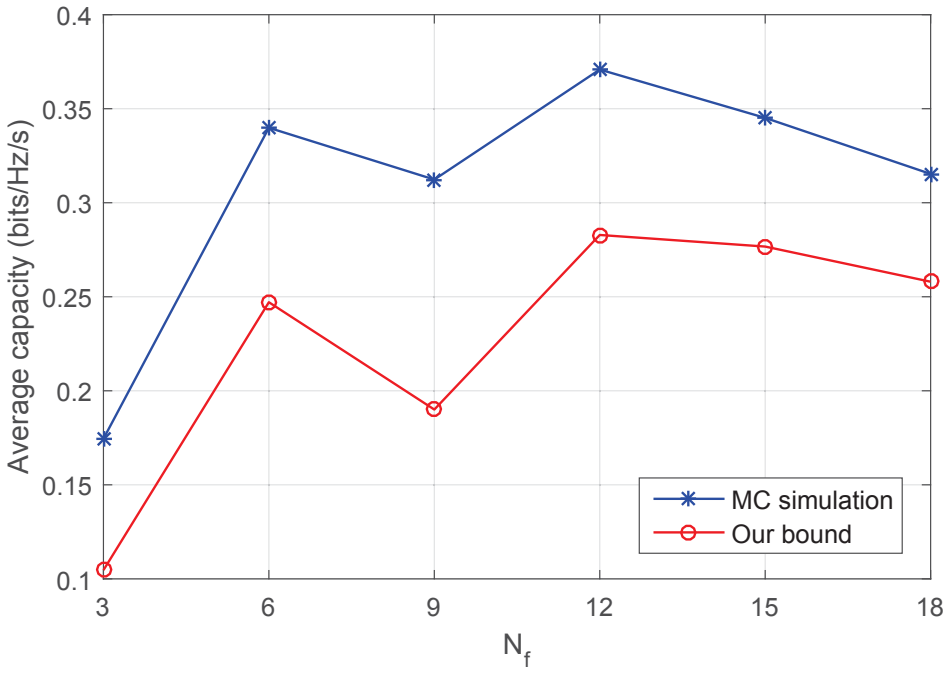

Figure 6.5: Average capacity with different N_f when $P_n = 0$ Watts.

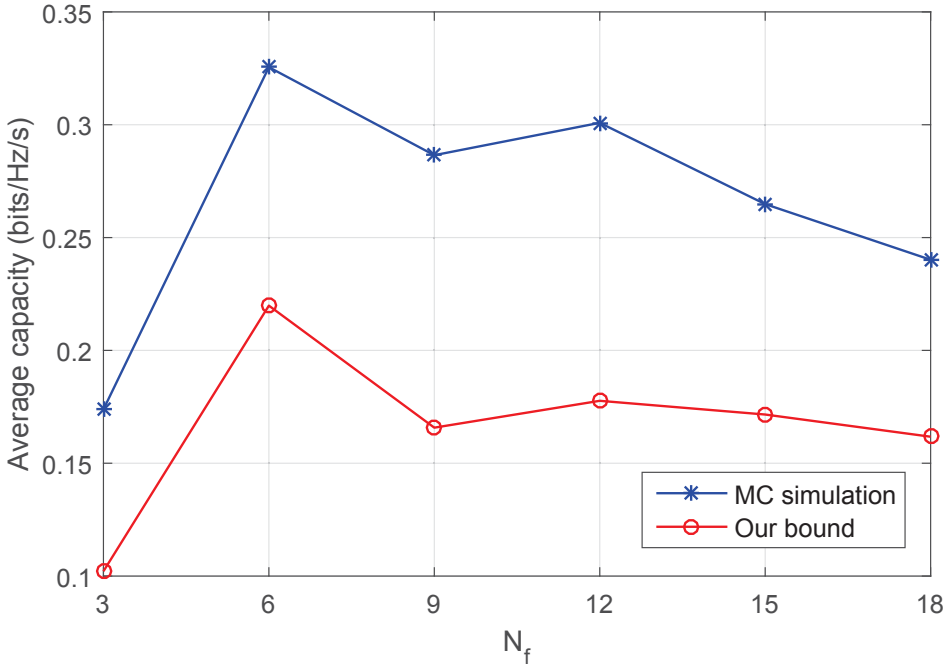

Figure 6.6: Average capacity with different N_f when $P_n = -73$ dBm.

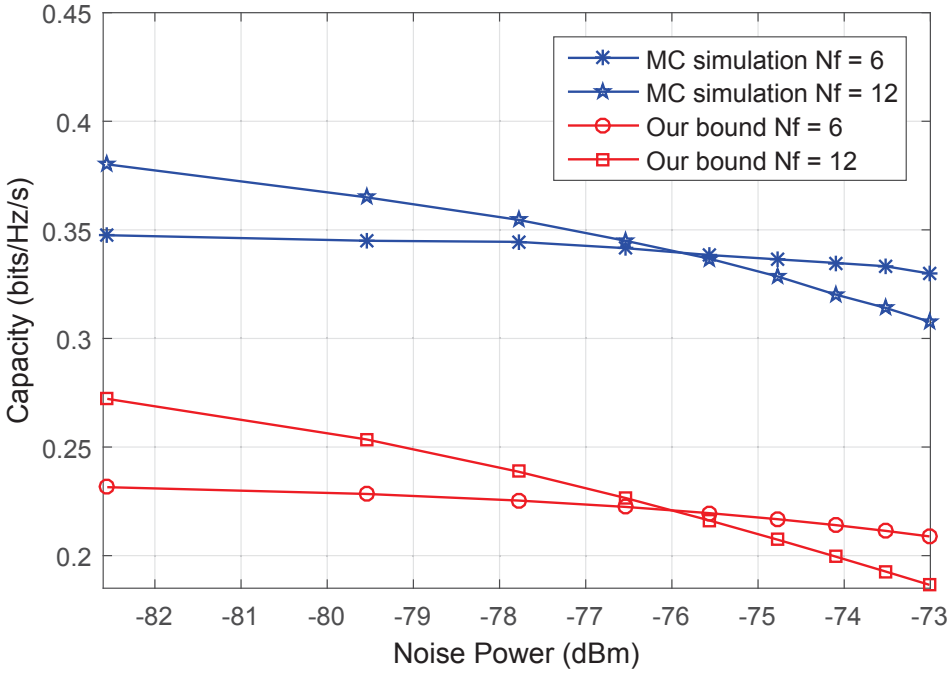

Figure 6.7: Optimum N_f with different values of noise power.

are illustrated in Figure 6.7. Our lower bound is also presented. The figure shows that there is a threshold of noise power $P_n \approx -76$ dBm. For $P_n \leq -76$ dBm, the optimum value is $N_f = 12$ and for -76 dBm $\leq P_n \leq -73$ dBm the optimum value is $N_f = 6$. There is a gap between the Monte-Carlo simulation and our bound because of the approximation of the upper bound in the interfering power in (6.10). However, the gap does not affect the result of the optimum value of N_f. The simulation and analytical bound produce the same result on the optimum value of N_f. Thus, our lower bound can be used for decision making in FFR resource allocation in C-RAN.

6.2 SNR threshold in C-RAN

In the previous sections, we have found that SNR has an important impact on the capacity of C-RAN with coordination. To compare the capacity of non-coordination scenario, in this section, we investigate the performance of using Cooperative Joint Transmission (CJT) and non-CJT schemes and find the SNR threshold for deciding whether or not to use coordination in C-RAN. Non-CJT represents one

base station transmit to a user with one antenna at the base station.

6.2.1 Problem formulation

We use the downlink ergodic capacity as the merit of the decision on whether to use CJT or non-CJT. If the ergodic capacity of CJT C_C is greater than the ergodic capacity of non-CJT C_N, i.e. $E[C_C] > E[C_N]$, CJT should be used to strengthen the performance, otherwise, we do not have to use CJT. Non-CJT can save the total power consumption compared with that of CJT because one user is supported by one antenna with transmit power P_t when no CJT is used, while one user is supported by multiple antennas both with transmit power P_t in the CJT scenario. Thus, Non-CJT should be selected, as long as it can provide receiving SINR that is higher than or equal to that of CJT. The problem is defined to find γ_{th}, the threshold of transmitting SNR as:

$$\mathcal{P}: \begin{cases} \text{find} & \gamma_{th} \\ \text{for} & \forall\ \gamma_0 \leq \gamma_{th}, \quad \text{s.t.} \quad E[C_C|\gamma_0] \geq E[C_N|\gamma_0] \\ \text{for} & \forall\ \gamma_0 > \gamma_{th}, \quad \text{s.t.} \quad E[C_C|\gamma_0] < E[C_N|\gamma_0] \end{cases} \tag{6.15}$$

For a fair comparison, the capacity is evaluated under the same bandwidth, FFR pattern and channel fading condition. We consider the receiving SINR as a function of the transmitting SNR γ_0. The value of transmitting SNR will affect the receiving SINR and the capacity, depending on the linear property, the constraints of the problem can be turned into the comparison between receiving SINR as:

$$\mathcal{P}: \begin{cases} \text{find} & \gamma_{th} \\ \text{for} & \forall\ \gamma_0 \leq \gamma_{th}, \quad \text{s.t.} \quad E[\gamma_C|\gamma_0] \geq E[\gamma_N|\gamma_0] \\ \text{for} & \forall\ \gamma_0 > \gamma_{th}, \quad \text{s.t.} \quad E[\gamma_C|\gamma_0] < E[\gamma_N|\gamma_0] \end{cases} \tag{6.16}$$

where γ_C is the receiving SINR when using CJT and γ_N is the receiving SINR when using non-CJT following (5.3). We assume the expectation of the small scale fading channel gain is constant $E[|g_{ik'}|^2] = G$, then:

$$E[\gamma_k|\gamma_0] = E\left[\frac{\sum_{j\in B_S} P_t|h_{jk}|^2}{\sum_{i\in B_I} P_t|h_{ik'}|^2 + P_n}\right] = \frac{\sum_{j\in B_S} P_t E[|h_{jk}|^2]}{\sum_{i\in B_I} P_t E[|h_{ik'}|^2] + N_0} \tag{6.17}$$

$$\approx \frac{\sum_{j\in B_S} P_t E[|g_{jk}|^2 L_j]}{\sum_{i\in B_I} P_t E[|g_{ik'}|^2 L_i] + P_n} = \frac{\sum_{j\in B_S} P_t L_j}{\sum_{i\in B_I} P_t L_i + P_n}$$
$$= \frac{\sum_{j\in B_S} E[L_j]}{\sum_{i\in B_I} E[L_i] + \hat{\gamma_0}^{-1}} \tag{6.18}$$

where $\hat{\gamma_0} = G\gamma_0$. We use the Jensen's inequality [107] to get an approximation of (6.17). Path loss is considered as the only factor in large-scale fading. We use the classical wireless path loss model proposed by Goldsmith in [88] given as $L_i = K(\frac{d_i}{d_0})^{-\beta}$, where K is a constant parameter related to the antenna features and channel attenuation, d_i is the distance between antenna i and users, d_0 is the reference distance and β is the path loss exponent, which is a fixed value under a certain configuration. Substituting (6.18) into (6.16), we obtain:

$$E[\gamma_C] > E[\gamma_N]$$
$$\frac{|B_S|E[L_j]}{\sum_{i\in B_I^C} E[L_i] + \hat{\gamma_0}^{-1}} \geq \frac{E[L_j]}{\sum_{i\in B_I^N} E[L_i] + \hat{\gamma_0}^{-1}}$$
$$2(\sum_{i\in B_I^N} L_i + \gamma_0^{-1}) > \sum_{i\in B_I^C} L_i + \gamma_0^{-1}$$
$$\hat{\gamma_0}^{-1} \geq \sum_{i\in B_{It1}^C} E[L_i] + \sum_{i\in B_{It2}^C} E[L_i] - |B_S| \sum_{i\in B_{It2}^N} E[L_i] \tag{6.19}$$

where B_I^C and B_I^N are the sets of interfering transmitting antennas in CJT and non-CJT cases respectively. B_{Iti}^C denotes the interfering transmitting antennas set in tier i, $i = 1, 2, 3$. In the CJT case, there is no co-ordination between neighbouring base stations, thus interference exists in both tier one and tier two, given as : $B_I^C = B_{It1}^C \cup B_{It2}^C$. However, in the non-CJT case, there is no interfering base station in tier one $B_{It1}^N = \emptyset$, thus the total interference of the non-CJT case is given as $B_I^N = B_{It2}^N$.

6.2.2 Expectation of distance between cell edge users and interfering base stations

According to [108], if mobile users are independently and uniformly distributed in their respective cells, the PDFs of the mobile users' locations polar coordinates

(r, θ) relative to the closest base station are given as:

$$\begin{cases} f_r(r) = \dfrac{2(r - R_0)}{(R - R_0)^2}, R_0 \leq r \leq R, \\ f_\theta(\theta) = \dfrac{1}{2\pi}, \qquad\qquad 0 \leq \theta \leq 2\pi \end{cases}$$

where R is the cell radius and R_0 is the cell centre radius. The distance between mobile users to the interfering cell base station is

$$d(r) = \sqrt{r^2 + 2rD\sin(\theta) + D^2} \tag{6.20}$$

where D is the distance between the mobile user's respective cell base station and its interfering base station.

The expectation of the interfering distance is:

$$\begin{aligned} E[d] &= \int_0^{2\pi} \int_{R_0}^{R} d(r) f_r(r) f_\theta(\theta) dr d\theta \\ &= \frac{2\int_0^{2\pi} \int_{R_0}^{R} \sqrt{r^2 + 2rD\sin(\theta) + D^2}(r - R_0) dr d\theta}{2\pi(R - R_0)^2}. \end{aligned} \tag{6.21}$$

Because there is no explicit solution for (6.21), we deduce it using an approximation for tier one and tier two. For tier one where $D = \sqrt{3}R$ and $R_0 = 2/3R$, we use the following approximation:

$$\int_0^{2\pi} \int_{R_0}^{R} \sqrt{r^2 + 2\sqrt{3}Rr\sin(\theta) + 3R^2} dr d\theta \leq 2\pi \int_{R_0}^{R} \sqrt{r^2 + 2\sqrt{2}Rr + 2R^2} dr \tag{6.22}$$

Hence, the resulting approximation for the expectation of the interfering distance is $D = 2\sqrt{3}R$ and $R_0 = 2/3R$:

$$E[d] \leq \frac{2\int_{R_0}^{R} (r + \sqrt{2}r)(r - R_0) dr}{(R - R_0)^2} = \left(\frac{5}{9} + \sqrt{2}\right) R \tag{6.23}$$

We use the following approximation for tier two where :

$$\int_0^{2\pi} \int_{R_0}^{R} \sqrt{r^2 + 4\sqrt{3}Rr\sin(\theta) + 12R^2} dr d\theta \leq 2\pi \int_{R_0}^{R} \sqrt{r^2 + 4\sqrt{2}Rr + 8R^2} dr \tag{6.24}$$

Hence, the resulting approximation for the expectation of the interfering distance is:

$$E[d] \leq \frac{2\int_{R_0}^{R} (r + 2\sqrt{2}r)(r - R_0) dr}{(R - R_0)^2} = \left(\frac{8}{9} + 2\sqrt{2}\right) R \tag{6.25}$$

Since we have used the approximation in the calculation of the expectation of the interfering distance, we have also checked the difference between the original expectation and the approximated one. The mean squared error (MSE) between (6.21) and (6.23) is -27.87 dB for tier one and -29.72 dB for tier two.

6.2.3 Decision making on Coordinated Joint Transmission or Non-Coordinated Joint Transmission

Substituting (6.23) and (6.25) into (6.19), we obtain the threshold for the transmitting SNR :

$$\gamma_{th} = \frac{(R/d_0)^{\beta}(GK)^{-1}}{((|B^C_{It1}|)A_1^{-\beta} + (|B^C_{It2}| - |B_S||B^N_{It2}|)A_2^{-\beta})} \tag{6.26}$$

where $A_1 = 5/9 + \sqrt{2}$ and $A_2 = 8/9 + 2\sqrt{2}$ from (6.23) and (6.25) respectively.

Therefore, our decision making on whether or not to use CJT is: For a given transmitting SNR γ_0, if $\gamma_0 < \gamma_{th}$, CJT should be used to obtain higher capacity; else if $\gamma_0 \geq \gamma_{th}$, non-CJT can obtain higher capacity and also save the total power consumption compared with that of CJT.

For a limited size cellular network, the parameters in (6.26) are all positive real and far less than infinity, the threshold of the transmitting SNR is positive real and far less than infinity, $0 < \gamma_{th} \ll +\infty$. Thus, the transmitting SNR is an important factor in the analysis of CJT in FFR aided DAS and cannot be assumed to be positive infinite. Thus, the scenarios in previous literature [87] [67] that assume noise is zero or small enough to be ignored are not suitable for the analysis of CJT in FFR aided DAS.

We select a classic FFR pattern. For other possible FFR patterns, considering the same transmission schemes, a more general expression can be given as:

$$\gamma_{th} = \frac{(R/d_0)^{\beta}(GK)^{-1}}{((|B^C_{It1}| - 2|B^N_{It1}|)A_1^{-\beta} + (|B^C_{It2}| - |B_S||B^N_{It2}|)A_2^{-\beta})} \tag{6.27}$$

where we assume

$$(|B^C_{It1}| - |B_S||B^N_{It1}|)A_1^{-\beta} + (|B^C_{It2}| - |B_S||B^N_{It2}|)A_2^{-\beta} > 0. \tag{6.28}$$

6.2.4 Simulation results

The channel model considered in the simulations follows that in Section 5.2.2. The path loss model follows the classical wireless path loss model proposed by Goldsmith in [88]. The path loss parameters configured for the simulations are transmit power $P_t = 43$ dBm, $d_0 = 100$ m and $\beta = 4$. Each cell has 120 random uniformly distributed single-antenna users. For the CJT case: $|B_S| = 2$, $|B_{It1}^C| = 2, |B_{It2}^C| = 9$ or $|B_S| = 3$, $|B_{It1}^C| = 4, |B_{It2}^C| = 12$; for the non-CJT case: $|B_S| = 1$, $|B_{It1}^N| = 0, |B_{It2}^N| = 6$.

Cumulative Distribution Function of the capacity

Firstly, we simulate the ergodic capacity for the cell edge users with the cell radius $R = 500$ m and two coordinated base stations $B_S = 2$ to illustrate the effect of the transmitting SNR on the capacity. Three transmitting SNR values ($\gamma_0 < \gamma_{th}$, $\gamma_0 = \gamma_{th}$ and $\gamma_0 > \gamma_{th}$) have been picked for illustration. The CDF of downlink ergodic capacity is evaluated using Monte-Carlo simulations. The results are shown in Figure 6.8 to 6.10 and match our analysis in (6.26). These results verify our analysis on the existence of the transmitting SNR threshold for the decision making of using CJT or non-CJT for all the cell edge users and also show that the transmitting threshold is far less than infinity thus the transmitting SNR should be considered as a key factor in the research on CJT in FFR aided DAS.

Receiving SINR

Secondly, we simulate the average receiving SINR with various transmitting SNR values and two cell radius settings $R = 300m$ and $R = 500m$. We use the differential receiving SINR as the illustration. The differential receiving SINR is given as:

$$\Delta\gamma = E[\gamma_C|\gamma_0] - E[\gamma_N|\gamma_0] \tag{6.29}$$

where $E[\gamma_C|\gamma_0]$ and $E[\gamma_N|\gamma_0]$ follow (6.17) for CJT and non-CJT configurations respectively.

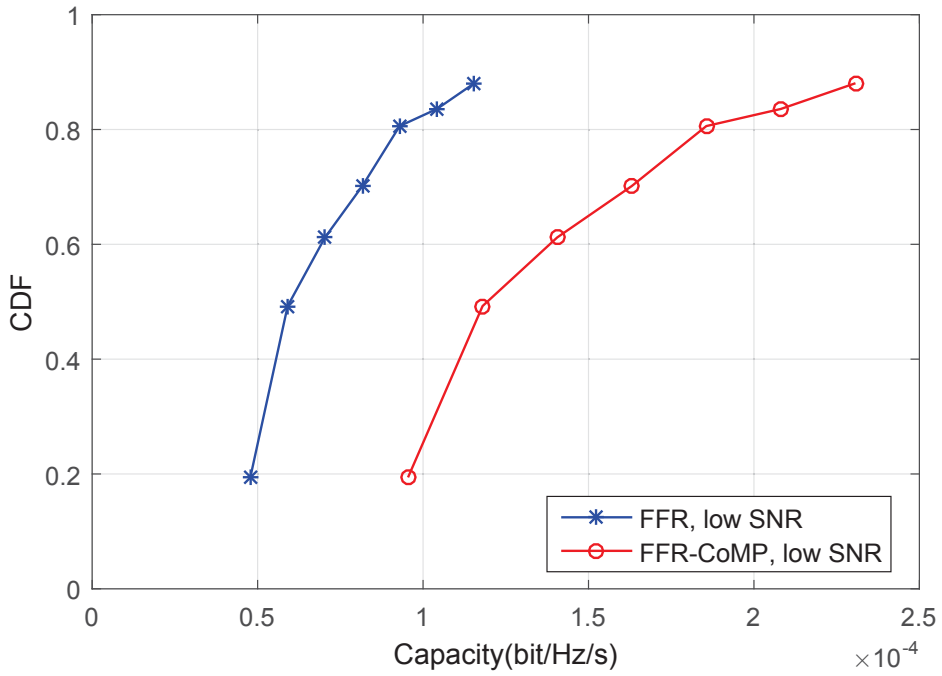

Figure 6.8: Capacity CDF in low SNR condition

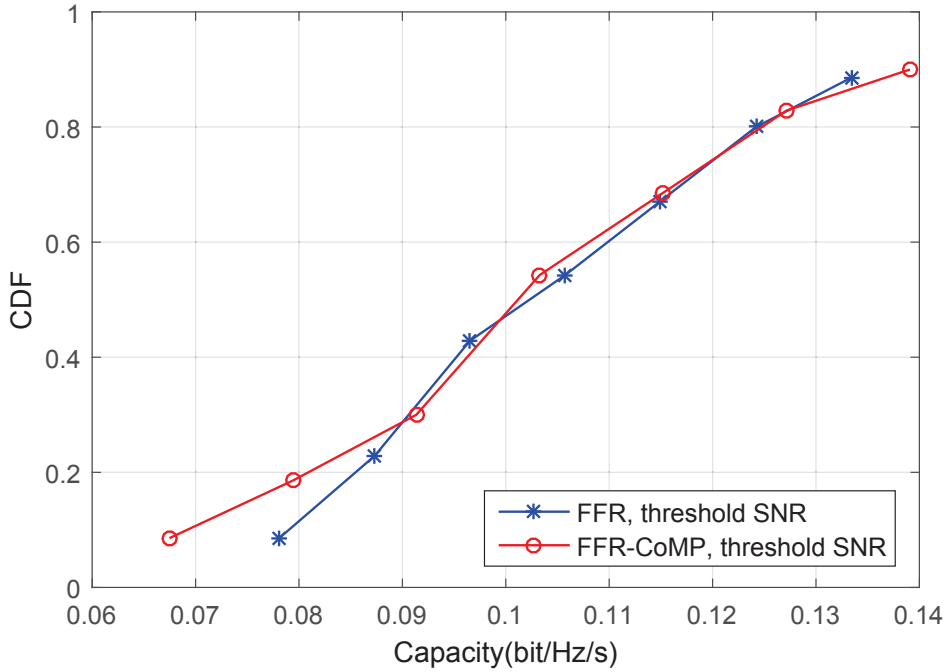

Figure 6.9: Capacity CDF in threshold SNR condition

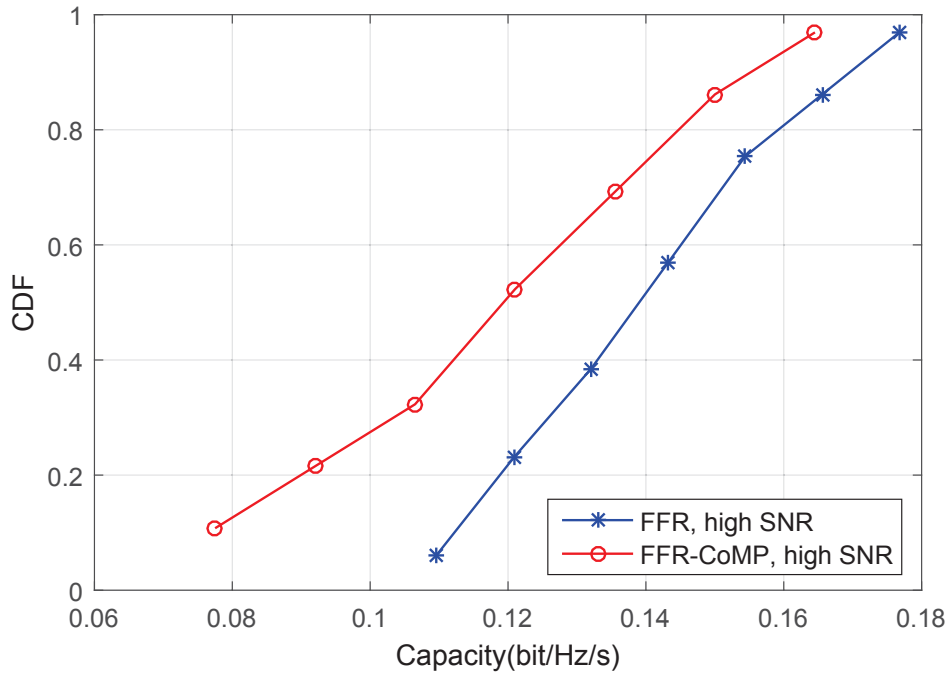

Figure 6.10: Capacity CDF in high SNR condition

According to our analytical result in (6.26), if $\gamma_0 < \gamma_{th}$, we have $\Delta\gamma > 0$, which means CJT provides better performance in lower SNR conditions; or if $\gamma_0 > \gamma_{th}$, we have $\Delta\gamma < 0$, which means non-CJT can provide better performance in high SNR conditions. The threshold will happen when $\gamma_0 = \gamma_{th}$ and $\Delta\gamma = 0$.

The simulation results in Figure 6.11 show the intersection of non-CJT and CJT differential receiving SINR curves with $B_S = 2$ and $B_S = 3$ respectively. Our analytical results on the SNR threshold obtained from (6.26) are also marked as dashed lines in the figures. The value of the transmitting SNR at the intersection of the curves with $\Delta\gamma = 0$ is slightly less than the SNR threshold obtained from (6.26). This also follows our analytical result, because we have used an upper bounded approximation.

Consider the thermal noise power density $N_0 = kT_0$ [88], where k is the Boltzmann's constant $k = 1.38 \times 10^{-23}$ J/K and $T_0 = 290$ K. Thus, the thermal noise power density is $N_0 = -174$ dBm/Hz, which is the value in the simulation of [87] and [67]). We assume that the transmit power is $P_t = 43$ dBm for 5 MHz bandwidth, the transmitting SNR is $\gamma_0 = 120$ dB, which is greater than the transmitting

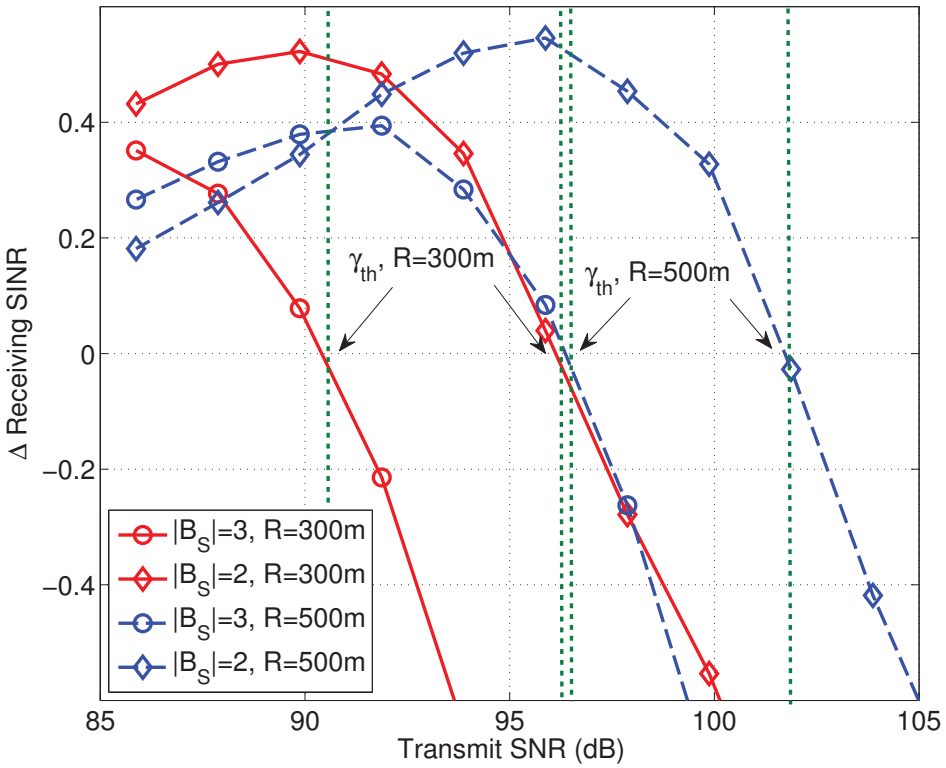

Figure 6.11: Differential receiving SINR as a function of transmitting SNR.

SNR threshold calculated from (6.26) which is also shown in Figure 6.11. If we only consider the thermal noise, we do not have to use CJT to enhance performance. However, if we consider other signals from other networks nearby operating in the same spectrum, e.g. femto-cell, the transmitting SNR may be less than the SNR threshold, and then CJT should be used.

Threshold accuracy evaluation

Thirdly, we evaluate the accuracy of our threshold expression in (6.26) under different cell radius settings from $R = 300$ m to $R = 500$ m and different path loss exponents $\beta = 2.5, 3.25$ and 4 with two coordinated base stations $B_S = 2$, as illustrated in Figure 6.12. The MSE between our threshold and the Monte-Carlo simulation is approximately -50.27 dB. Thus, the threshold obtained from (6.26) is a tight upper bound and from the figure, we can observe that it is more accurate for a larger cell radius.

The threshold increases with the increase of the cell radius and the increase

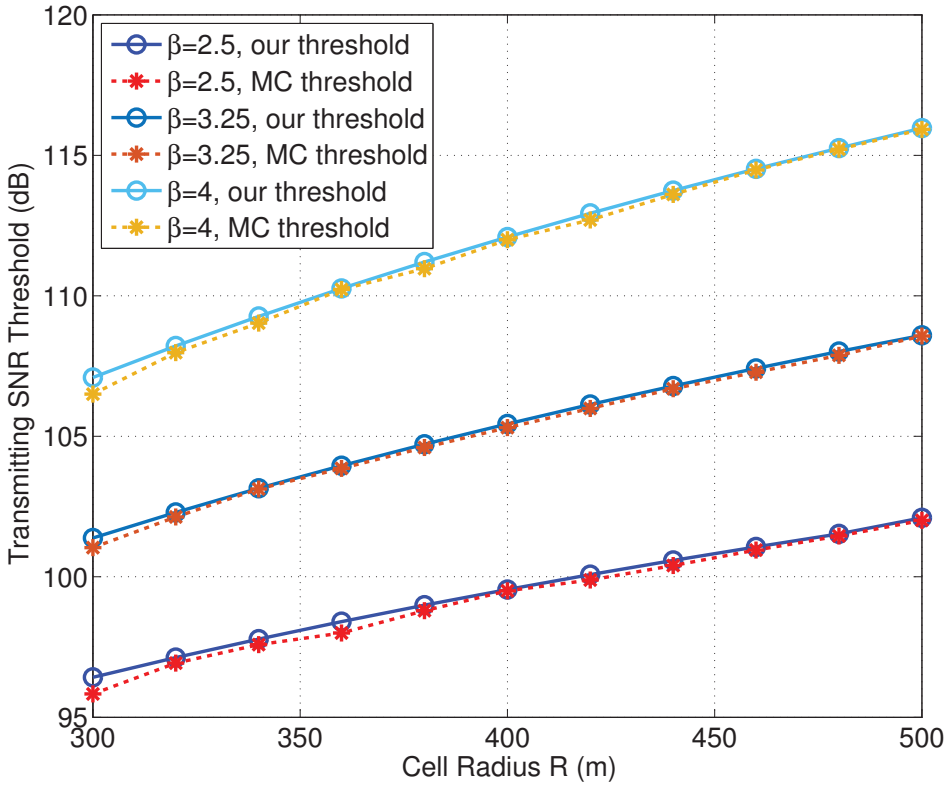

Figure 6.12: Transmitting SNR threshold as a function of cell radius, $B_S = 2$.

of the path loss exponent as illustrated in Figure 6.12. Because in larger cells or greater path loss scenarios, cell edge users will be further away from the transmitting antennas or experience deeper large scale fading, thus they need CJT to obtain more capacity. Moreover, larger cells or deeper path loss will decrease the inter-cell interference caused by CJT.

6.3 Summary

In this chapter, we studied capacity of the C-RAN using the Fractional Frequency Reuse scheme for resource allocation. A Multiset approach was used to model resource allocation and interference. A Multiset based frequency allocation algorithm was proposed to obtain the optimal frequency allocation and a closed-form lower bound of the downlink average capacity was derived. Simulation results validated the proposed algorithm.

We also derived a new threshold for the transmitting SNR to decide whether

or not to use Coordinated Joint Transmission in FFR aided C-RAN. Moreover, we have shown that the transmitting SNR is a key factor in the analysis of FFR aided DAS for both static and dynamically changing network topologies. Monte-Carlo simulations have also been carried out and the results match our analysis. The analytical expressions can be used as a guide for future wireless communication networks, such as C-RAN, without the need to carry out simulations.

Chapter 7

Conclusion

7.1 Remarks

This thesis presented research work on spectrum sharing in the next generation wireless communication networks. Interference mitigation, spectrum access and co-existence in the spectrum sharing frameworks - Licensed Shared Access (LSA) and Spectrum Access System (SAS) were investigated. Capacity and resource allocation in the Cloud Radio Access Network (C-RAN) were also analysed to enable spectrum sharing in cellular networks. Our work is timely aligned with the recent released ETSI documents [6] [35] [34] and FCC documents [7] [39]. The methods proposed in this thesis provided solutions and design reference for spectrum sharing in the future frameworks and within cellular networks in 5G.

The conclusions of this thesis are as follows:

- We proposed a method for inter-operator interference mitigation in Spectrum Access System between Priority Access and General Authorised Access base stations. Our method does not require or expose the exact locations of any base stations. GAA base stations share their location distribution and the number of transmitters in a closed finite census tract area and the PAL network can derive and calculate the distribution of aggregate interference from the GAA base stations. Furthermore, we considered the practical implementation with the Inverse Fast Fourier Transform and Discrete Fourier Transform. Moreover, we proposed a novel way of using the exclusion zone to protect PAL base

stations. According to the distribution of aggregate interference, the PAL network can design and optimise their exclusion zone size. We proposed a convex lower bound to approximate the non-convex optimisation problem. Simulation results show that the lower bound provides a good approximation. Our method meets the interference requirements of SAS, keeps fairness between PAL and GAA networks and protects the location information of both networks. Our approach reduces the exclusion zone size by over 40%, which gives significantly more spectral opportunities to GAA in the spatial domain.

- We proposed spectrum access and coexistence methods for users in different tiers in LSA and SAS. Our methods cover problems in all the levels in the LSA and SAS frameworks. For the access of all the secondary users, such as LSA licensees, PAL and GAA in SAS, to the incumbents' bands, we proposed interference measurement and user selection methods that can guarantee interference to incumbents below a certain threshold as well as enable more uplink transmission of the secondary network. Our methods guarantee the interference requirements are met. For the access of the third-tier user GAA to the second-tier user PAL in SAS, we proposed an efficient PAL detection method with sub-sampling. The detection approach leverages the characteristic reference signal in the LTE and processes multiple PALs in parallel. For the access and coexistence between cognitive basis secondary users, we proposed WiFi and LTE coexistence in the unlicensed band for the users' offloading to avoid collisions and keep fairness between secondary users.

- We considered the problem of deriving analytical bounds for the differential capacity of the cell edge users in Cloud Radio Access Networks (C-RAN) under low Signal-Noise-Ratio (SNR) conditions. We derived new closed-form upper and lower bounds by using the Moment Generating Function of SNR. Simulation results corroborate the analysis of the bounds under two different channel models. The numerical results show that the proposed upper bound is much tighter than the one in [69] and that the proposed bounds perform well under a realistic LTE channel model.

- We compared the capacity of SU-MISO with CoMP Joint Transmission and MU-MIMO with CoMP Coordinated Beamforming. Monte-Carlo simulations corroborate the analysis. The MU-MIMO scheme obtains approximately 6 dB gain over the SU-MISO case with the additional computational operations and constraints imposed by user paring and selection.

- We used the Licensed Shared Access concept in the analysis of the downlink capacity of cell edge users in C-RAN for resource allocation. We analysed and compared the capacity for using LSA with SU-MISO joint transmission with original MNO MU-MIMO coordinated beamforming. A threshold of the LSA bandwidth ratio for the average capacity and the average capacity gain were derived. Numerical results validate the analytical results. The analytical results provide a merit for the decision making of using LSA in 5G wireless communication systems without the need for simulation.

- We studied the capacity of C-RAN using the Fractional Frequency Reuse scheme for resource allocation. A Multiset based frequency allocation algorithm was proposed to obtain an optimal frequency allocation and a closed-form lower bound of the downlink average capacity is derived. Simulation results validate the proposed algorithm.

- We also derived a new threshold for the transmitting SNR to decide whether or not to use Coordinated Joint Transmission in FFR aided C-RAN. Moreover, we showed that the transmitting SNR is a key factor in the analysis of FFR aided DAS for both static and dynamically changing network topologies. Monte-Carlo simulations were also also carried out and the results match to our analysis. The analytical expressions can be used as a guide for future wireless communication networks, such as C-RAN, without the need to carry out simulations.

7.2 Future work

In this thesis, we addressed several key problems in spectrum sharing for next generation wireless communications and we have provided solutions. However, there are still some other problems or scenarios in spectrum sharing worth considering.

- Our proposed interference mitigation between PAL and GAA is focused on co-channel interference. We assume the adjacent channel interference can be neglected. It is worth taking adjacent channel interference into consideration when the cell size is small or one SAS does not own the licence for several continuous PAL channels.

- Our proposed work covers various aspects of secondary MNO networks. Another important component in spectrum sharing frameworks is also worth investigating. In SAS, there is a third party sensing network named Environmental Sensing Capability (ESC). ESC will sense the incumbent signal and provide the secondary user a binary decision when to start/stop transmission. The sensing and signal processing techniques in ESC are key aspects in SAS.

- Our proposed work follows the current released documents from ETSI and FCC and solves the problem in the defined spectrum sharing frameworks and 5G networks. The evolution of the spectrum frameworks should be considered in future work. How to further reduce the exclusion zone size to enable more cellular network usage is a main direction. In this respect, LTE/radar coexistence and low power communication are key enabling technologies that have not yet been investigated.

- Capacity and performance analysis of C-RAN in this thesis is provided from the network point of view. In the future, we can enhance performance by studying UEs behaviour. For example, the "tidal effect", at day time people are in the city area, at night time people are at a residential area. The pattern of network and service usage can be measured or monitored. With spectrum sharing and C-RAN, network performance in terms of capacity and energy consumption can be further increased.

- The C-RAN architecture that is used in this thesis is moving all distributed processing units into a central processing unit. In the future, we can consider pushing the cloud computing function further down to the UE level. The evolution of C-RAN with enabling UE's processing components as part of the cloud resource is an angle worth considering.

Abbreviations

3GPP	Third Generation Partnership Project
4G	4th Generation
5G	5th Generation
AS	Antenna Selection
ASIC	Application-Specific Integrated Circuit
AWGN	Additive White Gaussian Noise
BD	Block Diagonalisation
C-RAN	Cloud Radio Access Network
CA	Carrier Aggregation
CAZAC	Constant Amplitude Zero Autocorrelation
CB	Coordinated Beamforming
CBRS	Citizen's Broadband Radio Service
CBSD	Citizens Broadband Radio Service Device
CCA	Clear Channel Check
CDF	Cumulative Density Function
CF	Characteristic Function

CFR	Cooperative Frequency Reuse
CJT	Cooperative Joint Transmission
CoMP	Coordinated Multi-Point
CTS	Clear to Send
D2D	Device-to-Device
DAS	Distributed Antenna System
DCAP	Differential Capacity
DFT	Discrete Fourier Transform
DSP	Digital Signal Processor
EHF	Extremely High Frequency
ESC	Environmental Sensing Capability
ETSI	European Telecommunications Standards Institute
FFR	Fractional Frequency Reuse
FSS	Fixed Satellite Systems
GAA	General Authorised Access
H-CRAN	Heterogeneous Cloud Radio Access Network
HARQ	Hybrid Automatic Repeat reQuest
HT-GF	High Throughput Greenfield
ICI	Inter-Cell Interference
IDFT	Inverse Discrete Fourier Transform
IFFT	Inverse Fast Fourier Transform
JT	Joint Transmission

LBT	Listen-Before-Talk
LSA	Licensed Shared Access
LTE	Long-Term Evolution
MAC	Media Access Control
MC	Monte-Carlo
MGF	Moment Generating Function
MGR	Multi-sector Gradient
MIMO	Multiple-Input-Multiple-Output
MNO	Mobile Network Operators
MRT	Maximum Ratio Transmission
MSE	Mean Squared Error
MU-MIMO	Multi-User Multiple-Input-Multiple-Output
NLOS	Non-Line-of-Sight
NOI	Notice of Inquiry
NPRM	Notice of Proposed Rulemaking
NTIA	National Telecommunications and Information Administration
OFDM	Orthogonal Frequency-Division Multiplexing
OFDMA	Orthogonal Frequency Division Multiple Access
PAL	Priority Access Licensees
PDF	Probability Density Function
PPP	Poisson Point Process
PSS	Primary Synchronisation Sequence

QAM	Quadrature Amplitude Modulation
QoS	Quality-of-Service
RTS	Request to Send
SAS	Spectrum Access System
SDL	Supplementary Downlink
SFR	Soft Frequency Reuse
SINR	Signal-to-Interference-and-Noise-Ratio
SNR	Signal-to-Noise-Ratio
SU-MIMO	Single-User Multiple-Input-Single-Output
UC	User Clustering
UE	User Equipment
UFR	Universal Frequency Reuse
VHT	Very High Throughput
ZC	Zadoff-Chu

Bibliography

[1] "Ericsson mobility report," Ericsson, June 2016. [Online]. Available: https://www.ericsson.com/res/docs/2016/ericsson-mobility-report-2016.pdf

[2] "Cisco visual networking index: Global mobile data traffic forecast update, 2015-2020," Cisco, Feburary 2016. [Online]. Available: http://www.cisco.com/c/en/us/solutions/collateral/service-provider/visual-networking-index-vni/mobile-white-paper-c11-520862.pdf

[3] J. G. Andrews, S. Buzzi, W. Choi, S. V. Hanly, A. Lozano, A. C. K. Soong, and J. C. Zhang, "What will 5G be?" *IEEE Journal on Selected Areas in Communications*, vol. 32, no. 6, pp. 1065–1082, June 2014.

[4] B. Badic, C. Drewes, I. Karls, and M. Mueck, *Rolling out 5G: use cases, applications, and technology solutions*. Apress, 2016.

[5] A. Osseiran, F. Boccardi, V. Braun, K. Kusume, P. Marsch, M. Maternia, O. Queseth, M. Schellmann, H. Schotten, H. Taoka, H. Tullberg, M. A. Uusitalo, B. Timus, and M. Fallgren, "Scenarios for 5G mobile and wireless communications: the vision of the METIS project," *IEEE Communications Magazine*, vol. 52, no. 5, pp. 26–35, May 2014.

[6] "Electromagnetic compatibility and radio spectrum matters (ERM); system reference document (SRdoc); mobile broadband services in the 2300 MHz-2400 MHz frequency band under licensed shared access regime," ETSI Reconfigurable Radio Systems (RRS), ETSI TS 103 113 V1.1.1, Tech. Rep., July 2013.

[7] "Amendment of the commission rules with regard to commercial operations in the 3550-3650 mhz band," Federal Communications Commission, FCC 15-47 A1,GN Docket No. 12-354, Tech. Rep., April 2015.

[8] M. D. Mueck, S. Srikanteswara, and B. Badic, "Spectrum sharing: Licensed Shared Access (LSA) and Spectrum Access System (SAS)," Intel, October 2015. [Online]. Available: www.intel.com/content/dam/www/public/us/en/documents/white-papers/spectrum-sharing-lsa-sas-paper.pdf

[9] M. M. Sohul, M. Yao, T. Yang, and J. H. Reed, "Spectrum access system for the citizen broadband radio service," *IEEE Communications Magazine*, vol. 53, no. 7, pp. 18–25, July 2015.

[10] S. Bhaumik, S. Chandrabose, M. Jataprolu, G.Kumar, A. Muralidhar, P. Polakos, V. Srinivasan, and T. Woo, "CloudIQ: A framework for processing base stations in a data center," in *Proc. 18th annual international conference on Mobile computing and networking (Mobicom)*, 2012, pp. 125–136.

[11] "C-RAN the road towards green RAN-white paper," China Mobile Research Institute, October 2011. [Online]. Available: http://labs.chinamobile.com/cran/wp-content/uploads/CRAN_white_paper_v2_5_EN(1).pdf

[12] M. Mueck, W. Jiang, G. Sun, H. Cao, E. Dutkiewicz, and S. Choi, "Novel spectrum usage paradigms for 5G," *IEEE Technical Committee on Cognitive Networks (TCCN), White paper*, 2014.

[13] "3rd Generation Partnership Project; Technical Specification Group Radio Access Network; Evolved Universal Terrestrial Radio Access (E-UTRA); User Equipment (UE) radio transmission and reception (Release 13)," 3GPP, Tech. Spec. 36.101 v13.3.0, March 2016.

[14] M. Palolo, T. Rautio, M. Matinmikko, J. Prokkola, M. Mustonen, M. Heikkil, T. Kippola, S. Yrjl, V. Hartikainen, L. Tudose, A. Kivinen, J. Paavola, J. Okkonen, M. Mkelinen, T. Hnninen, and H. Kokkinen, "Licensed shared

access (LSA) trial demonstration using real LTE network," in *Proc. 9th International Conference on Cognitive Radio Oriented Wireless Networks and Communications (CROWNCOM)*, June 2014, pp. 498–502.

[15] G. A. Sanders, "Effects of radar interference on LTE (FDD) eNodeB and UE receiver performance in the 3.5 GHz band," U.S. Department of Commerce, National Telecommunications and Information Administration, 2014. [Online]. Available: www.its.bldrdoc.gov/publications/download/TR-14-506.pdf

[16] S. Kodituwakku, T. Lamahewa, and T. Dissanayake, "Impact on radar probability of detection due to interference from 4G communication signals," in *Proc. IEEE Global Electromagnetic Compatibility Conference (GEMCCON)*, November 2015, pp. 1–5.

[17] J. Mitola and G. Q. Maguire, "Cognitive radio: making software radios more personal," *IEEE Personal Communications*, vol. 6, no. 4, pp. 13–18, August 1999.

[18] "Notice of proposed rule making and order: Facilitating opportunities for flexible, efficient, and reliable spectrum use employing cognitive radio technologies," Federal Communications Commission and others, ET docket 03-108, 2005.

[19] "IEEE standard for information technology– local and metropolitan area networks– specific requirements– part 22: Cognitive wireless RAN medium access control (MAC) and physical layer (PHY) specifications: Policies and procedures for operation in the TV bands," IEEE Std 802.22-2011, July 2011.

[20] C. R. Stevenson, G. Chouinard, Z. Lei, W. Hu, S. J. Shellhammer, and W. Caldwell, "IEEE 802.22: The first cognitive radio wireless regional area network standard," *IEEE Communications Magazine*, vol. 47, no. 1, pp. 130–138, January 2009.

[21] "IEEE standard for information technology - telecommunications and information exchange between systems - local and metropolitan area networks -

specific requirements - part 11: Wireless LAN medium access control (MAC) and physical layer (PHY) specifications amendment 5: Television white spaces (TVWS) operation," IEEE Std 802.11af-2013 (Amendment to IEEE Std 802.11-2012, as amended by IEEE Std 802.11ae-2012, IEEE Std 802.11aa-2012, IEEE Std 802.11ad-2012, and IEEE Std 802.11ac-2013), February 2014.

[22] "MAC and PHY for operation in TV white space," ECMA International, June 2012. [Online]. Available: http://www.ecma-international.org/publications/files/ECMA-ST/ECMA-392.pdf

[23] "IEEE standard for information technology–telecommunications and information exchange between systems – local and metropolitan area networks – specific requirements – part 19: TV white space coexistence methods," IEEE Std 802.19.1-2014, June 2014.

[24] S. Filin, T. Baykas, H. Harada, F. Kojima, and H. Yano, "IEEE standard 802.19.1 for TV white space coexistence," *IEEE Communications Magazine*, vol. 54, no. 3, pp. 22–26, March 2016.

[25] C. X. Wang, F. Haider, X. Gao, X. H. You, Y. Yang, D. Yuan, H. M. Aggoune, H. Haas, S. Fletcher, and E. Hepsaydir, "Cellular architecture and key technologies for 5G wireless communication networks," *IEEE Communications Magazine*, vol. 52, no. 2, pp. 122–130, February 2014.

[26] S. Haykin, "Cognitive radio: brain-empowered wireless communications," *IEEE Journal on Selected Areas in Communications*, vol. 23, no. 2, pp. 201–220, February 2005.

[27] T. Yucek and H. Arslan, "A survey of spectrum sensing algorithms for cognitive radio applications," *IEEE Communications Surveys Tutorials*, vol. 11, no. 1, pp. 116–130, 2009.

[28] Y. C. Liang, Y. Zeng, E. C. Y. Peh, and A. T. Hoang, "Sensing-throughput tradeoff for cognitive radio networks," *IEEE Transactions on Wireless Communications*, vol. 7, no. 4, pp. 1326–1337, April 2008.

[29] H. T. Cheng and W. Zhuang, "Simple channel sensing order in cognitive radio networks," *IEEE Journal on Selected Areas in Communications*, vol. 29, no. 4, pp. 676–688, April 2011.

[30] Y. Xin, H. Zhang, and L. Lai, "A low-complexity sequential spectrum sensing algorithm for cognitive radio," *IEEE Journal on Selected Areas in Communications*, vol. 32, no. 3, pp. 387–399, March 2014.

[31] H. Zhang, H. C. Wu, and L. Lu, "Analysis and algorithm for robust adaptive cooperative spectrum-sensing," *IEEE Transactions on Wireless Communications*, vol. 13, no. 2, pp. 618–629, February 2014.

[32] E. Axell, G. Leus, E. G. Larsson, and H. V. Poor, "Spectrum sensing for cognitive radio : State-of-the-art and recent advances," *IEEE Signal Processing Magazine*, vol. 29, no. 3, pp. 101–116, May 2012.

[33] W. Zhang, C. K. Yeo, and Y. Li, "A MAC sensing protocol design for data transmission with more protection to primary users," *IEEE Transactions on Mobile Computing*, vol. 12, no. 4, pp. 621–632, April 2013.

[34] "Reconfigurable radio systems (RRS); system architecture and high level procedures for operation of licensed shared access (LSA) in the 2300 MHz-2400 MHz band," ETSI Reconfigurable Radio Systems (RRS), ETSI TS 103 235 V1.1.1, Tech. Rep., October 2015.

[35] "System requirements for operation of mobile broadband systems in the 2300 mhz - 2400 mhz band under licensed shared access (LSA)," ETSI Reconfigurable Radio Systems (RRS), ETSI TS 103 154 V1.1.1, Tech. Rep., October 2014.

[36] "LTE-U SDL coexistence specifications v1.3," LTE-U Forum, October 2015. [Online]. Available: http://www.lteuforum.org/uploads/3/5/6/8/3568127/lte-u_forum_lte-u_sdl_coexistence_specifications_v1.3.pdf

[37] "3rd Generation Partnership Project; Technical Specification Group Radio Access Network; Study on Licensed-Assisted Access to Unlicensed Spectrum; (Release 13)," 3GPP, Tech. Spec. 36.889 v13.0.0, June 2015.

[38] Y. Li, F. Baccelli, J. G. Andrews, T. D. Novlan, and J. C. Zhang, "Modeling and analyzing the coexistence of Wi-Fi and LTE in unlicensed spectrum," *IEEE Transactions on Wireless Communications*, vol. to be published, 2016.

[39] "Amendment of the commission rules with regard to commercial operations in the 3550-3650 mhz band," Federal Communications Commission, FCC 16-55 A1,GN Docket No. 12-354, Tech. Rep., May 2016.

[40] E. Drocella, J. Richards, R. Sole, F. Najmy, A. Lundy, and P. McKenna, "3.5 GHz exclusion zone analyses and methodology," NTIA Technical Report TR-15-517, June 2015. [Online]. Available: www.its.bldrdoc.gov/publications/download/TR-15-517r1.pdf

[41] S. Sesia, I. Toufik, and M. Baker, *LTE – The UMTS Long Term Evolution: From Theory to Practice*. Wiley, 2015.

[42] B. Jayawickrama, E. Dutkiewicz, M. Mueck, and Y. He, "On the usage of geolocation aware spectrum measurements for incumbent location and transmit power detection," *IEEE Transactions on Vehicular Technology*, to be published.

[43] L. Vijayandran, P. Dharmawansa, T. Ekman, and C. Tellambura, "Analysis of aggregate interference and primary system performance in finite area cognitive radio networks," *IEEE Transactions on Communications*, vol. 60, no. 7, pp. 1811–1822, July 2012.

[44] C. h. Lee and M. Haenggi, "Interference and outage in poisson cognitive networks," *IEEE Transactions on Wireless Communications*, vol. 11, no. 4, pp. 1392–1401, April 2012.

[45] S. Kusaladharma, P. Herath, and C. Tellambura, "Underlay interference analysis of power control and receiver association schemes," *IEEE Transactions on Vehicular Technology*, to be published.

[46] A. Shojaeifard, K. A. Hamdi, E. Alsusa, D. K. C. So, and J. Tang, "Exact SINR statistics in the presence of heterogeneous interferers," *IEEE Transactions on Information Theory*, vol. 61, no. 12, pp. 6759–6773, December 2015.

[47] J. Guo, S. Durrani, and X. Zhou, "Outage probability in arbitrarily-shaped finite wireless networks," *IEEE Transactions on Communications*, vol. 62, no. 2, pp. 699–712, February 2014.

[48] J. Guo, S. Durrani, and X. Zhou, "Performance analysis of arbitrarily-shaped underlay cognitive networks: Effects of secondary user activity protocols," *IEEE Transactions on Communications*, vol. 63, no. 2, pp. 376–389, February 2015.

[49] Z. Khalid and S. Durrani, "Distance distributions in regular polygons," *IEEE Transactions on Vehicular Technology*, vol. 62, no. 5, pp. 2363–2368, June 2013.

[50] C. W. Kim, J. Ryoo, and M. M. Buddhikot, "Design and implementation of an end-to-end architecture for 3.5 GHz shared spectrum," in *Proc. IEEE International Symposium on Dynamic Spectrum Access Networks (DySPAN)*, September 2015, pp. 23–34.

[51] J. Ojaniemi, J. H. Poikonen, and R. Wichman, "Optimization of secondary system antenna deployment in shared spectrum access," *IEEE Transactions on Vehicular Technology*, vol. 65, no. 5, pp. 3536–3546, May 2016.

[52] U. Tefek and T. J. Lim, "Interference management through exclusion zones in two-tier cognitive networks," *IEEE Transactions on Wireless Communications*, vol. 15, no. 3, pp. 2292–2302, March 2016.

[53] A. Ullah, S. Bhattarai, J. M. Park, J. H. Reed, D. Gurney, and B. Bahrak, "Multi-tier exclusion zones for dynamic spectrum sharing," in *Proc. IEEE*

International Conference on Communications (ICC), June 2015, pp. 7659–7664.

[54] S. Bhattarai, A. Ullah, J. M. J. Park, J. H. Reed, D. Gurney, and B. Gao, "Defining incumbent protection zones on the fly: Dynamic boundaries for spectrum sharing," in *Proc. IEEE International Symposium on Dynamic Spectrum Access Networks (DySPAN)*, September 2015, pp. 251–262.

[55] I. Chih-Lin, S. Han, Z. Xu, S. Wang, Q. Sun, and Y. Chen, "New paradigm of 5G wireless internet," *IEEE Journal on Selected Areas in Communications*, vol. 34, no. 3, pp. 474–482, March 2016.

[56] F. Boccardi, R. W. Heath, A. Lozano, T. L. Marzetta, and P. Popovski, "Five disruptive technology directions for 5G," *IEEE Communications Magazine*, vol. 52, no. 2, pp. 74–80, February 2014.

[57] P. Rost, C. J. Bernardos, A. D. Domenico, M. D. Girolamo, M. Lalam, A. Maeder, D. Sabella, and D. Wbben, "Cloud technologies for flexible 5G radio access networks," *IEEE Communications Magazine*, vol. 52, no. 5, pp. 68–76, May 2014.

[58] A. Checko, H. L. Christiansen, Y. Yan, L. Scolari, G. Kardaras, M. S. Berger, and L. Dittmann, "Cloud RAN for mobile networks - a technology overview," *IEEE Communications Surveys Tutorials*, vol. 17, no. 1, pp. 405–426, 2015.

[59] M. Peng, Y. Li, J. Jiang, J. Li, and C. Wang, "Heterogeneous cloud radio access networks: a new perspective for enhancing spectral and energy efficiencies," *IEEE Wireless Communications*, vol. 21, no. 6, pp. 126–135, December 2014.

[60] A. A. M. Saleh, A. Rustako, and R. Roman, "Distributed antennas for indoor radio communications," *IEEE Transactions on Communications*, vol. 35, no. 12, pp. 1245–1251, December 1987.

[61] L. Dai, S. Zhou, and Y. Yao, "Capacity analysis in CDMA distributed antenna systems," *IEEE Transactions on Wireless Communications*, vol. 4, no. 6, pp. 2613–2620, November 2005.

[62] W. Choi and J. G. Andrews, "Downlink performance and capacity of distributed antenna systems in a multicell environment," *IEEE Transactions on Wireless Communications*, vol. 6, no. 1, pp. 69–73, 2007.

[63] W. Roh and A. Paulraj, "MIMO channel capacity for the distributed antenna," in *Proc. IEEE 56th Vehicular Technology Conference (VTC)*, vol. 2, 2002, pp. 706–709.

[64] P. Marsch and G. Fettweis, "A framework for optimizing the uplink performance of distributed antenna systems under a constrained backhaul," in *Proc. IEEE International Conference on Communications (ICC)*, 2007, pp. 975–979.

[65] E. Park, S.-R. Lee, and I. Lee, "Antenna placement optimization for distributed antenna systems," *IEEE Transactions on Wireless Communications*, vol. 11, no. 7, pp. 2468–2477, 2012.

[66] S. R. Lee, S. H. Moon, J. S. Kim, and I. Lee, "Capacity analysis of distributed antenna systems in a composite fading channel," *IEEE Transactions on Wireless Communications*, vol. 11, no. 3, pp. 1076–1086, 2012.

[67] X. Zhang, Y. Sun, X. Chen, S. Zhou, J. Wang, and N. B. Shroff, "Distributed power allocation for coordinated multipoint transmissions in distributed antenna systems," *IEEE Transactions on Wireless Communications*, vol. 12, no. 5, pp. 2281–2291, May 2013.

[68] H. Zhu, "Performance comparison between distributed antenna and microcellular systems," *IEEE Journal on Selected Areas in Communications*, vol. 29, no. 6, pp. 1151–1163, 2011.

[69] D. Castanheira and A. Gameiro, "Distributed antenna system capacity scaling [Coordinated and Distributed MIMO]," *IEEE Wireless Communications*, vol. 17, no. 3, pp. 68–75, 2010.

[70] W. Feng, Y. Wang, N. Ge, J. Lu, and J. Zhang, "Virtual MIMO in multi-cell distributed antenna systems: Coordinated transmissions with large-scale CSIT," *IEEE Journal on Selected Areas in Communications*, vol. 31, no. 10, pp. 2067–2081, October 2013.

[71] J. Joung, Y. K. Chia, and S. Sun, "Energy-efficient, large-scale distributed-antenna system (L-DAS) for multiple users," *IEEE Journal of Selected Topics in Signal Processing*, vol. 8, no. 5, pp. 954–965, October 2014.

[72] Z. Jiang, S. Zhou, and Z. Niu, "Optimal antenna cluster size in cell-free large-scale distributed antenna systems with imperfect CSI and intercluster interference," *IEEE Transactions on Vehicular Technology*, vol. 64, no. 7, pp. 2834–2845, July 2015.

[73] "Simulation results on handover when DRX is used," 3GPP TSG RAN WG4 Meeting # 48 bis, NTT DOCOMO, R4-082347, October 2008.

[74] "Enhancing LTE cell-edge performance via PDCCH ICIC," Fujitsu Network Communications Inc., 2011. [Online]. Available: http://www.fujitsu.com/downloads/TEL/fnc/whitepapers/Enhancing-LTE-Cell-Edge.pdf

[75] "3rd Generation Partnership Project; Technical Specification Group Radio Access Network; Evolved Universal Terrestrial Radio Access (E-UTRA); Further advancements for E-UTRA physical layer aspects; (Release 9)," 3GPP, Tech. Spec. 36.889 v1.0.0, February 2009.

[76] V. Jungnickel, L. Thiele, T. Wirth, T. Haustein, S. Schiffermuller, A. Forck, S. Wahls, S. Jaeckel, S. Schubert, H. Gabler, C. Juchems, F. Luhn, R. Zavrtak, H. Droste, G. Kadel, W. Kreher, J. Mueller, W. Stoermer, and G. Wannemacher, "Coordinated multipoint trials in the downlink," in *Proc. IEEE Global Communications Conference (Globecom) Workshops*, November 2009, pp. 1–7.

[77] A. Ghosh, R. Ratasuk, B. Mondal, N. Mangalvedhe, and T. Thomas, "LTE-advanced: next-generation wireless broadband technology [invited paper]," *IEEE Wireless Communications*, vol. 17, no. 3, pp. 10–22, June 2010.

[78] G. Boudreau, J. Panicker, N. Guo, R. Chang, N. Wang, and S. Vrzic, "Interference coordination and cancellation for 4G networks," *IEEE Communications Magazine*, vol. 47, no. 4, pp. 74–81, April 2009.

[79] A. L. Stolyar and H. Viswanathan, "Self-organizing dynamic fractional frequency reuse for best-effort traffic through distributed inter-cell coordination," in *Proc. IEEE International Conference on Computer Communications (INFOCOM)*, April 2009, pp. 1287–1295.

[80] S. H. Ali and V. C. M. Leung, "Dynamic frequency allocation in fractional frequency reused OFDMA networks," *IEEE Transactions on Wireless Communications*, vol. 8, no. 8, pp. 4286–4295, August 2009.

[81] T. D. Novlan, R. K. Ganti, A. Ghosh, and J. G. Andrews, "Analytical evaluation of fractional frequency reuse for OFDMA cellular networks," *IEEE Transactions on Wireless Communications*, vol. 10, no. 12, pp. 4294–4305, December 2011.

[82] C. Wang, Q. Cui, S. Li, X. Tao, and X. Xu, "Multiuser pairing in uplink CoMP MU-MIMO systems using particle swarm optimization," in *Proc. IEEE Vehicular Technology Conference (VTC)*, September 2011, pp. 1–5.

[83] J. Liu, X. Li, H. Ji, and Y. Tang, "Traffic-pairing scheme based on particle swarm optimization in downlink CoMP-MU-MIMO system," in *Proc. IEEE Wireless Communications and Networking Conference (WCNC)*, April 2014, pp. 1779–1784.

[84] M. Matinmikko, H. Okkonen, M. Palola, S. Yrjola, P. Ahokangas, and M. Mustonen, "Spectrum sharing using licensed shared access: the concept and its workflow for LTE-advanced networks," *IEEE Wireless Communications*, vol. 21, no. 2, pp. 72–79, 2014.

[85] M. Mustonen, T. Chen, H. Saarnisaari, M. Matinmikko, S. Yrjola, and M. Palola, "Cellular architecture enhancement for supporting the european licensed shared access concept," *IEEE Wireless Communications*, vol. 21, no. 3, pp. 37–43, 2014.

[86] J. Li, H. Zhang, X. Xu, X. Tao, T. Svensson, C. Botella, and B. Liu, "A novel frequency reuse scheme for coordinated multi-point transmission," in *Proc. IEEE 71st Vehicular Technology Conference (VTC)*, 2010, pp. 1–5.

[87] J. Hwang, S. M. Yu, S. L. Kim, and R. Jantti, "On the frequency allocation for coordinated multi-point joint transmission," in *Proc. IEEE 75th Vehicular Technology Conference (VTC)*, May 2012, pp. 1–5.

[88] A. Goldsmith, *Wireless communications*. Cambridge university press, 2005.

[89] H. Tanizaki, *Computational methods in statistics and econometrics*. CRC Press, 2004.

[90] A. Rényi, *Foundations of Probability*. Courier Corporation, 2007.

[91] V. Skorokhod, *Basic principles and applications of probability theory*. Springer Science & Business Media, 2005.

[92] Y. He, J. Wang, Y. Su, E. Dutkiewicz, X. Huang, and J. Shi, "An efficient implementation of PRACH generator in LTE UE transmitters," in *Proc. 7th International Wireless Communications and Mobile Computing Conference (IWCMC)*, July 2011, pp. 2226–2230.

[93] "3rd Generation Partnership Project; Technical Specification Group Radio Access Network; Evolved Universal Terrestrial Radio Access (E-UTRA); Further advancements for E-UTRA physical layer aspects (Release 9)," 3GPP, Tech. Spec. 36.814 v9.0.0, March 2010.

[94] "3rd Generation Partnership Project; Technical Specification Group Radio Access Network; Evolved Universal Terrestrial Radio Access (E-UTRA); Physical layer procedures (Release 8)," 3GPP, Tech. Spec. 36.213 v8.7.0, May 2009.

[95] "3rd Generation Partnership Project; Technical Specification Group Radio Access Network; Evolved Universal Terrestrial Radio Access (E-UTRA); Physical Channels and Modulation (Release 8)," 3GPP, Tech. Spec. 36.211 v8.7.0, May 2009.

[96] "IEEE standard for information technology– telecommunications and information exchange between systemslocal and metropolitan area networks– specific requirements–part 11: Wireless LAN medium access control (MAC) and physical layer (PHY) specifications–amendment 4: Enhancements for very high throughput for operation in bands below 6 GHz." IEEE Std 802.11ac-2013 (Amendment to IEEE Std 802.11-2012, as amended by IEEE Std 802.11ae-2012, IEEE Std 802.11aa-2012, and IEEE Std 802.11ad-2012), December 2013.

[97] Lo and T. KY, "Maximum ratio transmission," in *Proc. IEEE International Conference on Communications,(ICC)*, vol. 2, 1999, pp. 1310–1314.

[98] A. Papoulis and S. U. Pillai, *Probability, random variables, and stochastic processes*. Tata McGraw-Hill Education, 2002.

[99] D. Castanheira and A. Gameiro, "Distributed MISO system capacity over rayleigh flat fading channels," in *Proc. IEEE 19th International Symposium on Personal, Indoor and Mobile Radio Communications (PIMRC)*, September 2008, pp. 1–5.

[100] F. Héliot, R. Hoshyar, and R. Tafazolli, "An accurate closed-form approximation of the distributed MIMO outage probability," *IEEE Transactions on Wireless Communications*, vol. 10, no. 1, pp. 5–11, 2011.

[101] A. Sibille, C. Oestges, and A. Zanella, *MIMO: from theory to implementation*. Academic Press, 2010.

[102] Q. H. Spencer, A. L. Swindlehurst, and M. Haardt, "Zero-forcing methods for downlink spatial multiplexing in multiuser MIMO channels," *IEEE Transactions on Signal Processing*, vol. 52, no. 2, pp. 461–471, 2004.

[103] W. Feng, Y. Li, S. Zhou, J. Wang, and M. Xia, "Downlink capacity of distributed antenna systems in a multi-cell environment," in *Proc. IEEE Wireless Communications and Networking Conference (WCNC)*, April 2009, pp. 1–5.

[104] Y. He, E. Dutkiewicz, G. Fang, and J. Shi, "Differential capacity bounds for distributed antenna systems under low SNR conditions," in *Proc. IEEE International Conference on Communications (ICC)*, June 2014, pp. 5550–5554.

[105] E. Pateromichelakis, M. Shariat, R. Tafazolli *et al.*, "On the evolution of multi-cell scheduling in 3gpp lte/lte-a," *IEEE Communications Surveys & Tutorials*, vol. 15, no. 2, pp. 701–717, 2013.

[106] D. E. Knuth, "The art of computer programming, 3rd edn., vol. 2," *Seminumerical Algorithms*, 1998.

[107] D. Chandler, "Introduction to modern statistical mechanics," *Oxford University Press*, 1987.

[108] M. S. Alouini and A. J. Goldsmith, "Area spectral efficiency of cellular mobile radio systems," *IEEE Transactions on Vehicular Technology*, vol. 48, no. 4, pp. 1047–1066, 1999.